EVALUATING CLIMATE VARIABILITY AND COUPLING STRENGTH OF LAND-ATMOSPHERE INTERACTIONS ACROSS THE AMAZON BASIN

By

Nafiseh Haghtalab

A DISSERTATION

Submitted to
Michigan State University
in partial fulfillment of the requirements
for the degree of

Geography—Doctor of Philosophy

2021

ABSTRACT

EVALUATING CLIMATE VARIABILITY AND COUPLING STRENGTH OF LAND-ATMOSPHERE INTERACTIONS ACROSS THE AMAZON BASIN

By

Nafiseh Haghtalab

The Amazon basin, which contains about 60% of tropical rainforests in the world, plays vital roles in regulating climate patterns, sustaining ecosystem services, contributing to global biodiversity, and cycling nutrients. These services, however, have been disrupted by human activities within the region due to infrastructure development and resource extraction. These land-use changes have impacts from local to global scales, particularly on climate and hydrologic cycles, but the extent to which is unclear. Therefore, it is essential to examine precipitation variability and look for drivers of changes at multiple spatio-temporal scales. Analysis of hot spots of land-atmosphere interactions highlights the areas where changes in land surface characteristics influence the atmosphere behavior the most.

This dissertation focuses on climate variability and land-atmosphere coupling across the Amazon basin. Research questions are addressed in three self-contained chapters. Chapter 2 examines the changes in precipitation amount and intensity using a high-resolution (0.05^{o} spatial resolution) gridded data set (CHIRPS) from 1982 to 2018. Several precipitation indices are developed to analyze trends using the Mann-Kendall test. Our results show landscape-scale changes in the timing and intensity of rainfall events. Specifically, wet areas of the western basin have become significantly wetter since 1982, with an increase of 182 mm of rainfall per year. In the eastern and southern regions, where deforestation is widespread, a significant drying trend is evident.

In chapter 3, we aim to examine the impacts of potential tropical reforestation on surface energy and moisture budgets, including precipitation. We simulated changes in heat and moisture fluxes due to tropical reforestation using WRF.V3.9 (Weather Research and Forecast model) to analyze the sensitivity and magnitude of changes to the surface fluxes due to reforestation in the Amazon Basin. We found that the effects of reforestation on the atmosphere were more evident during the dry season; spatial patterns of the changes in atmospheric behavior due to reforestation were consistent with the pattern of land cover change, and the cooling effect of reforestation was evident at seasonal time scale.

In chapter 4, following the results of chapter 3 on the effects of land surface characteristics on atmosphere behavior, we aim to find hot spots of strong land-atmosphere (L-A) coupling across the basin at regional scales. Strong land-atmosphere coupling is critical to understanding precipitation dynamics. Therefore, we applied two commonly used coupling approaches at the regional spatial scale and monthly temporal scale. Ultimately, we recommend a new metric considering more physical relationships, interactions, and lag times between variables. We found that the spatial pattern of hot spots is highly dependent on the temporal and spatial scales of analysis. Also, the interactions among variables within the boundary layer play a more important role in determining the hot spots of strong L-A coupling.

Overall, the evidence provided here suggests that (1) precipitation distribution has changed over time (1982-2018) with wet areas getting wetter and dry areas getting drier across the Amazon basin; (2) reforestation of deforested regions across the basin moderates atmospheric patterns and behavior; (3) hot spots of strong L-A coupling are highly dependent on temporal and spatial scales of analysis as well as parameters interactions within the boundary layer.

ACKNOWLEDGMENTS

This Ph.D. journey has been a life-changing experience for me. With all ups and downs, it would be impossible without the guidance and support of many people.

First and foremost, I would like to thank my Ph.D. advisor, Dr. Nathan Moore, for listening, guiding, encouraging, inspiring, and advising, with wisdom and good humor always.

I would like to express my deepest appreciation to my Ph.D. research committee Dr. Joe Messina, Dr. Jeff Andresen, and Dr. Pouyan Nejadhashemi for valuable and timely feedback at key stages in the research process and for writing recommendation letters at very short notice. I also, want to thank Dr. David Hyndamn for providing insightful feedback and guidance on my work. I would like to thank Dr. Emilio Moran for involving me in the INFEWs project and providing partial funding for my research. It was a great opportunity for me to learn and grow.

Thanks to my wonderful colleagues and friends in the geography department. A special note of thanks to Leah Mungai for her everyday support and friendship. I would love to thank my friends in the Iranian community and SWIG for their supports.

I would like to acknowledge the Department of Geography, Environment, and Spatial Sciences, the graduate school, the center for global change and observations, ESPP at Michigan State University for supporting me financially, and NCAR for technical support. This dissertation was also supported by an MSU Graduate School Dissertation Completion Fellowship and NSF INFEWS/T3 grant No. 1639115. Partial support also came from NIFA Hatch Grant Accession No. 1007604.

I cannot begin to express my thanks to the love of my life Mohsen. I am truly grateful for his love, support, and patience. Without him, I would not have been able to thrive in my doctoral

program or balance my research with everything else. Thanks to my daughter Hannah for bringing joy and happiness to our family.

Finally, I would like to extend my sincere thanks to my parents, my siblings, and my in-laws for their years of continual support, inspiration, and involvement.

TABLE OF CONTENTS

LIST OF TABLES ix

LIST OF FIGURES x

CHAPTER 1. INTRODUCTION 1
- Research Context 1
- Dissertation Focus and Organization 5

REFERENCES 7

CHAPTER 2. EVALUATING SPATIAL PATTERNS IN PRECIPITATION TRENDS ACROSS THE AMAZON BASIN DRIVEN BY LAND COVER AND GLOBAL SCALE FORCINGS 12
- Introduction 12
- Material and methods 16
  - Study area 16
  - Data 18
    - Rain gauge data 18
    - Remotely sensed precipitation data 19
    - Precipitation indices 19
  - Methodology 20
    - Changepoint detection 20
    - Statistical analysis of rainfall trends 21
- Results 22
  - Gridded data validation 22
  - Interannual precipitation trend analysis 23
    - MAP trend analysis 24
    - NDD trend analysis 25
    - NXE trend analysis 27
  - Quantifying the trend magnitude 28
    - MAP trend magnitude 29
    - NDD trend magnitude 30
    - NXE trend magnitude 32
  - Aggregated change analysis 34
- Discussion 35
- Conclusion 40

APPENDIX 41

REFERENCES 47

CHAPTER3. ANALYZING THE FIRST-ORDER RESPONSES OF ATMOSPHERE TO THE POTENTIAL REFORESTATION ACROSS THE AMAZON BASIN 55
- Introduction 55
- Materials and Methods 58

Study area and simulation domain 58
Data 60
WRF model setup 61
Results and Discussion 62
Model validation 62
Land cover change scenarios 64
The sensitivity of fluxes and Precipitation to land cover change across the basin 65
Heat flux 65
Moisture flux and precipitation 70
Conclusion 73
APPENDIX 75
REFERENCES 81

CHAPTER 4. MULTIVARIATE PREDICTORS OF SOIL MOISTURE - PRECIPITATION COUPLING AT THE REGIONAL SCALE 89
Introduction 89
Materials and Methods 93
Simulation set-up 93
Land-atmosphere coupling metrics 94
A: Variance based metric 94
B: Correlation-based metric 95
C: Multivariable predictor of hot spots of strong coupling 97
Results 97
A:Variance based metric 97
B: Correlation-based metric 99
Discussion 102
Terrestrial Segment 102
Atmosphere Segment 104
Deficiencies of available metrics 106
Conclusion 110
APPENDIX 113
REFERENCES 120

CHAPTER 5. CONCLUSIONS 126
Summary and Opportunities for Future Research 126
Broader Impacts 131
REFERENCES 134

LIST OF TABLES

Table 1. Summary of defined indices to quantify the precipitation variability 20

Table 2. Correlation between CHIRPS and ANA gauges as well as PERSIANN and ANA gauges for each location. 42

Table 3. WRF parameterizations 62

Table 4. Key parameters in land-atmosphere coupling 115

LIST OF FIGURES

Figure 1. Map of the Amazon basin..... 18

Figure 2. Amazon Basin Precipitation Map..... 23

Figure 3. The trend of mean annual precipitation (MAP) 25

Figure 4. The trend of the number of dry days (NDD)..... 26

Figure 5. The trend of the number of extreme events (NXE)..... 28

Figure 6. Magnitude of changes in mean annual precipitation (MAP)..... 30

Figure 7. Magnitude of changes in the number of dry days (NDD)..... 31

Figure 8. Magnitude of changes in NXE during May-Nov and Dec-Apr 33

Figure 9. Aggregated significant changes in all indices 34

Figure 10. The Amazon basin. 60

Figure 11. Model output validation 63

Figure 12. Correlation between topography and model performance 64

Figure 13. ESA land cover map used in the simulation..... 65

Figure 14. Mean daily seasonal Latent Heat Flux (LH) 67

Figure 15. Mean daily seasonal sensible heat flux (SH)..... 68

Figure 16. Mean daily seasonal skin temperature (TSK) 69

Figure 17. Mean daily seasonal Upward Moisture Flux (QFX) 71

Figure 18. Mean daily seasonal precipitation (mm) 72

Figure 19. Differences of LH (wm^{-2})..... 76

Figure 20. Differences of upward moisture flux (wm^{-2})..... 77

Figure 21. Differences of precipitation (mm)..... 78

Figure 22. Differences of precipitation (mm) 79

Figure 23. Differences of T_{sk} (^{o}C) 80

Figure 24. GLACE-type L-A coupling measurement at a regional scale. 99

Figure 25. Correlation-based Coupling Index (I) for SM_LH on the left and SM_SH on the right 100

Figure 26. Correlation-based Coupling Index (I) for SM_QFX on the left and SM_SpH on the right 101

Figure 27. Correlation-based Coupling Index (I) for LH_prcp on the left and SH_prcp on the right 102

Figure 28. multivariable regression index at monthly time scale. 109

Figure 29. Soil texture categories 114

Figure 30. Land cover change from forest to agriculture across the Amazon Basin. 118

CHAPTER 1. INTRODUCTION

Research Context

The Amazon Basin contains about 60% of tropical rainforests in the world (Laurance et al. 2002, Arvor et al. 2017), and plays vital roles in sustaining climate and ecosystem services, and contributes to global biodiversity and nutrient cycling. However, these services have been altered by human disturbances within the region. Deforestation is the dominant human disturbance in this region, replacing forests with pasture and agriculture across the "Arc of Deforestation" in the south of the Amazon Basin (Fearnside 2000, Moore et al. 2007, Costa and Pires 2010, Davidson et al. 2012). These land-use changes have local to global impacts, particularly on climate and hydrologic cycles (Longobardi et al. 2016). The climate of the Amazon Basin is varied from a wet northwest with almost no dry season to a dry southeast with a long dry season. This gradient is coincident with the gradient of land cover change with more agriculture in the south and east of the basin indicating the interconnectedness of socio-economic and biophysical processes. On the other hand, large scale circulations such as ENSO (El Nino-Southern Oscillation) and MJO (Madden-Julian Oscillation) largely affect the rainfall variability of the basin. ENSO cycles that occur every 3 to 7 years, can exacerbate droughts during the dry season (Laurance et al. 2002). Conversely, when the Northern tropical Atlantic and equatorial Pacific are anomalously cold, a rainier wet season is observed. In addition, when specific oceanic events are combined (e.g. cold SSTs and El Nino), the northern Amazon faces very strong negative rainfall anomalies (Ronchail et al. 2002). Therefore, quantifying changes in precipitation variability is essential to analyze the strength of land-atmosphere coupling and assessing impacts on ecosystems. To capture this variability, a high-resolution analysis of rainfall over the Amazon is needed. Precipitation at the regional scale is far from uniform (Laurance et al. 2002) and at finer scales is influenced by convection (Funatsu et al.

2012). Air blowing from the Atlantic brings about two-thirds of the moisture to the basin, while the rest is supplied through hydrologic recycling of ET (Evapotranspiration) driven by the Amazon forests (Costa and Foley 1998). Several studies examined precipitation variability across Amazon, but they are based on either gauge measurements (Santos et al. 2015; Longobardi et al. 2016), which are spatially insufficient, or coarse resolution (> 0.25°) gridded datasets (e.g. Arvor et al. 2017; Silva Junior et al. 2018). Thus, analyzing the precipitation variability across the Amazon Basin, using CHIRPS as a high spatial resolution gridded data (0.05°) with a long-time span (1982-2018) is necessary.

Several studies have identified that the rapidly rising human population, industrial logging, mining, expanding roads and networks, agriculture expansion, and human-caused fires are the primary drivers of precipitation variability (e.g., Laurence 2002; Costa and Pires 2010; Butt et al. 2011; Bagley et al. 2014). Thus, it is essential to correlate significant and spatially cohesive precipitation variability to causal factors.

Land cover change (LCC), which for Amazonia primary means replacing forests and natural grasslands with crops and farms or grazing, influences the regional climate (Forster, et al. 2007). At this scale, the effects of LCC are highly varied. The major parameters that are altered as a result of LCC are net radiation, partitioning of available energy between sensible and latent heat, surface albedo/radiative forcing, the aerodynamics of the surface roughness, boundary layer temperature, and partitioning of precipitation between runoff and evaporation (Pitman 2003; Ramaswamy et al. 2007; Pielke et al. 2011). Deforestation makes the air above it warms quickly (more sensible heat) and rise, which draws the moisture from the surrounding area triggering shallow convection. The convective cell can be advected away from the surface conditions that triggered it, which can lead to a decrease in precipitation in the forest area and increase the cloudiness, rainfall, and

thunderstorms downwind (Avissar and Schmidt 1998; Davidson et al. 2012). This process is called the "vegetation breeze" (Sheil and Murdiyarso 2009; Nobre et al. 2016; Laurance et al. 2018). Also, large-scale heterogeneous deforestation has been shown to suppresses rainfall on the core forest especially at the onset and cessation of the rainy season (Butt et al. 2011; Knox et al. 2011).

Numerical models consistently suggest that if deforestation happens at a scale more than 10^5 km^2, a basin-wide decrease in precipitation will happen (Oyama and Nobre 2003, Coe et al. 2009), which is due to (1) a decline in ET from the deforested area; and (2) a decline in net absorbed solar energy and a general weakening of the continental scale low-pressure system that drives the precipitation over the basin.

Based on the theory, observations, and models, the evidence of LCC effects across the Amazon is strong (Pielke et al. 2011). Regional and global climate modeling experiments have demonstrated impacts of LCC on rainfall, surface temperature, and turbulent energy fluxes (Henderson-Sellers and Gornitz 1984; Chase et al. 2000; Werth 2002; Findell et al. 2006). Global model studies (e.g. Feddema et al. 2005), are able to show significant regional effects of LCC, however, they are unable to simulate substantial changes in the global average radiative forcings (Pielke et al. 2011). This is because models testing positive radiative forcings due to LCC are balanced by areas with negative radiative forcings. However, there is a disagreement among researchers about the degree to which the experimental results are model-dependent and to what extent they can bias the results (Seneviratne et al. 2006). Two different AGCMs can lead to two contradictory results regarding the degree to which deforestation affects the climate (e.g., Pitman et al. 2009) because the way they consider the process of land surface interactions in the climate simulations may be totally different.

The disagreement between those climate model results are mainly due to 1) different representation of crop phenology; 2) varied implementation of land cover characteristics in spite of the same land cover maps; 3) different representation of ET for different land cover type, and 4) different parametrization of albedo (Pitman et al. 2009). Several studies have addressed these discrepancies in climate models. For instance, the Land Use Change IDentification experiment (LUCID: Pitman et al., 2009) found no teleconnection between LCC and its effects on remote climate. Their results were limited because they used fixed SST values. In the other experiments, Koster et al. (2004) and Seneviratne et al. (2006) showed that land-atmosphere coupling strength is highly varied from region to region and from model to model. This shows a major difference between climate models in terms of implementing the effects of LCC on the simulations and feedback analysis. Still, there is a big gap in measuring the strength of land-atmosphere coupling for any given region. For instance, many studies of land-atmosphere coupling strength did not consider autocorrelation in the statistical analysis (e.g., student's t-test) which can overestimate the significance of the changes in the climate. Other studies still use the first generation of the land surface schemes (Pitman 2003) which may overestimate the impacts of perturbation (Chen et al. 2008) since they do not represent the coupled effects of water, energy, and carbon cycles. However, when state-of-the-art land cover schemes are used, there is still disagreement on how to apply changes in the partitioning between latent and sensible heat fluxes to the simulations. Phenologically, the way that models deal with land cover data through LSMs differ; for example, some of them calculate daily leaf area index (LAI) and others prescribe LAI from observations (Pielke et al. 2011). Other biophysical variables are similarly inconsistent.

In summary, simulations and observational studies of Amazonia have suggested that the nature of land cover can significantly influence the surface energy and moisture budget and

eventually the atmospheric circulation (Betts et al. 2004). The climate of Amazonia can be dramatically altered by changes in the extent of forest cover. Therefore, deforestation across the Amazon Basin can exert feedbacks on precipitation reduction through changes in the biophysical characteristics of the land surface (Betts et al. 2004). Consequently, using a numerical climate model coupled with a state-of-the-art land surface scheme to simulate land-atmosphere coupling strength across Amazon is of critical importance.

Dissertation Focus and Organization

The central objective of this dissertation is to quantitatively evaluate land-atmosphere interactions across the Amazon basin. Chapters 2 through 4 are self-contained studies respectively addressing three interrelated research questions:

1. How has precipitation amount, intensity, and timing changed over time and space across the Amazon Basin?
2. What are the responses of the atmosphere to the potential reforestation across the Amazon Basin?
3. Where are the robust hot spots of strong land-atmosphere coupling?

Chapter 2 addresses the spatio-temporal variability of precipitation from 1982 to 2018 using high spatial resolution gridded data (0.05°) at a daily time scale. In this chapter, I developed multiple indices to examine variabilities in timing, amount, and intensity of precipitation through statistical analysis and change detection techniques. Also, the potential drivers of changes are introduced. The results of this chapter highlight the hot spots of changes in precipitation patterns and picture the regions with the highest rate of extreme events and unreliable precipitation.

Chapter 3 uses the results of chapter 2 as a reference to the effects of deforestation on atmosphere behavior in the Amazon Basin. In this chapter using WRFV3.9, the sensitivity of the

atmosphere to potential reforestation across the basin is examined. The main goal of this chapter is to evaluate the extent to which changes in biophysical characteristics of the land surface force the atmosphere behavior. A detailed analysis of atmosphere behavior in response to reforestation is provided.

Chapter 4 quantifies the land-atmosphere coupling strength at the regional scale. In this chapter, using 10 years of simulations, hot spots of strong land-atmosphere coupling are identified. Also, a detailed analysis of physical processes involved in land-atmosphere interaction is provided. Finally, a novel multivariable metric is presented.

Chapter 5 summarizes the proceeding chapters' results, describes their contributions to the field of atmospheric sciences, and identifies a path for future research.

REFERENCES

REFERENCES

Arvor, Damien, Beatriz M. Funatsu, Véronique Michot, and Vincent Dubreui. 2017. "Monitoring Rainfall Patterns in the Southern Amazon with PERSIANN-CDR Data: Long-Term Characteristics and Trends." Remote Sensing 9 (9). https://doi.org/10.3390/rs9090889.

Avissar, Roni, and Tatyana Schmidt. 1998. "An Evaluation of the Scale at Which Ground-Surface Heat Flux Patchiness Affects the Convective Boundary Layer Using Large-Eddy Simulations." Journal of the Atmospheric Sciences 55 (16): 2666–89. https://doi.org/10.1175/1520-0469(1998)055<2666:AEOTSA>2.0.CO;2.

Betts, R. A., P. M. Cox, M. Collins, P. P. Harris, C. Huntingford, and C. D. Jones. 2004. "The Role of Ecosystem-Atmosphere Interactions in Simulated Amazonian Precipitation Decrease and Forest Dieback under Global Climate Warming." Theoretical and Applied Climatology 78 (1–3): 157–75. https://doi.org/10.1007/s00704-004-0050-y.

Butt, Nathalie, Paula Afonso De Oliveira, and Marcos Heil Costa. 2011. "Evidence That Deforestation Affects the Onset of the Rainy Season in Rondonia, Brazil." Journal of Geophysical Research Atmospheres 116 (11): 2–9. https://doi.org/10.1029/2010JD015174.

Chase, T. N., R. A. Pielke Sr., T. G. F. Kittel, R. R. Nemani, and S. W. Running. 2000. "Simulated Impacts of Historical Land Cover Changes on Global Climate in Northern Winter." Climate Dynamics 16 (2–3): 93–105. https://doi.org/10.1007/s003820050007.

Chen, Mingyue, Wei Shi, Pingping Xie, Viviane B. S. Silva, Vernon E. Kousky, R. Wayne Higgins, and John E. Janowiak. 2008. "Assessing Objective Techniques for Gauge-Based Analyses of Global Daily Precipitation." Journal of Geophysical Research 113 (D4): D04110. https://doi.org/10.1029/2007JD009132.

Coe, M. T., M. H. Costa, and B. S. Soares Filho. 2009. "The Influence of Historical and Potential Future Deforestation on the Stream Flow of the Amazon River - Land Surface Processes and Atmospheric Feedbacks." Journal of Hydrology (Amsterdam) 369 (1/2): 165–74. https://doi.org/10.1016/j.jhydrol.2009.02.043.

Costa, Marcos Heil, and Jonathan A. Foley. 1998. "A Comparison of Precipitation Datasets for the Amazon Basin." Geophysical Research Letters 25 (2): 155–58. https://doi.org/10.1029/97GL03502.

Costa, Marcos Heil, and Gabrielle Ferreira Pires. 2010. "Effects of Amazon and Central Brazil Deforestation Scenarios on the Duration of the Dry Season in the Arc of Deforestation." International Journal of Climatology 30 (13): 1970–79. https://doi.org/10.1002/joc.2048.

Davidson, Eric A., Alessandro C. De Araüjo, Paulo Artaxo, Jennifer K. Balch, I. Foster Brown, Mercedes M. Mercedes, Michael T. Coe, et al. 2012. "The Amazon Basin in Transition." Nature 481 (7381): 321–28. https://doi.org/10.1038/nature10717.

Fearnside, Philip. 2000. “Global Warming and Tropical Land-Use Change: Greenhouse Gas Emissions from Biomass Burning, Decomposition and Soils in Forest Conversion, Shifting Cultivation and Secondary Vegetation.” Climatic Change 46: 115–58. https://doi.org/10.1023/A:1005569915357.

Feddema, Johannes J., Oleson W. Keith, Gordon Bonan B., Linda O. Mearns, Lawrence E. Buja, Gerald A Meehl, and Warren M Washington. 2005. “How Much More Global Warming and Sea Level Rise?” Science (New York, N.Y.) 307 (5716): 1769–72. https://doi.org/10.1126/science.1106663.

Findell, Kirsten L., Thomas R. Knutson, P. C. D. Milly, Kirsten L. Findell, Thomas R. Knutson, and P. C. D. Milly. 2006. “Weak Simulated Extratropical Responses to Complete Tropical Deforestation.” Journal of Climate 19 (12): 2835–50. https://doi.org/10.1175/JCLI3737.1.

Funatsu, Beatriz M., Vincent Dubreuil, Chantal Claud, Damien Arvor, and Manoel A. Gan. 2012. “Convective Activity in Mato Grosso State (Brazil) from Microwave Satellite Observations: Comparisons between AMSU and TRMM Data Sets.” Journal of Geophysical Research Atmospheres 117 (16): 1–16. https://doi.org/10.1029/2011JD017259.

Henderson-Sellers, A., and V. Gornitz. 1984. “Possible Climatic Impacts of Land Cover Transformations, with Particular Emphasis on Tropical Deforestation.” Climatic Change 6 (3): 231–57. https://doi.org/10.1007/BF00142475.

Knox, Ryan, Gautam Bisht, Jingfeng Wang, Rafael Bras, Ryan Knox, Gautam Bisht, Jingfeng Wang, and Rafael Bras. 2011. “Precipitation Variability over the Forest-to-Nonforest Transition in Southwestern Amazonia.” Journal of Climate 24 (9): 2368–77. https://doi.org/10.1175/2010JCLI3815.1.

Laurance, William F., José L.C. Camargo, Philip M. Fearnside, Thomas E. Lovejoy, G. Bruce Williamson, Rita C.G. Mesquita, Christoph F.J. Meyer, Paulo E.D. Bobrowiec, and Susan G.W. Laurance. 2018. “An Amazonian Rainforest and Its Fragments as a Laboratory of Global Change.” Biological Reviews 93 (1): 223–47. https://doi.org/10.1111/brv.12343.

Laurance, William F, Thomas E Lovejoy, Heraldo L Vasconcelos, Emilio M Bruna, Raphael K Didham, Philip C Stouffer, Claude Gascon, et al. 2002. “Ecosystem Decay of Amazonian Forest Fragments: A 22-Year Investigation.” Conservation Biology 16 (3): 605–18. http://www.wec.ufl.edu/academics/courses/wis4554/WebUpdate/ReadingsWIS5555/Habitat_fragmentation/Laurance et al_2002_ConBio.pdf.

Longobardi, Patrick, Alvaro Montenegro, Hugo Beltrami, and Michael Eby. 2016. “Deforestation Induced Climate Change: Effects of Spatial Scale.” Edited by Juan A. Añel. PLoS ONE 11 (4): e0153357. https://doi.org/10.1371/journal.pone.0153357.

Malhi, Y., Luiz E. O. C. Aragao, David Galbraith, Chris Huntingford, Rosie Fisher, Przemyslaw Zelazowski, Stephen Sitch, Carol McSweeney, and Patrick Meir. 2008. “Hipoacusia Tubotimp’Anica. Concepto Fisiopatol’Ogico.” PANS 106 (49): 20610–15. https://doi.org/10.1073/pnas.0804619106.

Moore, Nathan, Eugenio Arima, Robert Walker, and Renato Ramos da Silva. 2007. “Uncertainty and the Changing Hydroclimatology of the Amazon.” Geophys. Res. Lett 34: 14707. https://doi.org/10.1029/2007GL030157.

Nobre, Carlos A., Gilvan Sampaio, Laura S. Borma, Juan Carlos Castilla-Rubio, José S. Silva, and Manoel Cardoso. 2016. “Land-Use and Climate Change Risks in the Amazon and the Need of a Novel Sustainable Development Paradigm.” Proceedings of the National Academy of Sciences 113 (39): 10759–68. https://doi.org/10.1073/pnas.1605516113.

Oyama, Marcos Daisuke, and Carlos Afonso Nobre. 2003. “A New Climate-Vegetation Equilibrium State for Tropical South America.” Geophysical Research Letters 30 (23): n/a--n/a. https://doi.org/10.1029/2003GL018600.

Ramaswamy Forster P., V., Artaxo T., Berntsen R., Betts D.W., Fahey J., Haywood J., Lean D.C., et al. 2007. “Changes in Atmospheric Constituents and in Radiative Forcing.” Climate Change 2007: The Physical Science Basis 30 (22): 129–234. https://doi.org/10.1103/PhysRevB.77.220407.

Pielke, Roger A., Andy Pitman, Dev Niyogi, Rezaul Mahmood, Clive McAlpine, Faisal Hossain, Kees Klein Goldewijk, et al. 2011. “Land Use/Land Cover Changes and Climate: Modeling Analysis and Observational Evidence.” Wiley Interdisciplinary Reviews: Climate Change 2 (6): 828–50. https://doi.org/10.1002/wcc.144.

Pitman, A. J. 2003. “The Evolution of, and Revolution in, Land Surface Schemes Designed for Climate Models.” International Journal of Climatology 23 (5): 479–510. https://doi.org/10.1002/joc.893.

Pitman, A. J., N. De Noblet-Ducoudré, F. T. Cruz, E. L. Davin, G. B. Bonan, V. Brovkin, M. Claussen, et al. 2009. “Uncertainties in Climate Responses to Past Land Cover Change: First Results from the LUCID Intercomparison Study.” Geophysical Research Letters 36 (14): 1–6. https://doi.org/10.1029/2009GL039076.

Ronchail, Josyane, Gérard Cochonneau, Michel Molinier, Jean Loup Guyot, Adriana Goretti De Miranda Chaves, Valdemar Guimarães, and Eurides De Oliveira. 2002. “Interannual Rainfall Variability in the Amazon Basin and Sea-Surface Temperatures in the Equatorial Pacific and the Tropical Atlantic Oceans.” International Journal of Climatology 22 (13): 1663–86. https://doi.org/10.1002/joc.815.

Santos, Eliane Barbosa, Paulo Sérgio Lucio, and Cláudio Moisés Santos e Silva. 2015. “Precipitation Regionalization of the Brazilian Amazon.” Atmospheric Science Letters 16 (3): 185–92. https://doi.org/10.1002/asl2.535.

Seneviratne, Sonia I., Daniel Lüthi, Michael Litschi, and Christoph Schär. 2006. “Land–Atmosphere Coupling and Climate Change in Europe.” Nature 443 (7108): 205–9. https://doi.org/10.1038/nature05095.

Sheil, Douglas, and Daniel Murdiyarso. 2009. “How Forests Attract Rain: An Examination of a New Hypothesis.” BioScience 59 (4): 341–47. https://doi.org/10.1525/bio.2009.59.4.12.

Shukla, J, Y Mintz, Randal D. Koster, Paul A. Dimeyer, J Shukla, Y Mintz, Zhichang Guo, et al. “Influence of Land-Surface Evapotranspiration on the Earth’s Climate.” Science (New York, N.Y.), March. http://www.ncbi.nlm.nih.gov/pubmed/17788673.

Silva Dias, M. A.F., S. Rutledge, P. Kabat, P. L. Silva Dias, C. Nobre, G. Fisch, A. J. Dolman, et al. 2002. “Cloud and Rain Processes in a Biosphere-Atmosphere Interaction Context in the Amazon Region.” Journal of Geophysical Research D: Atmospheres 107 (20). https://doi.org/10.1029/2001JD000335.

Silva Junior, Celso H.L., Catherine T. Almeida, Jessflan R.N. Santos, Liana O. Anderson, Luiz E.O.C. Aragão, and Fabrício B. Silva. 2018. “Spatiotemporal Rainfall Trends in the Brazilian Legal Amazon between the Years 1998 and 2015.” Water (Switzerland) 10 (9): 1–16. https://doi.org/10.3390/w10091220.

Werth, David. 2002. “The Local and Global Effects of Amazon Deforestation.” Journal of Geophysical Research 107 (D20). https://doi.org/10.1029/2001jd000717.

CHAPTER 2. EVALUATING SPATIAL PATTERNS IN PRECIPITATION TRENDS ACROSS THE AMAZON BASIN DRIVEN BY LAND COVER AND GLOBAL SCALE FORCINGS

Citation: Haghtalab, N., Moore, N., Heerspink, B. P., Hyndman, D. W. (2020) Evaluating spatial patterns in precipitation trends across the Amazon basin driven by land cover and global scale forcings, Theoretical and Applied Climatology. DOI: 10.1007/s00704-019-03085-3

Introduction

The Amazon basin, which contains about 60% of tropical rainforests in the world (Laurance et al. 2002; Arvor et al. 2017), plays vital roles in regulating climate patterns, sustaining ecosystem services, contributing to global biodiversity, and cycling nutrients. These services, however, have been disrupted by human activities within the region due to infrastructure development and resource extraction. Deforestation is the dominant human disturbance in this region, replacing forests with pasture and agriculture across the "Arc of Deforestation" in the southern headwaters of the Amazon basin (Fearnside 2000; Costa and Pires 2010; Moore et al. 2007; Davidson et al. 2012). These land-use changes have impacts from local to global scales, particularly on climate and hydrologic cycles (Longobardi et al. 2016). The land cover change affects land surface characteristics including surface albedo, roughness, and reflectance, which directly alter surface energy and water fluxes. Partitioning of these fluxes is the most important parameter in the spatial distribution and seasonal variability of rainfall. In the Amazon basin, changes in the magnitude and variability of precipitation have caused both intensified drought recurrence and flood frequency (Silva et al. 2018). Khanna et al. (2017) found that a reduction in surface roughness due to deforestation plays an important role in the region's dry season hydroclimate and that deforestation "is sufficiently advanced to have caused a shift from a thermally to a dynamically-driven hydroclimate regime." Simulations of the Amazon basin's hydroclimatology suggest that

deforestation-induced declines in rainfall across the basin's eastern and southern ecotones could lead to permanently drier conditions (Moore et al. 2007). Simulations also show that preserving forests helps maintain precipitation amounts (Walker et al. 2009). Evapotranspiration (especially transpiration) increases shallow convection, which destabilizes the atmosphere during the transition from dry to wet season. Therefore, interactions between land surface processes, atmospheric convection, and biomass burning are related to the deforestation effects on the dry season (May-Nov) length and enhance regional vulnerability to drought (Wright et al. 2017). Soil moisture and vegetation cover type affect the net radiation through changes in sensible and latent heat fluxes over the basin (Li et al. 2006), which are important factors for determining the wet season onset and the dry season length (Li and Fu 2004). This possible anthropogenic shift towards permanent savannization is not a new concept (Oyama and Nobre 2003), but evidence for the phenomenon has not been shown via broad analyses of Amazon precipitation data.

Extreme climate events across the basin are influenced not only by deforestation but also are affected by synoptic-scale processes and global circulations including the El Niño-Southern Oscillation (ENSO) and the Pacific Decadal Oscillation (PDO) (J. A. Marengo and Espinoza 2016). The observed intensification of rainfall at the regional scale is most likely due to higher sea surface temperatures in the Atlantic (Gloor et al. 2013). This is consistent with an intensification of the global water cycle. Specifically, ENSO cycles that occur every 3 to 7 years can exacerbate droughts during the dry season (Laurance et al. 2002). Conversely, when equatorial Pacific and Northern tropical Atlantic are anomalously cold, a rainier wet season is commonly observed. In addition, when some oceanic events are combined, such as cold SSTs and El Niño, the northern Amazon faces strong negative rainfall anomalies (Ronchail et al. 2002). Therefore, changes in precipitation in the Amazon basin can be related to sea surface temperature fluctuations, ENSO,

the Pacific Decadal Oscillation (Marengo and Espinoza 2016), and deforestation (Khanna et al. 2017). However, changes in each factor may manifest differently within the hydro-climatic cycle, and across portions of the basin.

Quantifying changes in precipitation amount, intensity, and seasonality is essential to analyze effects on ecosystems. To capture variability, a high spatial and temporal resolution analysis of rainfall over the entire Amazon basin is needed. Precipitation at the regional scale (e.g. continental scale) is far from uniform (Laurance et al. 2002); at finer scales (e.g. basin-scale), it is influenced by convection resulting in enhanced spatiotemporal variability (Funatsu et al. 2012). For example, Marengo (2004) found a negative trend in rainfall for the entire Amazon basin based on gauge measurements from 1929 to 1998, while the Mann– Kendall test used on multi-decadal station datasets found only weak trends (Satyamurty et al. 2010). Trend analysis of daily gauge precipitation data of 305 weather stations from 1983 to 2012 showed a significant positive trend in the number of days with precipitation more than 50 and 95 percentiles in the northeast region and a significant decreasing trend in the number of days with precipitation above 95 percentile in the south of the basin (Santos et al. 2015). Using rain gauges 1971-2010 Debortoli et al (2015) found decreasing precipitation trends in the transitional month from wet to dry (Apr-May) and from dry to wet (Nov-Dec) on deforested areas. They also found a later onset and earlier cessation of the rainy season at 88% of the rain gauges In contrast, Almeida et al. (2016) found no trend at most of the 47 weather stations in the Brazilian Legal Amazon from 1973 to 2013. Remotely sensed data have been used to evaluate synaptic changes in rainfall patterns due to insufficient spatial distribution of weather stations and inconsistent temporal measurements of gauge data (Arvor et al. 2017; Silva et al. 2018).

Salviano et al. (2016) used the Climate Research Unit (CRU) monthly precipitation data (1961–2011) and the Mann–Kendall test to estimate rainfall trends across Brazil and found an insignificant positive trend in Jan-Apr and an insignificant negative trend in the Jun-Sep. Analysis of PERSIANN_CDR (Precipitation Estimation from Remotely Sensed Information using Artificial Neural Networks—Climate Data Record (Ashouri et al. 2015) daily precipitation data detected significant decreasing rainfall trends associated with the contracting wet season in the southern Amazon basin, possibly connected to human drivers (Arvor et al. 2017). Tropical Rainfall Measuring Mission satellite (TRMM) data from 1998 to 2015 were analyzed using the Mann–Kendall test to quantify precipitation trends over the Brazilian Legal Amazon and an annual pixel-by-pixel analysis showed that 92.3% of the Brazilian Amazon had no rainfall trend, while 4.2% had significant negative trends ($p \leq 0.05$) and 3.5% had significant positive trends (Silva et al. 2018). Arvor et al. (2017) analyzed changes in the seasonality of the Southern Amazon from 1983 to 2014 and found a contraction of the rainy season by several days. Also, the frequency of dry days in the southern Amazon has increased significantly, and total rainfall has decreased. Wet day frequency has increased across the northern Amazon along with an increase in total rainfall of about 17% (Espinoza et al. 2019).

Previous publications on precipitation changes in the Amazon basin provided contradictory results, perhaps due to either insufficient spatial distribution of weather stations, the low spatial resolution gridded datasets, or analysis limited to subregions of the basin. This discrepancy motivates our analysis of variability in higher spatial resolution precipitation datasets at daily timescales. Here, we analyze changes in precipitation over time and space for the entire Amazon Basin. We examine the trends and change points using CHIRPS data from 1982 to 2019 along with possible drivers such as deforestation, ENSO, and/or changes in the Southern American

Convergence Zone (SACZ). We define indices of Number of Dry Days (NDD) and Number of eXtreme Events (NXE) aggregated in Dec-Apr and May-Nov seasonal timescales and Mean Annual Precipitation (MAP) per day to analyze changes beyond wet days and dry days since the combination of these changes can provide new insights on how different processes are changing across seasons. Ultimately, the aim is to correlate significant and spatially cohesive precipitation variability to causal factors.

Material and methods

Study area

The Amazon basin, which spans ~ 6 million km^2, is drained by the Amazon River and its tributaries. It covers portions of Brazil, Colombia, Peru, Bolivia, Ecuador, Guyana, Suriname, and Venezuela and includes the Andes Cordillera where the transition between lowland and mountains results in the rainiest areas of the basin (Espinoza et al. 2015; Paccini et al.2018) (Figure 1). The river system is a hotspot of ecological diversity and ecosystem function; it provides more than 20% of the world's freshwater discharge, and its forest biomass holds about 100 billion tons of carbon (Malhi et al. 2006; Saatchi et al. 2007). Forest vegetation cover has decreased to 80% of its pre-1960s area (Instituto Nacional de Pesquisas Espaciais and National Institute for Space Research Projeto Prodes Monitoramento da Florsta Amazonica Brasileira por Sate'lite Prodes 2011). The rate of deforestation decreased from 28,000 km^2/year in 2004 to less than 7000 km^2/year in 2011 (Davidson et al. 2012); however, it is increasing again (Fearnside 2015). In addition to landscape changes, the population of the Brazilian Amazon increased from ~ 6 million in 1960 to ~ 25 million in 2010 (Davidson et al. 2012).

The climate varies over the region, from the continuously rainy northwest to the wet/dry transitional climate and long dry season in the south and east (Sombroek 2001; Davidson et al.

2012). The climate gradient is consistent with the land cover change gradient, with more conversion to agriculture in the dry east and south of the region referred to as the "Arc of Deforestation." The eastern basin is strongly influenced by ENSO (Marengo 2004), in which flow in the Amazon River decreases during El Niño years; correspondingly, flooding increases during La Nina years (Coe et al. 2002). The Atlantic Multi-decadal Oscillation also affects the region; for example, the severe drought of 2005 is linked to this oscillation (Marengo et al. 2008). In the southern portion of the basin, maximum rainfall occurs during DJF (the austral summer) related to the South American Monsoon System (SAMS; Vera et al. 2006), which brings moisture from the equatorial regions such as the tropical Atlantic Ocean. The SACZ contributes to rainfall variability across southern Amazonia during JJA (the austral winter), which is an elongated northwest/southeast band of convection (Carvalho et al. 2004). The ITCZ highly influences MAM rainfall regime, but it is highly variable (e.g., Fu et al. 2001).

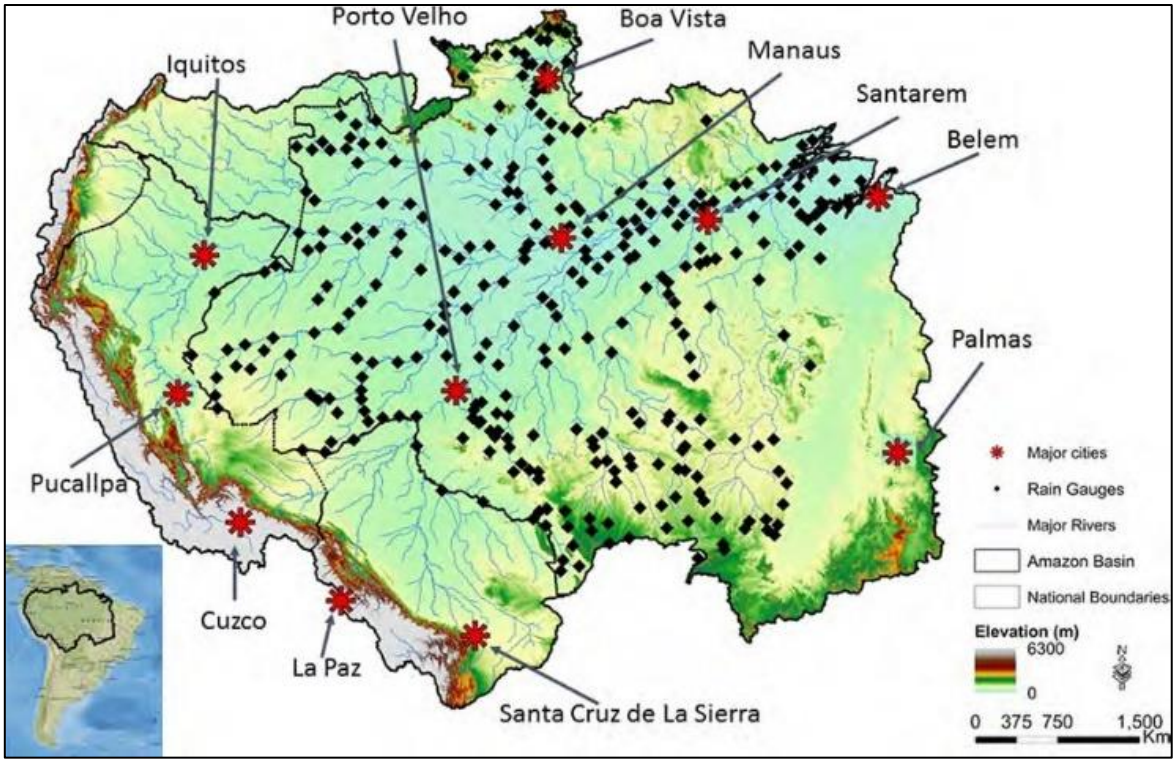

Figure 1. Map of the Amazon basin *shown with shaded topography, along with ANA gauge precipitation stations, major rivers, and cities.*

Data

Rain gauge data

Daily rainfall datasets from 1982 to 2018 for the Brazilian Amazon basin were acquired from a network of 424 rain gauging stations operated by the Brazilian National Water Agency (ANA). For this analysis, we excluded all stations missing greater than 5% of data per year, then subsequently excluded all stations with a record shorter than 10 years after 1982. This resulted in 198 stations over the study area, which had at least 10 years of daily data with less than 5% of daily values missing per year.

Remotely sensed precipitation data

We examined several gridded datasets available at different spatial and temporal resolutions for the region. TRMM 3- hourly data with 0.25° spatial resolution is available starting in 1998 (Huffman et al. 2007), but it has a relatively coarse spatial resolution, and its temporal extent is insufficient for climate analysis (20 years of data). PERSIANN–CDR data contains daily precipitation estimates from 1983 to present, with 0.25° spatial resolution (Ashouri et al. 2015). This dataset also has coarse spatial resolution and artifacts for several dates in the western Amazon. The Climate Hazards Group InfraRed Precipitation with Stations (CHIRPS) dataset has 0.05° spatial resolution that incorporates satellite imagery to represent sparsely gauged locations. It used interpolation techniques to blend station data with remotely sensed data to provide high spatial and temporal resolution of record precipitation estimates based on infrared cold cloud duration (CCD) observations (Funk et al. 2015). CHIRPS has been checked for consistency with Global Precipitation Climatology Center (GPCC) precipitation estimates and performs better than other gridded datasets (Funk et al. 2015). More information about CHIRPS is available at chg.geog.ucsb.edu/data/chirps/. In this paper, we used CHIRPS data for precipitation, and the ANA gauge data were used to assess the findings from the CHIRPS data.

Precipitation indices

We defined several indices to quantify precipitation variability including the number of dry days (NDD), the number of extreme events (NXE) over two time spans Dec-Nov and May-Nov (calculated separately), and mean annual precipitation per day (MAP) for a water year (Dec-Nov) (Table 1). In the next step, we ran a pixel-based non-parametric Mann–Kendall test for each of these indices. We used both Kendall's Tau coefficient and Sen's Slope estimator to detect significant time-series trends from 1982 to 2018. Third, we ran a change point detection

algorithm to identify anomalies and abrupt changes in all indices for regions that show statistically significant changes. Based on the water year, we separately analyzed data during Dec-Nov and May-Nov. Here, we define the water year as the time span starting December 1 of the previous year and ending November 30 of the current year. Changes in seasonality of the Southern Amazon by Arvor et al. (2017) found a contraction of the rainy season by several days. Similarly, Debortoli et al. (2015) found that the rainy season became shorter at 88% of rain gauges from 1971 to 2010. Also, Fu et al. (2013) projected an increase in consecutive dry days and a decrease in consecutive wet days by the end of the twenty-first century. We thus used three separate indices to examine trends in total rainfall and extremes in rainfall for the distinct seasons in the Amazon. Table 1 summarizes these indices.

Table 1. Summary of defined indices to quantify the precipitation variability

Index	Definition
Mean Annual Precipitation (MAP) by day	Mean Annual Daily Precipitation (mm)
Number of Dry Days (NDD)	Days <= 2 mm total precipitation
Number of Extreme Events (NXE)	Days => than 20 mm total precipitation
Water Year	Dec 1st of the previous year to Nov 30th of the current year

Methodology

Changepoint detection

To identify the most significant breakpoint in a large dataset, we applied the binary segmentation method (Fryzlewicz 2014). The binary segmentation method is suitable for consistent estimation of the number and location of multiple change points in data. Cost functions are used in binary segmentation to penalize a high amount of change points in order to avoid overfitting. In a given time series $\{y\tau + 1,. .., yn\}$, if the distribution of $\{y1,. .., y\tau\}$ and $\{y\tau + 1,. .., yn\}$ differ at time τ with respect to at least one parameter such as mean, variance, or

regression structure, then a change point will be detected (Rohrbeck 2013). We used the model to select the most significant breakpoint in each data series.

Statistical analysis of rainfall trends

First, we developed the indices of MAP, NXE, and NDD aggregated over Dec-Nov and May-Nov in Python version 2.7.5. and mapped the results. Then, we performed our statistical analysis of the results in R statistical software (version 3.3.4; R Core Team 2018).

MAP, NXE, and NDD were calculated and sorted using Python version 2.7.5. Statistical analyses were done using R statistical software (version 3.3.4; R Core Team 2018). Pixel-by-pixel analysis identified the spatial distributions of the trends. We used two non-parametric methods to identify the strengths and magnitudes of the trends in both gridded data and gauge measurements as these data are not normally distributed, and non-parametric tests are less sensitive to outliers. The Mann–Kendall test was used to analyze trends in the climate data (e.g., Wilks 2011; Zilli et al. 2017). The non-parametric Mann–Kendall test examines whether there is a trend in the data regardless of the distribution. The null hypothesis is there is no trend in the data over time and space. (Mann 1945; Kendall 1995).

We calculated the test statistic Tau using the "Kendall" package in R. The range of Tau is −1 to + 1, with negative values showing a decreasing trend (more negative "steps") and positive values showing an increasing trend (more upward "steps"). We used a significance level of $\alpha = 0.05$ to identify significant trends.

To quantify the trend magnitude for the three indices, the Mann–Kendall test was used with the non-parametric and robust Sen's slope estimator (e.g., Gocic and Trajkovic 2013; Partal and Kahya 2006; Sharma and Babel 2014; Xu et al. 2003). Again, the distribution may deviate

significantly from a normal/Gaussian distribution for this method. This test is not sensitive to skewness or large outliers (Kumar Sen 1968).

Results

Gridded data validation

To validate the gridded data, we compared ANA rain gauge measurements to CHIRPS data. We compared all 198 ANA gauges that have more than 10 years of data after 1982 with the corresponding CHIRPS pixel values at the same location. The spatial average of 9 neighbors around each point was calculated to reduce bias and errors in the comparison. Figure 2 shows the spatial distribution of mean daily annual precipitation out of CHIRPS (1982–2018) and ANA stations for comparison. The significant correlations at 5% are marked by stars and at 10% are marked with double circles in Figure 2. The results reflect that the northwestern portion of the Amazon basin is the wettest, and the south and southeast portions are the driest. Most of the basin receives 3 to 9 mm/day with a maximum of ~12 mm/d.

We evaluated correlations between both PERSIANN_CDR and CHIRPS against ANA gauge data. The correlation between ANA and CHIRPS was more than 0.6 at 12% of the sites, but the correlation between PERSIAN and ANA is mostly around 0.2, and there are no correlations above 0.6 (Figure 2, bottom inset). This is not surprising as some gauge stations are used in the development of the CHIRPS product. We also encountered numerous artifacts, non-physical patterns, and missing values in the PERSIANN-CDR data. Due to this and bias corrections based on gauge data, we opted to conduct our full analysis with CHIRPS data.

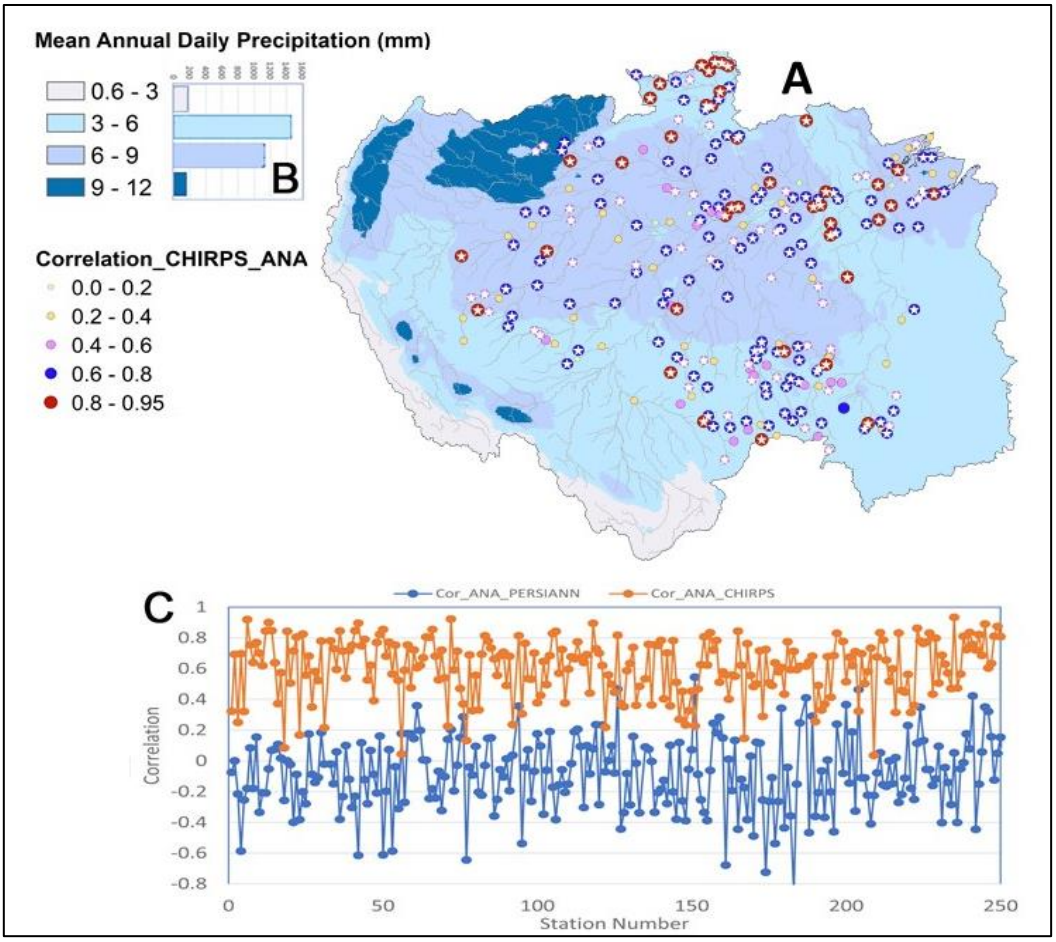

Figure 2. Amazon Basin Precipitation Map*; (A) using CHIRPS daily values 1982–2018. Circles on the map show the correlations between CHIRPS and ANA gauges. The size and color of the circle indicate the strength of correlation and stars indicate the significant correlations at 95%. (B) Distribution of daily rainfall across categories based on CHIRPS daily values 1982–2018. (C) Correlation between daily rain gauges (ANA) and daily CHIRPS data in blue and rain gauges and PERSIANN in orange. A table of correlation values for each of these gauges is included in Supplemental Materials.*

Interannual precipitation trend analysis

The Tau statistic of the Mann–Kendall test is used to assess significant non-parametric trends in time series. This section reports the Tau statistic and the Sen's slope results for the CHIRPS precipitation data. In this chapter we are confident about the trends, but not about the amount of changes. For this reason, the significant level of 95% has been applied in our analysis.

MAP trend analysis

Figure 3 shows the Tau values for gridded data and gauge measurements. Only gauges with statistically significant trends are shown on the map. Forty-one of the 54 gauges with trends (circles) are consistent with CHIRPS (background colors); hatched areas indicate significance at the 0.05 level. The western and northern parts of the domain show significant increasing trends with Tau > 0.3 while "hot spots" around Porto Velho and Santa Cruz de la Sierra show significant decreasing trends with Tau < 0.3.

To capture abrupt changes in time series, we chose areas with a significant change to look at local precipitation variability. All significant CHIRPS pixels in each lettered sub-region on the following figures were spatially averaged for this test. The lettered regions were selected based on the outlined significance levels. Regions A (north-central basin), B (central basin), and C (south-central basin) of Fig. 3 show Tau values < − 0.3, indicating that there are year-to-year decreases 30% more often than the rest of the time series. Regions A, B, and C show decreasing trends with significant variability. Also, a huge difference between the amount of rainfall in 2013 and 2015 is considerable. Changepoint detection shows abrupt decreases in daily precipitation across regions A (1998), B (1995), and C (1992), which all are severe drought years across the basin, especially in the northeast. These are also ENSO years, which combined with anomalous heating in the Atlantic Ocean can cause less rainfall across the basin. Region D shows a positive Tau value of > 0.3 indicating an increasing trend in MAP, with an abrupt increase after 1999; several other regions have similar positive trends across the basin. Together, these results suggest a significant shift in mean annual precipitation across all four regions during the 1990s.

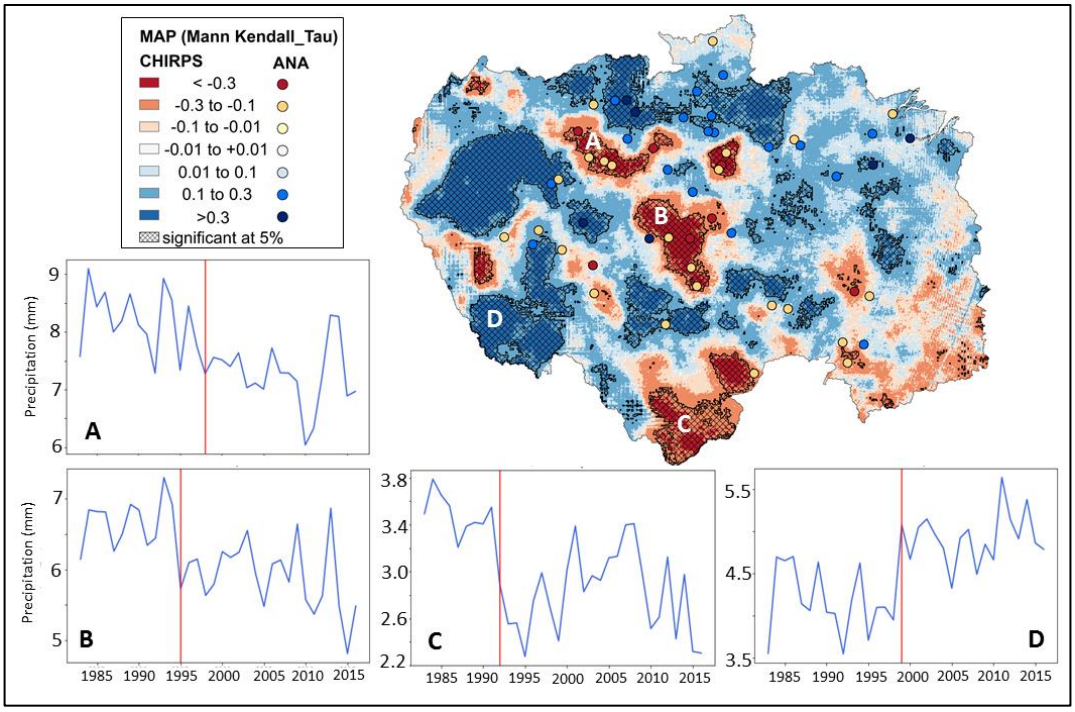

Figure 3. The trend of mean annual precipitation (MAP) *by day is shown on the map. Hatches show significant trends at a 5% confidence level. Graphs show the abrupt changes in the amount of mean annual daily precipitation.*

NDD trend analysis

Figure 4 shows the trends in NDD aggregated in Dec-Nov and May-Nov time spans. All selected regions show an increasing trend of NDD. During May-Nov, NDD increased significantly over the "arc of deforestation" in the southern and eastern portions of the basin. Increasing NDD during May-Nov in the southern basin (region E on Fig. 4) shows a graduate rise across the study period, with a sharp rise in 2010, which was an extreme El Niño year and extreme drought across the basin. 2010 was characterized by a weak SACZ, positive anomalies in the SST in the central Pacific Ocean, and negative anomalies in SST in the Southern Tropical Atlantic Ocean, and a displacement of the ITCZ to the north (Coelho et al. 2013). In region F, which covers a large area east of Palmas, the abrupt change point in NDD occurred in 2004 proceeding with an increasing trend in the number of dry days. There are two extreme decreases

in NDD in 1989 and 2008, both reaching a historic low of 157 dry days, while the average number of dry days during May-Nov is approximately 170 days for region F.

During Dec-Apr, changes in NDD are spatially heterogeneous based on our analysis of station data and prior research (c.f., Fig. 4 in Silva et al. 2018). Only one location shows a significant increasing/drying trend (region G). The time series for G shows high variability for this very rainy region, but the overall increasing trend is clearly recognizable. For example, NDD in 1982 was 65 days, while by 2017, it had shifted to 84 days—an increase of 20 days around Pucallpa, Peru. There was also a steep decline in NDD in 1988, to only 54 dry days within Dec-Apr. The changepoint analysis identified 2001 as a significant break after which the average NDD remains consistently higher than before 2001. There is a notable inconsistency between the gauge and gridded statistics for the number of dry days during Dec-Apr in the Northern Basin.

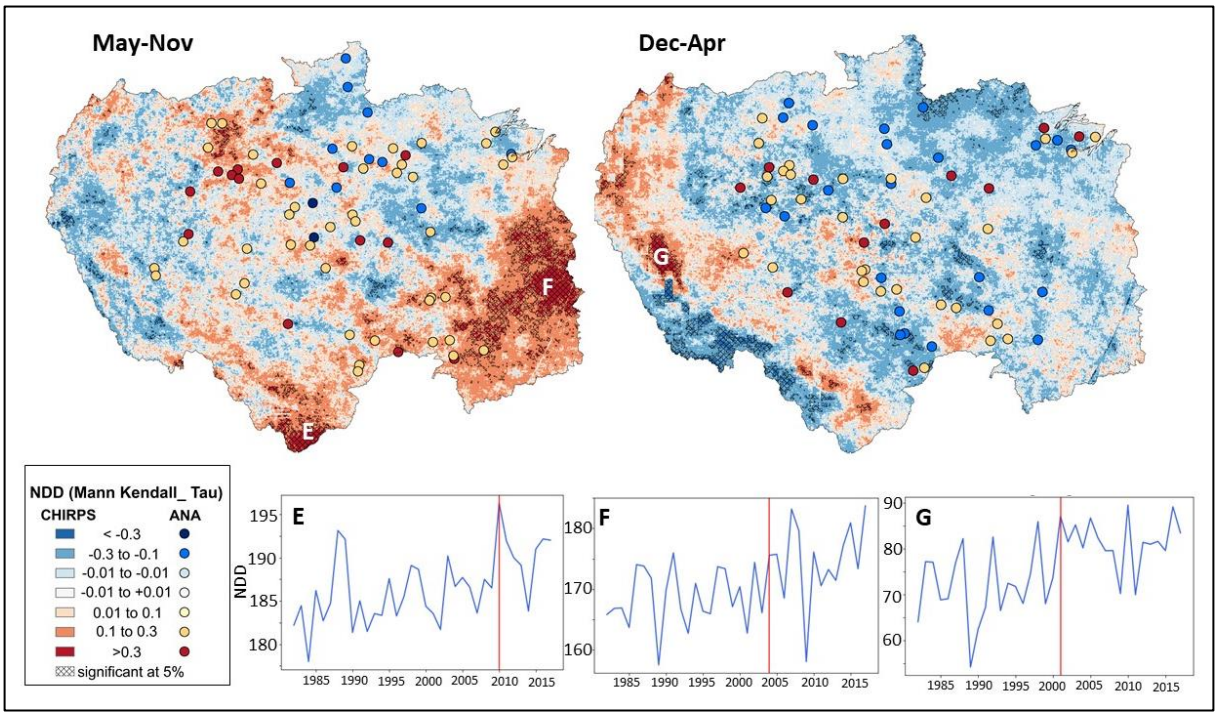

Figure 4. The trend of the number of dry days (NDD) *during May-Nov and Dec-Apr using CHIRPS as a gridded data and ANA rain gauge measurements to validate the results. Graphs on the bottom show the NDD anomalies for each season. Note that vertical axis scales are different*

NXE trend analysis

Changes in NXE during May-Nov and Dec-Apr are shown in Figure 5. Regions H, which is located on the western part of the basin, shows an increasing trend of NXE during May-Nov and Dec-Apr. But all other regions show a decreasing trend in NXE. The warmer (red) colors indicate a decrease in NXE, while cooler (blue) colors show an increase in NXE. Similar to MAP trends, NXE for May-Nov shows a significant increasing trend in the west, especially around Iquitos. There is a strip in the center of the basin from north to south that shows a decreasing trend in extreme events. Gridded and station data show high consistency for the NXE metric across the domain. Region H shows that the NXE during May-Nov doubled after 2012 relative to the earlier average of 11 extreme events. Region J (around Porto Velho extending in a northwest strip) shows a large decreasing trend in NXE, with one dramatic rise in extreme events in 1989. Changepoint detection identifies a significant shift in NXE in 1997, which was an extreme drought year. Before this point, NXE generally remained above 8 days per year, and afterward falls, and has a maximum of 7 days per year. Conversely, in the Santa Cruz de la Sierra (Region K), a noticeable and consistent drop in NXE variability occurs after 1988 (also, a severe drought year). Significant breakpoints in the patterns of NXE vary temporally across these three regions.

During Dec-Apr shows more complex patterns of change and different regions of statistical significance. Similar to NDD, there is a slight inconsistency between gauges and gridded data in the north of the region, where fewer gauges are available, and reporting is less consistent. Changes in NXE during Dec-Apr are not as strongly clustered or as intense as for May-Nov.

Region L in the western basin shows a slightly increasing trend with an average of 13 extreme days per year until the change point in 2012, after which NXE rises to a maximum of 23 events per year. Regions M and N, around Porto Velho and Santa Cruz, show a decreasing trend

in NXE. In the Porto Velho area (M), NXE changed from 26 days in 1982 to 22 days in 2017 with change point analysis showing a significant shift trend in 1995. Region N exhibits a complex but decreasing trend that is significant but not very abrupt. There is a peak in 1988 where NXE is equal to 21 days, with a clear decline after 1992 when a severe basin-wide drought occurred. It is worth mentioning that the breakpoints for NXE in both seasons occur at nearly the same time for regions H/L and J/M.

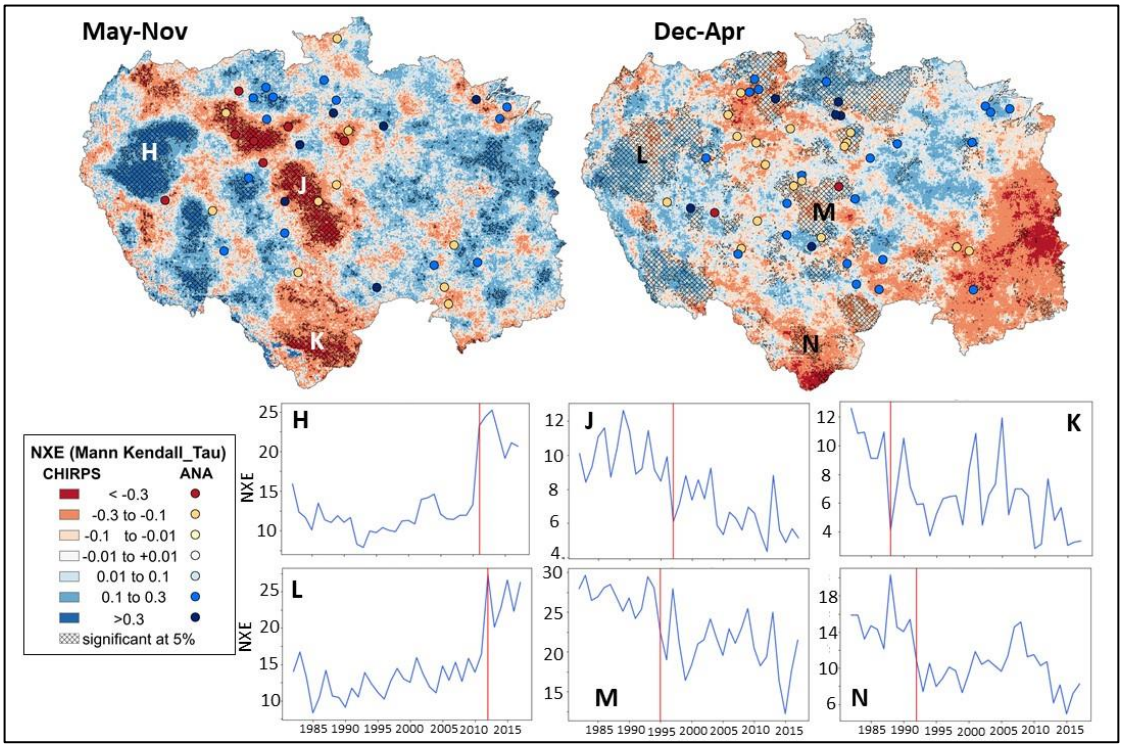

Figure 5. The trend of the number of extreme events (NXE) *during May-Nov and Dec-Apr using CHIRPS as a gridded data and ANA as rain gauge measurements to validate the results. Graphs 5H to 5N show the NXE change*

Quantifying the trend magnitude

Sen's slope is a common non-parametric method that has been used to quantify the magnitude of slope (changes per unit of time) as opposed to the "step" counting of the Tau statistic. In this section, we discuss the magnitude of trends for each variable. Figures 6, 7, and 8 show both a standard regression line and Sen's non-parametric slope, as well as outliers and

intervals. Categories and color schemes are consistent in the Figures. 6, 7, and 8 to facilitate comparison between the three indices. For changes of magnitude in individual years, please refer back to Figures. 3,4, and 5.

MAP trend magnitude

Figure6 shows Sen's slopes of the trend line for MAP. Most of the basin show statistically significant increasing trends (blue) broken up by clusters of negative trends along the Porto Velho northwest strip. Region O (see inset graph in Fig. 6, averaged over the significant area) shows almost sinusoidal changes with a gradual decline. This trend differs from region P near Porto Velho, which suggests a different physical process. For region O, MAP decreased by ~ 0.2 mm/year on average over 37 years. The confidence intervals of the trend line show several outliers in the dataset that each has a different influence on the trend magnitude. 1983 was an extreme wet year for this area at a MAP rate of 9.1 mm/day. 2010 and 2011 were extreme dry years with 6 mm/day.

In region P around Porto Velho, MAP decreases annually at a rate of 0.3 mm/day. Sen's slope is approximately the same as at region O, and the overall change for 37 years is 10 mm/day less in this very wet region. In 1993, an extreme wet year, region O had a MAP rate of 7.4 mm/day, and at the dry extreme (2015), a rate of 4.6 mm/day. This region barely registered the drought of 2005. However, the effects of the drought of 2015 are clear in regions O and P.

Region T, around Santa Cruz, saw a decrease of ~11 mm/ year in MAP over 37 years, equivalent to 407 mm since 1982. This contiguous area of significant change spans ~172,000 km2. There was a period of low variability prior to 2000, while in 2008 and 2009, and there was a sharp decline to 2.2 mm/day after 2016. Region R around and north of Cuzco shows a significant increasing and spatially cohesive trend with a magnitude of 10.1 mm/day over all the

study period 1982, 1992, and 1995 are identified as the driest years with 3.6, 3.5, and 3.7 mm/day of precipitation, whereas 2012 is the wettest year with 5.6 mm/day of rain.

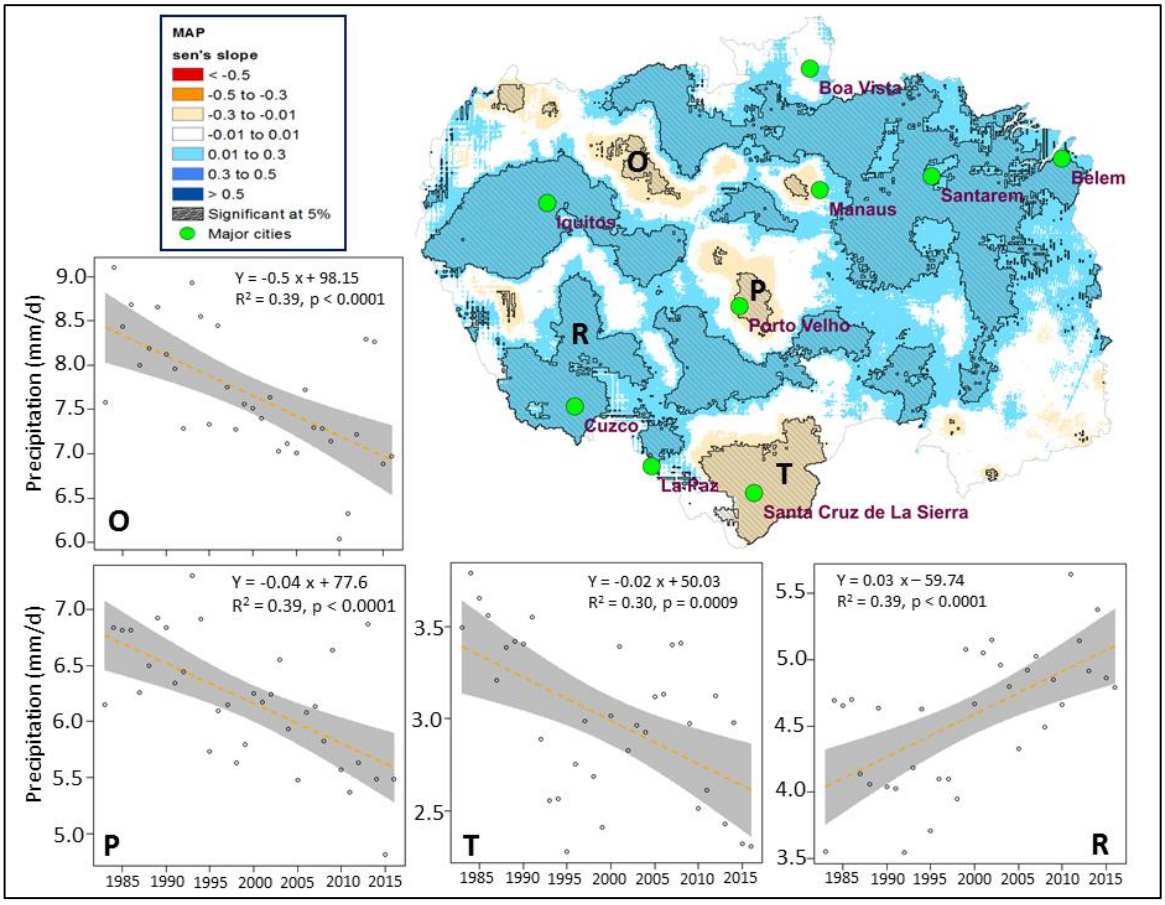

Figure 6. Magnitude of changes in mean annual precipitation (MAP)*. Hatches on the map show the significant changes at 5%. Graphs show the trend line and associated equation for the significant changes with 5% confidence intervals around the trend*

NDD trend magnitude

Sen's slope analysis for NDD shows similar areas of significant change as the Tau method; however, magnitudes of change differ. Figure 7 shows changes of NDD across the basin assessed using Sen's slope, which for region S indicates that the NDD during May-Nov increased by about 0.3 days per year, or 11 days total over the last 37 years. Extreme values in the dataset affect the slope significantly for region S. The lowest NDD was 1984 with 176 dry days during

May-Nov, and 1988 and 2011 had the driest May-Nov with 193 and 197 dry days per season accordingly.

Across region U, NDD increased by 0.5 days per May-Nov time span or 18 days over the entire period. 1989 and 2009 had the wettest May-Nov with 156 dry days, and 2007 and 2017 had the longest May-Nov seasons with ~ 183 dry days. NDD fluctuations in this region occur in 10-year cycles, indicating a strong influence by the Pacific Decadal Oscillation.

Region V is the only area that showed a significant increasing trend in NDD for the Dec-Apr at the 0.05 level. NDD increased by more than 18 days over 37 years shifting from 54 days in 1989 to 89 days in 2016. This region is on the wet western edge of the basin, but the drying trend is spatially consistent with extreme increases in oil palm cultivation and fire expansion (Gutiérrez- Vélez et al. 2011).

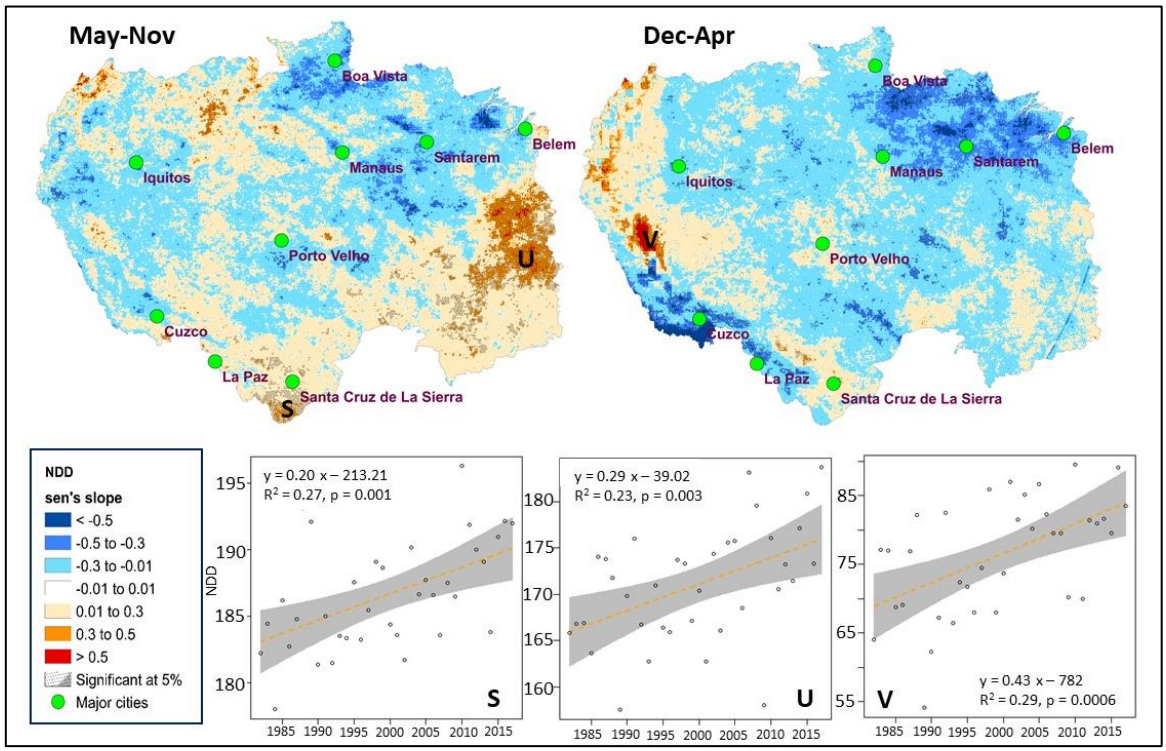

Figure 7. Magnitude of changes in the number of dry days (NDD) *during May-Nov and Dec-Apr. Hatches on the map show areas with significant changes at 5%. Graphs show trend lines*

for significant changes with 5% confidence intervals around the trend. Note that vertical axis scales are different.

NXE trend magnitude

The Sen's slope estimators are shown spatially in Figure 8, with selected time series in the inset boxes. Changes in NXE during May-Nov show a similar pattern with those of MAP, which indicates the intensification of the hydrologic cycle. NXE during May-Nov showed a large increase over most of the western region. We will use the term "events" for days that had an extreme event.

For region W during May-Nov, the magnitude of changes for much of the area was + 0.5 events/year, which amounts to an additional 18 extreme events on average over 37 years during May-Nov. These significant changes that are tightly clustered in the last 7 years show a strong and significant increasing trend with a maximum of 26 days during May-Nov of 2013.

Regions X and Y show a significant decreasing trend with 10.8 days on average over the study period, but the distribution of extreme events over time is very different. For region X, the range of NXE spans from 1989 with 13 extreme days to 2011 with 5 days—is the lowest over the 37 years. But, in region Y, NXE shows a prominent decline after 1990. The maximum NXE occurred in 1982 with 13 events, while after 2010, there were consistently less than four extreme days except for a jump in 2012 to 8 days. The minimum NXE was in 2010 at 2 extreme events.

During Dec-Apr, region Z (Figure. 8, inset) shows an increasing trend, echoing the May-Nov timeline in trend and location near Iquitos. The largest number of extreme rainfall events was in 2012, at 29 events; the following years were all well above normal and influenced the entire time series, which increased the slope of the trend line dramatically. The NXE change amount added 18 event days on average for the study period. 1985 had the fewest NXE at about

7 days, while 2012 had 29 for Dec-Apr. The data show a strong discontinuity starting around 2012, before which no year had more than 20 events during Dec-Apr.

Zones AZ and BZ both have a nonlinear interannual pattern with a local minimum in the late 1990s. NXE decreased by more than 18 events in AZ and 11 events in BZ overall 37 years during Dec-Apr. NXE across AZ changed from a maximum of 30 events in 1983 and 1993 to a minimum of 11 events in 2015. While in BZ the maximum NXE was 20 in 1988, and the minimum NXE within Dec-Apr was 5 events/year in 2015 (Figure 8).

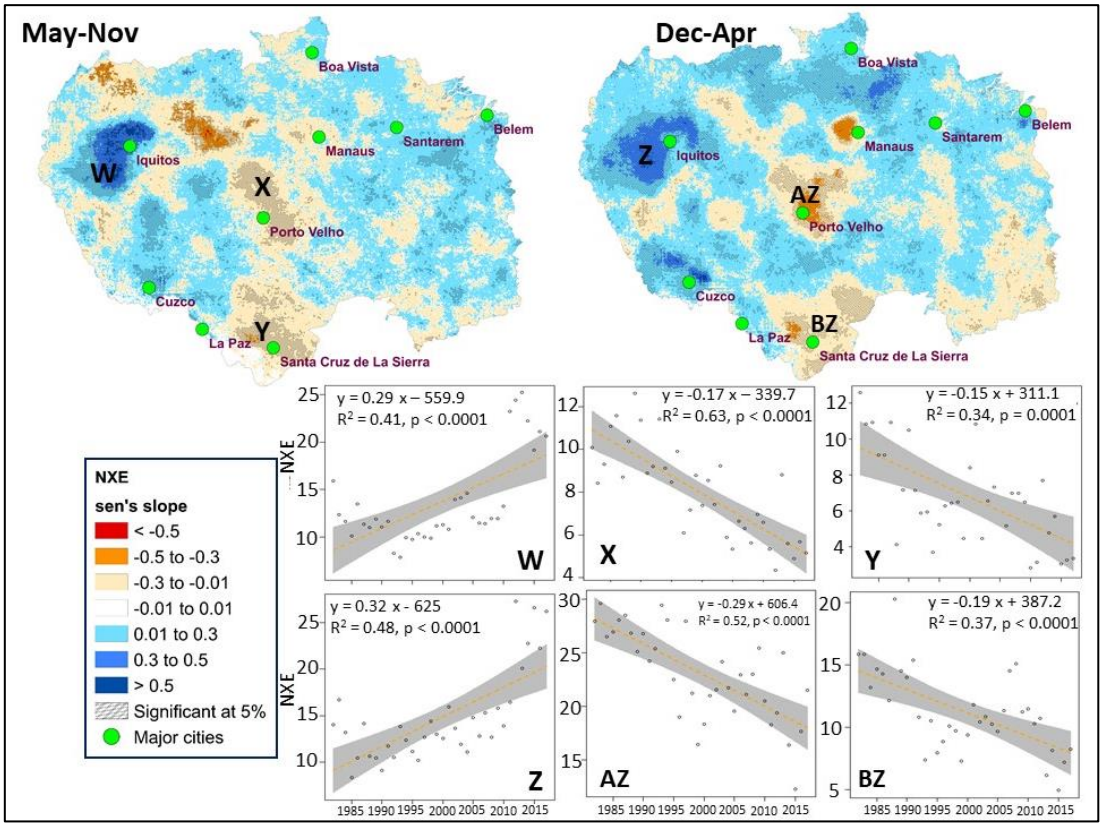

Figure 8. Magnitude of changes in NXE during May-Nov and Dec-Apr*. Hatches on the map show areas with significant changes at 5%. Graphs show the trend line and associated equation for the significant changes with 5% confidence intervals around the trend. Note that vertical axis scales are different*

Aggregated change analysis

Figure 9 shows deforested areas in yellow from 1992 to 2015, overlain with areas of significant change in all indices to illustrate the extent to which deforested regions are aligned with the areas of significant precipitation changes. Areas around Porto Velho and Santa Cruz show the highest amount of deforestation and the largest extent and greatest magnitude of dryness. All indices show less precipitation for these regions. Loss of tropical rain forests is expected to have the largest landscape conversion-related effect on precipitation. The yellow shaded areas on the map represent the loss of forest land, but do not capture the conversion of the native Cerrado in the far eastern side of the basin. The most significant deforestation occurred there from 1994 to 2005. These heavily deforested areas (Figure. 9) are spatially aligned with the regions with the highest precipitation variability, according to Figure. 4.

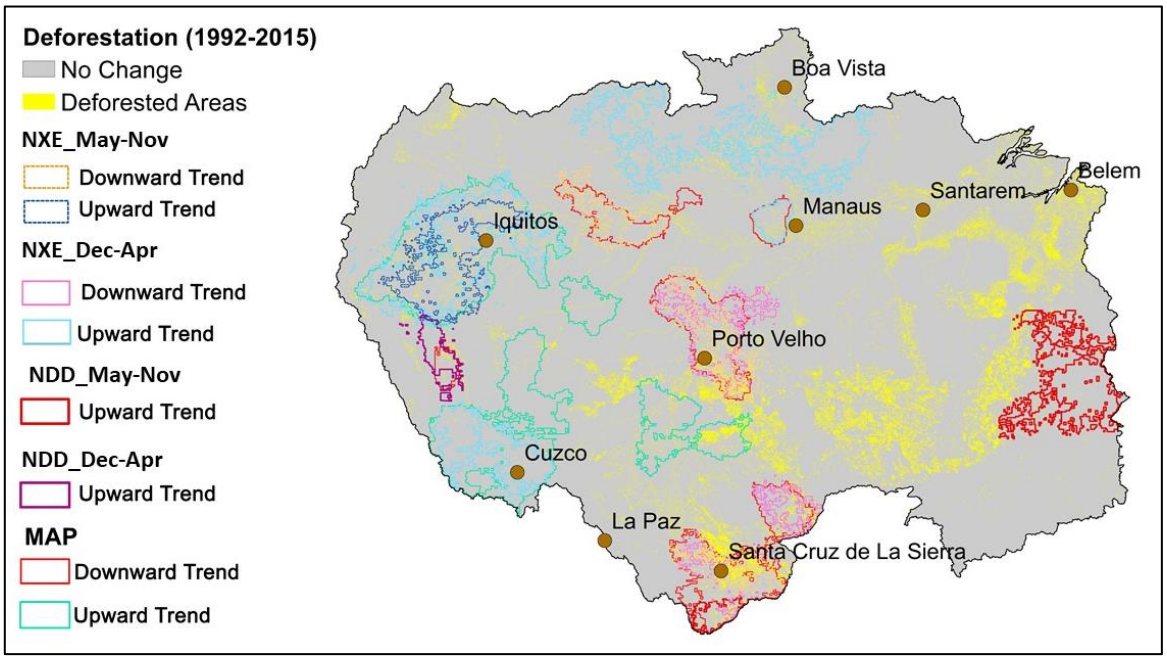

Figure 9. Aggregated significant changes in all indices*; Deforested areas from 1992 to 2015 are shown in yellow. Significant changes in all indices are plotted on top to show the spatial agreement between deforestation and precipitation changes. The warmer colors in the legend indicate regions with drying trends and cool (blue) colors show regions with increasing*

precipitation (NXE: number of extreme events; NDD: number of dry days; MAP: mean annual precipitation by day)

Discussion

The Amazon basin continues to have a rainy northwestern region, a wet/dry cyclical climate in the center of the domain, and a long dry season in the south and east (Davidson et al. 2012). Due to the Andes Mountains on the western edge of the basin, moisture cannot easily escape; our analysis finds no change in the precipitation behavior of this portion of the domain. Moisture flux from the Atlantic continues to drive the overall seasonality and transport of rainfall. However, these results show that the spatiotemporal variability of rainfall from 1982 to 2018 across the Amazon basin is locally more complex than the common refrain "wet gets wetter and dry gets drier" (Donat et al. 2016). This is especially true in the extreme western and southeastern parts of the domain. We find two broad patterns of change: a synoptic-scale shift of more dry days to the south and east and spatially cohesive regions with drying and wetting trends over hundreds of km^2. This study does not investigate causality; determining drivers of rainfall change would require process-based regional climate models. Instead, we refer to patterns found from this work that have been causally linked by other literature. We then consider possible drivers of precipitation change to motivate further investigation of causal mechanisms.

In our analysis, we found five important characteristics of changing rainfall patterns. First, estimates of spatial changes in MAP align with those in NXE based on both the Tau statistic and Sen's slope. This indicates that increasing frequencies of heavy rainfall days are strongly related to increases in total annual rainfall while decreasing heavy rainfall days decreases total annual rainfall. This change shows that the distribution of rainfall has changed to more intense rainfall in some areas and reduced intensity in others. Haylock et al. (2006) reported similar results for extreme events across South America, noting that "the pattern of extreme events was generally

the same as that for total annual rainfall." NDD is notably different than NXE and MAP, indicating broadly a different set of climatic processes driving these changes. For eastern Brazil, the "wet gets wetter, dry gets drier" mnemonic holds for NDD. The change point analysis showed that mean MAP changed abruptly in the 1990s for all regions, NDD trend changed in 2000s, and NXE of western wet of the basin changed in 2010s (regions H and L, Figure. 5). NXE of regions around Porto Velho (regions J and M, Figure. 5) changed abruptly nearly at the same time in both May-Nov and Dec-Apr seasons in the 1990s, while it is not the case for the south of the basin.

Second, changes in land use—particularly shifts in deforested areas—are spatially associated with regions of modified rainfall. Figure 9 illustrates this similarity, with deforested areas near many of the regions of changed precipitation analyzed here. Higher precipitation events have been connected to the "vegetation breeze" in the Amazon (Laurance et al. 2018; Nobre et al. 2016; Sheil and Murdiyarso 2009). In such cases, large convective circulations can develop from differential heating, and be advected downwind such that the landscape change generating the convection does not receive the rainfall. This essentially rearranges rainfall into a wet/dry "dipole" associated with forest removal and road development (Moore et al. 2007; Saad et al. 2010). Thus, the extreme events may still be generated by landscape heterogeneities, but those extreme events are often advected elsewhere; for example, extreme events have declined in both the Porto Velho and Santa Cruz regions throughout a year with MAP increases nearby. However, the main deforestation wave occurred primarily from 1992 to 2015. Since our study looked at trends during 1982–2018, this indicates other factors are likely at play, including effects associated with elevated greenhouse gases.

Third, these basin-wide results are consistent with previous rainfall studies that identified similar spatial anomalies (e.g., Ronchail et al. 2002; Silva et al. 2018) and declines in the number of extreme events in the south of the basin (e.g., Santos et al. 2015). General circulation model (GCM) outputs show highly varied historical changes over the Amazon but are not entirely consistent. IPCC AR5 results do not have sufficient resolution to characterize such changes in precipitation. Several regional climate projections at finer resolutions match some of the features found here, such as Fig. 4.4 in (Marengo and Espinoza 2016) for the 2011–2040 period. However, five of the 11 models in Ronchail et al. (2002) and Li et al. (2006) predicted an increase in annual rainfall, while three others showed a decrease, and the remainder produced no significant changes in the rainfall amount for the entire basin. NXE during Dec-Apr (Figure 5) somewhat matches maps showing fire risk by 2050 (Figure. 4 in Davidson et al. 2012), but projections are equivocal at best in matching overall historical patterns. Attribution to these changes is often difficult and requires finer-scale simulations forced with historical boundary conditions to assess causality.

Fourth, a “diagonal pattern” of decreased rainfall from the Porto Velho region to the northwestern edge of the domain appears in both NXE and MAP but is not associated with deforested regions or other major surface cover changes. A similar diagonal structure is evident in Silva et al. (2018) albeit with lower statistical significance using TRMM through 2015. The wet/dry “dipole” pattern noted above may amplify this pattern. The reduction is stronger in May-Nov when prevailing winds are from the south. This bimodal pattern is not produced in studies exploring land cover change alone (Bagley et al. 2014; Wu et al. 2017). However, the drying diagonal pattern shows spatial similarity with rainfall correlations to South Atlantic SST (Yoon and Zeng 2010). The South American low-level jet and the South American Convergence Zone

that affects rainfall in the western part of the basin are currently exhibiting higher variability (Liebmann et al. 2004). Grimm and Zilli (2009) showed that changes in precipitation variability are likely connected to ENSO and other global phenomena such as SST anomalies in the southern tropical Atlantic. Across the equatorial Amazon, Atlantic SST is strongly correlated with the timing of rainy season onset and end, especially during the transition between wet and dry regimes (Liebmann and Marengo 2001).

Fifth, a pattern of less precipitation in the south, consistent with reduced rainfall recycling (Eltahir and Bras 1994), makes seasonal changes more broadly consistent with an intensifying Hadley circulation. The weakening of poleward expansion of Hadley cells over South America has significant effects on precipitation anomalies (Freitas and Ambrizzi 2015) and has thus increased the dryness over the region, especially in north-eastern Brazil (Lau and Kim 2015). Stronger Hadley and Walker circulations are associated with a lengthening dry season in South America (Agudelo et al. 2018). That moisture is moved to the interior; wetting trends in much of the Amazon basin are influenced by a strengthening Walker circulation (Barichivich et al. 2018), which we identified in the northern and western parts of the basin (Figure 3). Yin et al. (2014) reported competing causes of variability in wet season onset that include SSTs and more local factors. The patterns we find for both NDD and NXE affirm this picture of multiple competing drivers.

Some significant changes in specific locations are worth noting. In the western basin, around Iquitos, MAP has increased by 10.8 mm/day over the 37 years with a clear trend, with erratic behavior in May-Nov extreme events. Most of the increase occurred due to Dec-Apr extreme events (18 additional events over 37 years). There is significant deforestation in this region due to increased economic activity, including palm oil cultivation. The region around Porto Velho

has declined in both MAP and NXE, and a smaller decline in NDD is evident. This is similar to the pattern identified in Silva et al. (2018) using TRMM data, and the wet/dry pattern matches the significant agricultural expansion in Rondonia along highway BR-364. The region around Santa Cruz has seen both significant deforestations similar to Porto Velho but also experiences the broader southern drying trend connected to global circulations. The Eastern Basin has witnessed the most dramatic shrinking of rainy days, with NDD during May-Nov increasing by more than 18 days over the study period. This drying pattern in the east, spanning the cerrado-moist forest ecotone, is likely related to agricultural expansion. Spera et al. (2016)) showed that when cerrado vegetation is replaced by agriculture, rainfall declines of up to 3% are possible.

The wet get wetter, dry gets drier narrative is only true for some regions. The dry season has lengthened in most of the eastern and northern regions of the basin to 9 months (Li et al. 2006). And, in the Iquitos region, topographic moisture convergence forced against the eastern slope of the Andes by easterly trade winds from the Atlantic causes a shorter dry season and wetter wet season (Kleeman 1989). However, correlations to other drivers make the results complex. For example, the eastern region is highly influenced by ENSO (Coe et al. 2009; Marengo 2004). The long dry season here is also driven by subsidence connected to both ITCZ (Fu et al. 2001) and SSTs (Yoon and Zeng 2010). Looking broadly at specific variables, dry season length is highly influenced by both the SST of tropical oceans (Liebmann and Marengo 2001) and local soil moisture and vegetation cover (Nepstad et al. 2008; Li and Fu 2004). Ronchail et al. (2002) found that the colder northern tropical Atlantic and equatorial Pacific make the northern part of the basin wetter, as Tropical SST significantly influences this region. The shorter and drier rainy season is associated with El Niño events.

Conclusion

Precipitation is changing in multiple ways across the Amazon basin. Here, we show that most of the Amazon basin has experienced climatic changes, many of which are significant. Generally, while the western regions have trended wetter, the eastern and southern regions trended dryer. Wetting trends occur following the spatial pattern of extreme rainfall events, with very little similarity to changes in the number of dry days. We found statistically significant changes of precipitation from 1982 to 2018 at the 0.05 level for MAP across much of the domain. Our results broadly echo those of Silva et al. (2018) but over a longer time period and with additional variables. Their constraint of a 0.05 significance level was more rigorous but may have excluded noisier but important trends.

To the best of our knowledge, this is the first study to consider the analysis of dry day occurrence and extreme rainfall event frequency during the May-Nov and Dec-Apr seasons for the entire Amazon basin using high temporal and spatial resolution data. The spatial pattern drivers of climate and its variability are complicated over the basin. The patterns we identified are likely a combination of factors including ENSO, SSTs, the ITCZ/SACZ transition, strengthening Hadley and Walker circulations, and deforestation. Future research should be directed towards identifying causality for these processes using high-resolution regional models. Our next steps are to simulate the effects of deforestation with and without elevated greenhouse gases to map where each process dominates and to quantify the magnitude of each perturbation. Ultimately, these simulations along with the analysis presented above will be crucial to understand changes in streamflow and hydrology, including those in flood and drought frequency across the basin.

APPENDIX

Table 2. Correlation between CHIRPS and ANA gauges as well as PERSIANN and ANA gauges for each location.

Station Code	Long	Lat	Correlation CHIRPS_ANA	P	Correlation PERSIANN_ANA	p
49009	-49.93940	-0.98530	0.28	0.40	0.15	0.67
49010	-49.97860	-0.16560	0.64	0.05	0.15	0.68
49011	-48.95970	-1.01580	0.08	0.81	-0.32	0.34
51005	-51.62390	-0.79470	0.37	0.10	0.00	1.00
52003	-52.07750	-0.45667	0.85	0.00	-0.31	0.30
60001	-60.69080	-0.22750	0.07	0.77	0.15	0.49
61001	-61.93170	-0.87310	0.37	0.21	0.11	0.71
63001	-62.77530	-0.36720	0.68	0.02	-0.41	0.21
65001	-65.01530	-0.42030	0.34	0.23	0.31	0.28
67002	-67.53580	-0.34440	0.55	0.01	-0.05	0.83
149003	-49.86360	-2.00190	0.38	0.12	-0.12	0.62
149004	-49.38170	-1.89750	0.54	0.01	0.15	0.49
150003	-50.43470	-1.79170	0.71	0.01	-0.04	0.89
151002	-51.26220	-1.21310	0.65	0.00	-0.24	0.32
151003	-51.91780	-1.58250	0.17	0.43	-0.22	0.29
152005	-52.57830	-1.52640	0.33	0.32	-0.37	0.27
152006	-53.15750	-1.08190	0.67	0.00	-0.04	0.85
154003	-54.73920	-1.94280	0.43	0.08	-0.09	0.71
155002	-55.11556	-1.88806	0.26	0.27	0.07	0.78
157001	-57.82750	-1.43780	0.60	0.00	-0.16	0.45
157002	-57.05060	-1.86830	0.67	0.00	-0.17	0.45
162002	-62.43670	-1.88720	-0.03	0.91	-0.11	0.63
169002	-69.11670	-1.73330	-0.05	0.85	-0.22	0.41
250001	-50.36860	-1.99170	0.64	0.00	-0.13	0.56
250002	-50.92280	-2.45330	0.59	0.01	0.00	0.99
250003	-50.62972	-2.24500	0.71	0.00	-0.08	0.70
252001	-52.91860	-2.33640	0.78	0.00	-0.14	0.49
253000	-53.59944	-1.17889	0.64	0.00	-0.35	0.10
255000	-55.48060	-2.26830	0.45	0.08	-0.39	0.14
255001	-55.72060	-2.65080	0.88	0.00	-0.49	0.03
256001	-56.08750	-2.15220	0.44	0.10	-0.18	0.52
256002	-56.71060	-2.18970	0.72	0.00	-0.20	0.47
257001	-57.06440	-2.79220	0.61	0.01	-0.09	0.70
257002	-57.59000	-2.97030	0.51	0.11	-0.23	0.50
257003	-57.28250	-2.45560	0.21	0.45	0.06	0.83
258001	-58.50580	-2.29110	0.43	0.25	0.37	0.33
259004	-59.69970	-2.70030	0.32	0.23	0.15	0.59
260006	-60.94780	-2.62000	-0.13	0.57	-0.36	0.10
260007	-60.02580	-2.04170	0.51	0.02	-0.02	0.94

Table 2 (cont'd)

261000	-61.54140	-2.02470	0.45	0.04	-0.23	0.32
265000	-65.11670	-2.35000	0.54	0.01	-0.01	0.98
267001	-67.56670	-2.75000	-0.05	0.80	-0.15	0.48
268000	-68.79860	-2.88060	-0.11	0.62	-0.36	0.11
269001	-69.69310	-2.92970	0.34	0.34	0.10	0.77
351002	-51.56810	-3.72310	0.60	0.00	-0.09	0.68
352005	-52.54190	-3.30780	0.44	0.03	-0.13	0.55
355001	-54.88690	-3.49360	0.52	0.02	-0.25	0.28
356002	-56.58610	-3.22810	-0.11	0.68	0.04	0.90
357003	-57.50420	-3.89670	0.49	0.01	-0.17	0.42
357004	-57.30310	-3.77280	0.60	0.01	-0.20	0.42
358003	-58.28610	-3.81670	0.31	0.20	-0.34	0.16
359004	-59.13390	-3.57640	0.61	0.00	-0.15	0.52
359005	-59.99440	-3.10000	0.14	0.67	-0.19	0.56
361001	-61.21330	-3.32970	0.20	0.55	0.23	0.50
361002	-61.37830	-3.58110	-0.15	0.52	0.03	0.91
362002	-62.67860	-3.41830	0.47	0.03	-0.19	0.42
363002	-63.39220	-3.45640	0.32	0.17	-0.10	0.67
364001	-64.30690	-3.59030	0.22	0.36	-0.35	0.14
366001	-65.94190	-2.98110	0.30	0.23	-0.42	0.08
367001	-67.48890	-3.33720	0.33	0.18	-0.08	0.76
369000	-69.37080	-3.57310	0.19	0.57	-0.50	0.12
454001	-54.64190	-3.96640	0.40	0.18	-0.20	0.51
455004	-54.90280	-4.08940	0.61	0.02	0.16	0.56
456001	-56.88220	-4.94690	0.03	0.90	-0.07	0.75
456002	-56.30000	-4.55000	0.58	0.01	0.16	0.52
458001	-58.67140	-4.23080	0.43	0.19	-0.06	0.87
459000	-59.59830	-4.39140	-0.22	0.30	-0.33	0.12
459001	-59.24940	-4.74970	-0.24	0.37	0.00	0.99
462001	-62.15190	-4.74080	0.38	0.13	0.51	0.04
462002	-62.86830	-4.85860	0.11	0.63	0.01	0.98
465000	-65.20170	-4.29220	0.63	0.02	0.06	0.84
468003	-68.66330	-4.89670	0.43	0.04	-0.07	0.77
470005	-70.54890	-4.13440	0.29	0.18	-0.08	0.72
555002	-55.49580	-6.67140	0.42	0.13	-0.06	0.83
560001	-60.70060	-5.29640	0.32	0.23	-0.04	0.87
560002	-60.37360	-5.58920	-0.07	0.78	0.34	0.18
563002	-63.51080	-5.72190	0.33	0.19	0.12	0.64
564001	-64.33530	-5.58310	-0.14	0.71	-0.28	0.43
564002	-64.31640	-5.95330	0.20	0.43	-0.22	0.38
567002	-67.40580	-5.46080	0.38	0.09	0.24	0.29

Table 2 (cont'd)

568001	-68.99830	-5.38080	0.53	0.02	-0.05	0.85
572000	-72.81360	-5.13750	0.10	0.77	0.15	0.68
655001	-55.26360	-7.51080	0.27	0.21	0.12	0.60
655003	-55.83330	-5.50000	0.22	0.34	0.03	0.90
655004	-55.77330	-6.25750	0.34	0.14	0.04	0.85
657000	-57.77560	-6.23580	-0.06	0.85	-0.08	0.81
661001	-61.76670	-6.36060	-0.06	0.87	0.04	0.90
662001	-62.78720	-7.00830	0.38	0.13	-0.15	0.56
664000	-64.88610	-6.31920	0.07	0.77	-0.08	0.70
669001	-69.13330	-6.61670	-0.18	0.44	-0.51	0.02
670000	-70.65000	-6.80000	0.30	0.40	-0.32	0.37
750000	-50.82890	-7.82830	0.15	0.53	0.20	0.41
759000	-59.89220	-7.20080	0.51	0.02	0.05	0.83
762003	-62.34780	-7.80280	-0.12	0.73	-0.30	0.37
763001	-63.02860	-7.51530	-0.17	0.54	0.11	0.69
765001	-65.35000	-7.51890	0.00	1.00	0.32	0.16
767002	-67.55920	-7.55000	0.21	0.53	0.36	0.27
770001	-70.98330	-7.26670	0.14	0.53	-0.04	0.86
771000	-71.68420	-7.05080	-0.45	0.09	-0.57	0.03
771001	-71.48220	-7.95110	0.25	0.25	-0.04	0.85
772002	-72.33360	-7.23580	-0.06	0.81	-0.45	0.04
772003	-72.01920	-7.85030	0.15	0.55	0.02	0.93
867002	-67.36670	-8.25000	0.42	0.09	0.31	0.23
869000	-69.26810	-8.88420	0.07	0.79	0.55	0.02
870002	-70.35640	-8.16360	0.15	0.54	-0.15	0.54
872001	-72.73440	-8.26750	0.43	0.03	0.05	0.82
954001	-54.88640	-9.81860	0.03	0.92	0.12	0.68
956001	-56.01860	-9.64330	0.25	0.47	-0.44	0.18
957001	-57.39470	-9.56640	0.59	0.05	-0.71	0.01
961003	-61.97890	-9.68140	-0.20	0.38	0.01	0.98
962001	-62.95310	-9.17920	0.05	0.87	-0.17	0.61
963009	-63.25000	-9.46670	-0.51	0.05	-0.10	0.73
966001	-65.99310	-9.69030	0.30	0.19	0.34	0.15
967005	-67.13920	-9.88810	0.01	0.97	0.17	0.57
968004	-68.28330	-9.56670	-0.43	0.22	-0.27	0.46
969001	-68.99330	-9.11030	0.27	0.34	0.13	0.66
972000	-72.70250	-9.40170	0.17	0.52	0.05	0.86
1052001	-52.18060	-10.55330	0.07	0.83	-0.41	0.17
1055002	-55.44860	-10.79860	0.39	0.13	-0.23	0.39
1055003	-55.54860	-10.95420	0.60	0.00	-0.06	0.80
1057001	-57.13310	-9.94170	0.50	0.05	0.31	0.24

Table 2 (cont'd)

1058003	-58.50170	-10.31250	0.41	0.15	0.13	0.66
1058004	-58.80330	-10.83420	0.19	0.48	0.15	0.59
1058005	-58.86780	-10.58860	-0.23	0.39	0.12	0.65
1061002	-61.04530	-10.39690	-0.52	0.05	-0.04	0.89
1061003	-62.00140	-10.51690	-0.05	0.84	-0.47	0.05
1062003	-62.65610	-11.00360	0.12	0.70	0.02	0.94
1062004	-62.34580	-10.23640	-0.36	0.12	-0.24	0.31
1067003	-67.67670	-10.57580	0.55	0.07	0.12	0.70
1154001	-54.99810	-11.92920	-0.09	0.77	0.11	0.72
1156000	-56.43330	-11.47140	0.60	0.02	-0.28	0.32
1156001	-55.44860	-11.69140	-0.02	0.95	0.06	0.83
1157001	-57.50670	-11.25310	0.19	0.45	-0.58	0.01
1158002	-58.71860	-11.40810	0.63	0.05	0.33	0.35
1158003	-58.04720	-11.71780	0.03	0.93	-0.33	0.35
1160002	-60.86780	-11.74890	0.42	0.05	0.25	0.25
1161002	-61.77640	-11.74970	0.44	0.08	0.07	0.80
1168001	-68.73500	-11.02330	0.38	0.10	0.24	0.30
1251000	-51.69690	-12.16420	-0.16	0.48	0.15	0.50
1251001	-51.82640	-12.93970	0.58	0.03	0.30	0.30
1254001	-54.75170	-12.81310	0.35	0.23	0.13	0.65
1256002	-56.31560	-12.98060	0.28	0.19	0.06	0.78
1257000	-58.00030	-12.11640	0.42	0.07	-0.15	0.53
1264000	-64.42250	-12.42690	0.62	0.02	-0.54	0.06
1352000	-52.41280	-13.88360	-0.23	0.38	-0.11	0.66
1352001	-52.45440	-13.49560	0.18	0.58	-0.51	0.09
1352002	-52.02670	-13.70530	0.21	0.42	0.16	0.55
1353001	-53.24170	-13.84190	-0.25	0.28	-0.07	0.77
1353002	-53.07440	-13.57000	0.77	0.00	-0.04	0.91
1355001	-55.33170	-13.55640	0.22	0.38	-0.46	0.05
1356002	-56.12220	-13.81560	-0.32	0.31	0.23	0.48
1357000	-57.11330	-13.06610	0.05	0.85	0.42	0.08
1358001	-58.28920	-13.64140	-0.02	0.94	-0.02	0.94
1358002	-58.97500	-13.46670	0.20	0.36	-0.38	0.08
1358005	-58.89810	-13.91000	0.38	0.08	-0.43	0.04
1359000	-59.87690	-13.18310	0.02	0.95	0.17	0.48
1359001	-59.76750	-13.77810	0.26	0.35	0.08	0.77
1360000	-60.54830	-13.11420	0.15	0.57	-0.43	0.09
1360001	-60.82330	-13.19670	-0.57	0.03	0.05	0.87
1360002	-61.04640	-13.47970	0.00	1.00	0.12	0.61
1360003	-60.58830	-13.73060	0.35	0.18	0.22	0.41
1452004	-52.15030	-14.07640	-0.48	0.03	0.23	0.33

Table 2 (cont'd)

1454002	-54.97280	-14.92610	0.06	0.83	#DIV/0!	#DIV/0!
1457003	-57.50690	-14.18330	0.34	0.14	0.37	0.11
1458002	-58.23440	-14.38420	-0.39	0.09	-0.31	0.18
1459003	-59.59390	-14.46940	-0.20	0.47	-0.38	0.16
1560000	-60.03170	-15.40030	0.32	0.18	0.24	#NUM!
8050000	-50.74830	0.50810	-0.49	0.04	-0.27	0.29
8051010	-51.12667	0.30333	0.07	0.82	0.38	0.23
8059001	-59.42830	0.80690	-0.10	0.72	-0.42	0.10
8059002	-59.91390	0.95780	0.08	0.72	-0.03	0.91
8059003	-59.31670	0.93330	0.09	0.72	-0.22	0.39
8060000	-60.46610	0.51780	-0.01	0.97	-0.12	0.67
8062000	-62.62220	0.88420	0.33	0.23	-0.53	0.04
8066002	-66.64920	0.38750	-0.18	0.48	-0.17	0.51
8067002	-67.94580	0.17580	-0.40	0.14	-0.17	0.53
8067003	-67.80640	0.58780	0.02	0.95	0.01	0.98
8068001	-68.83280	0.43250	-0.07	0.84	-0.37	0.24
8069004	-69.21330	0.14280	-0.05	0.87	-0.71	0.01
8160003	-60.76750	1.46080	-0.05	0.84	-0.05	0.85
8162000	-62.28330	1.75000	-0.51	0.03	-0.57	0.01
8260002	-60.67280	2.41330	-0.31	0.17	-0.55	0.01
8260003	-60.32500	2.76060	-0.55	0.10	-0.29	0.42
8260004	-60.91780	2.47140	0.13	0.58	0.02	0.92
8261001	-60.97280	2.26280	0.28	0.24	-0.10	0.69
8263000	-63.64170	2.83580	-0.28	0.33	-0.33	0.26
8359000	-59.81560	3.37830	-0.37	0.19	0.01	0.97
8361001	-61.28810	3.29060	-0.07	0.80	-0.09	0.73
8361004	-61.08830	3.28720	0.01	0.97	-0.28	0.43
8361005	-61.71810	3.75920	0.22	0.35	0.23	0.33
8362000	-62.39890	3.63190	0.05	0.86	-0.12	0.70
8363000	-63.16920	3.54970	0.14	0.63	-0.23	0.43
8459000	-59.85890	4.45170	-0.15	0.57	0.16	0.54
8460001	-60.79390	4.19610	-0.22	0.37	-0.46	0.05
8460003	-60.49640	4.64280	0.07	0.82	-0.01	0.97
8460004	-60.16640	4.59860	-0.51	0.05	-0.54	0.04
8461000	-61.15170	4.48030	-0.44	0.13	-0.67	0.01
8464001	-64.32470	4.00310	0.63	0.01	0.00	1.00

REFERENCES

REFERENCES

Agudelo, J., Arias, P. A., Vieira, S. C., & Martínez, J. A. (2018). Influence of longer dry seasons in the Southern Amazon on patterns of water vapor transport over northern South America and the Caribbean. Climate Dynamics, 52(5), 1–19. http://doi.org/10.1007/s00382-018-4285-1

Almeida, T. D. C., Oliveira-Júnior, J. F., & Cubo, P. (2016). Spatiotemporal rainfall and temperature trends throughout the Brazilian Legal Amazon, 1973-2013: Rainfall and temperature trends throughout the brazilian legal amazon. Article in International Journal of Climatology. http://doi.org/10.1002/joc.4831

Arvor, D., Funatsu, B. M., Michot, V., & Dubreui, V. (2017). Monitoring rainfall patterns in the southern amazon with PERSIANN-CDR data: Long-term characteristics and trends. Remote Sensing, 9(9). http://doi.org/10.3390/rs9090889

Ashouri, H., Hsu, K.-L., Sorooshian, S., Braithwaite, D. K., Knapp, K. R., Cecil, L. D., … Prat, O. P. (2015). PERSIANN-CDR: Daily Precipitation Climate Data Record from Multisatellite Observations for Hydrological and Climate Studies. Bulletin of the American Meteorological Society, 96(1), 69–83. http://doi.org/10.1175/BAMS-D-13-00068.1

Bagley, J. E., Desai, A. R., Harding, K. J., Snyder, P. K., & Foley, J. A. (2014). Drought and deforestation: Has land cover change influenced recent precipitation extremes in the Amazon? Journal of Climate, 27(1), 345–361. http://doi.org/10.1175/JCLI-D-12-00369.1

Barichivich, J., Gloor, E., Peylin, P., Brienen, R. J. W., Schöngart, J., Espinoza, J. C., & Pattnayak, K. C. (2018). Recent intensification of Amazon flooding extremes driven by strengthened Walker circulation. Science Advances, 4(9), eaat8785. http://doi.org/10.1126/sciadv.aat8785

Carvalho, L. M. V., Jones, C., Liebmann, B., Carvalho, L. M. V., Jones, C., & Liebmann, B. (2004). The South Atlantic Convergence Zone: Intensity, Form, Persistence, and Relationships with Intraseasonal to Interannual Activity and Extreme Rainfall. Journal of Climate, 17(1), 88–108. http://doi.org/10.1175/1520-0442(2004)017<0088:TSACZI>2.0.CO;2

Coe, M. T., Costa, M. H., Botta, A., & Birkett, C. (2002). Long-term simulations of discharge and floods in the Amazon Basin. Journal of Geophysical Research, 107(D20), 8044. http://doi.org/10.1029/2001JD000740

Coe, M. T., Costa, M. H., & Soares Filho, B. S. (2009). The influence of historical and potential future deforestation on the stream flow of the Amazon River - land surface processes and atmospheric feedbacks. Journal of Hydrology (Amsterdam), 369(1/2), 165–174. http://doi.org/10.1016/j.jhydrol.2009.02.043

Costa, M. H., & Pires, G. F. (2010). Effects of Amazon and Central Brazil deforestation

scenarios on the duration of the dry season in the arc of deforestation. International Journal of Climatology, 30(13), 1970–1979. http://doi.org/10.1002/joc.2048

Da Silva, P. E., Santos e Silva, C. M., Spyrides, M. H. C., & Andrade, L. de M. B. (2019). Precipitation and air temperature extremes in the Amazon and northeast Brazil. International Journal of Climatology, 39(2), 579–595. http://doi.org/10.1002/joc.5829

Davidson, E. A., De Araüjo, A. C., Artaxo, P., Balch, J. K., Brown, I. F., Mercedes, M. M., … Wofsy, S. C. (2012). The Amazon basin in transition. Nature, 481(7381), 321–328. http://doi.org/10.1038/nature10717

Donat, M. G., Lowry, A. L., Alexander, L. V., O'Gorman, P. A., & Maher, N. (2016). More extreme precipitation in the world's dry and wet regions. Nature Climate Change, 6(5), 508–513. http://doi.org/10.1038/nclimate2941

ElNesr, M. N., Abu-Zreig, M. M., Alazba, A. A., ElNesr, M. N., Abu-Zreig, M. M., & Alazba, A. A. (2010). Temperature trends and distribution in the Arabian Peninsula. American Journal of Environmental Sciences, 6(2), 191–203. http://doi.org/10.3844/ajessp.2010.191.203

Eltahir, E. A. B., & Bras, R. L. (1994). Precipitation recycling in the Amazon basin. Quarterly Journal of the Royal Meteorological Society, 120(518), 861–880. http://doi.org/10.1002/qj.49712051806

Espinoza, J. C., Chavez, S., Ronchail, J., Junquas, C., Takahashi, K., & Lavado, W. (2015). Rainfall hotspots over the southern tropical Andes: Spatial distribution, rainfall intensity, and relations with large-scale atmospheric circulation. Water Resources Research, 51(5), 3459–3475. http://doi.org/10.1002/2014WR016273

Espinoza, J. C., Ronchail, J., Marengo, J. A., & Segura, H. (2019). Contrasting North–South changes in Amazon wet-day and dry-day frequency and related atmospheric features (1981–2017). Climate Dynamics, 52(9–10), 5413–5430. http://doi.org/10.1007/s00382-018-4462-2

Fearnside, P. M. (2000). Global warming and tropical land-use change: greenhouse gas emissions from biomass burning, decomposition and soils in forest conversion, shifting cultivation and secondary vegetation. Climatic Change, 46(1/2), 115–158. http://doi.org/10.1023/A:1005569915357

Fearnside, P. M. (2015). Deforestation soars in the Amazon. Nature, 521(7553), 423–423. http://doi.org/10.1038/521423b

Freitas, A. C. V., & Ambrizzi, T. (2015). Recent changes in the annual mean regional hadley circulation and their impacts on south america. Advances in Meteorology, 2015. http://doi.org/10.1155/2015/780205

Fryzlewicz, P. (2014). Wild binary segmentation for multiple change-point detection. The Annals of Statistics, 42(6), 2243–2281. http://doi.org/10.1214/14-AOS1245

Fu, R., Dickinson, R. E., Chen, M., Wang, H., Fu, R., Dickinson, R. E., … Wang, H. (2001). How do tropical sea surface temperatures influence the seasonal distribution of precipitation in the Equatorial Amazon? Journal of Climate, 14(20), 4003–4026. http://doi.org/10.1175/1520-0442(2001)014<4003:HDTSST>2.0.CO;2

Funatsu, B. M., Dubreuil, V., Claud, C., Arvor, D., & Gan, M. A. (2012). Convective activity in Mato Grosso state (Brazil) from microwave satellite observations: Comparisons between AMSU and TRMM data sets. Journal of Geophysical Research Atmospheres, 117(16), 1–16. http://doi.org/10.1029/2011JD017259

Funk, C., Peterson, P., Landsfeld, M., Pedreros, D., Verdin, J., Shukla, S., … Michaelsen, J. (2015). The climate hazards infrared precipitation with stations—a new environmental record for monitoring extremes. Scientific Data, 2, 150066. http://doi.org/10.1038/sdata.2015.66

Gloor, M., Brienen, R. J. W., Galbraith, D., Feldpausch, T. R., Schöngart, J., Guyot, J.-L., … Phillips, O. L. (2013). Intensification of the Amazon hydrological cycle over the last two decades. Geophysical Research Letters, 40(9), 1729–1733. http://doi.org/10.1002/grl.50377

Gocic, M., & Trajkovic, S. (2013). Analysis of changes in meteorological variables using Mann-Kendall and Sen's slope estimator statistical tests in Serbia. Global and Planetary Change, 100, 172–182. http://doi.org/10.1016/j.gloplacha.2012.10.014

Grimm, A. M., & Zilli, M. T. (2009). Interannual variability and seasonal evolution of summer monsoon rainfall in South America. Journal of Climate, 22(9), 2257–2275. http://doi.org/10.1175/2008JCLI2345.1

Gutiérrez-Vélez, V. H., DeFries, R., Pinedo-Vásquez, M., Uriarte, M., Padoch, C., Baethgen, W., … Lim, Y. (2011). High-yield oil palm expansion spares land at the expense of forests in the Peruvian Amazon. Environmental Research Letters, 6(4), 044029. http://doi.org/10.1088/1748-9326/6/4/044029

Haylock, M. R., Peterson, T. C., Alves, L. M., Ambrizzi, T., Anunciação, Y. M. T., Baez, J., … Vincent, L. A. (2006). Trends in total and extreme south american rainfall in 1960–2000 and links with sea surface temperature. Journal of Climate, 19(8), 1490–1512. http://doi.org/10.1175/JCLI3695.1

Huffman, G. J., Bolvin, D. T., Nelkin, E. J., Wolff, D. B., Adler, R. F., Gu, G., … Stocker, E. F. (2007). The TRMM Multisatellite Precipitation Analysis (TMPA): Quasi-Global, Multiyear, Combined-Sensor Precipitation Estimates at Fine Scales. Journal of Hydrometeorology, 8(1), 38–55. http://doi.org/10.1175/JHM560.1

Instituto Nacional de Pesquisas Espaciais &National Institute for Space Research Projeto Prodes Monitoramento da Florsta Amazonica Brasileira por Sate´lite Prodes. (2011). Retrieved April 16, 2019, from http://www.obt.inpe.br/OBT/assuntos/programas/amazonia/prodes

Kendall, M. G. (Maurice G. (1970). Rank correlation methods. London: Griffin. Retrieved from

https://www.worldcat.org/title/rank-correlation-methods/oclc/3827024

Khanna, J., Medvigy, D., Fueglistaler, S., & Walko, R. (2017). Regional dry-season climate changes due to three decades of Amazonian deforestation. Nature Climate Change, 7(3), 200–204. http://doi.org/10.1038/nclimate3226

Killick, R., Fearnhead, P., & Eckley, I. A. (2012). Optimal detection of changepoints with a linear computational cost. Journal of the American Statistical Association, 107(500), 1590–1598. http://doi.org/10.1080/01621459.2012.737745

Kleeman, R. (1989). CLIMA AMERICA DEL SUR.pdf.

Kumar Sen, P. (1968). Estimates of the Regression Coefficient Based on Kendall's Tau. Journal of the American Statistical Association (Vol. 63). Retrieved from https://www.pacificclimate.org/~wernera/zyp/Sen 1968 JASA.pdf

Lau, W. K. M., & Kim, K.-M. (2015). Robust Hadley Circulation changes and increasing global dryness due to CO 2 warming from CMIP5 model projections . Proceedings of the National Academy of Sciences, 112(12), 201418682. http://doi.org/10.1073/pnas.1418682112

Laurance, W. F., Camargo, J. L. C., Fearnside, P. M., Lovejoy, T. E., Williamson, G. B., Mesquita, R. C. G., … Laurance, S. G. W. (2018). An Amazonian rainforest and its fragments as a laboratory of global change. Biological Reviews, 93(1), 223–247. http://doi.org/10.1111/brv.12343

Laurance, W. F., Lovejoy, T. E., Vasconcelos, H. L., Bruna, E. M., Didham, R. K., Stouffer, P. C., … John Heinz, H. (2002). Ecosystem Decay of Amazonian Forest Fragments: a 22-Year Investigation. Conservation Biology (Vol. 16). Retrieved from http://www.wec.ufl.edu/academics/courses/wis4554/WebUpdate/ReadingsWIS5555/Habitat_fragmentation/Laurance et al_2002_ConBio.pdf

Li, W., & Fu, R. (2004). Transition of the Large-Scale Atmospheric and Land Surface Conditions from the Dry to the Wet Season over Amazonia as Diagnosed by the ECMWF Re-Analysis. Journal of Climate, 17(13), 2637–2651. http://doi.org/10.1175/1520-0442(2004)017<2637:TOTLAA>2.0.CO;2

Li, W., Fu, R., & Dickinson, R. E. (2006). Rainfall and its seasonality over the Amazon in the 21st century as assessed by the coupled models for the IPCC AR4. Journal of Geophysical Research Atmospheres, 111(2), 1–14. http://doi.org/10.1029/2005JD006355

Liebmann, B., Kiladis, G. N., Vera, C. S., Saulo, A. C., & Carvalho, L. M. V. (2004). Subseasonal variations of rainfall in South America in the vicinity of the low-level jet east of the Andes and comparison to those in the South Atlantic convergence zone. Journal of Climate, 17(19), 3829–3842. http://doi.org/10.1175/1520-0442(2004)017<3829:SVORIS>2.0.CO;2

Liebmann, B., & Marengo, J. A. (2001). Interannual Variability of the Rainy Season and Rainfall in the Brazilian Amazon Basin. Journal of Climate, 14(22), 4308–4318.

http://doi.org/10.1175/1520-0442(2001)014<4308:IVOTRS>2.0.CO;2

Longobardi, P., Montenegro, A., Beltrami, H., & Eby, M. (2016). Deforestation induced climate change: Effects of spatial scale. PLoS ONE, 11(4). http://doi.org/10.1371/journal.pone.0153357

Malhi, Y., WOOD, D., BAKER, T. R., WRIGHT, J., PHILLIPS, O. L., COCHRANE, T., … VINCETI, B. (2006). The regional variation of aboveground live biomass in old-growth Amazonian forests. Global Change Biology, 12(7), 1107–1138. http://doi.org/10.1111/j.1365-2486.2006.01120.x

Mann, H. B. (1945). Nonparametric Tests Against Trend. ECONOMETRICA, 13(3), 245–259. Retrieved from https://www.jstor.org/stable/pdf/1907187.pdf

Marengo, J. A. (2004). Interdecadal variability and trends of rainfall across the Amazon basin. Theoretical and Applied Climatology, 78(1–3), 79–96. http://doi.org/10.1007/s00704-004-0045-8

Marengo, J. A., & Espinoza, J. C. (2016). Extreme seasonal droughts and floods in Amazonia: Causes, trends and impacts. International Journal of Climatology, 36(3), 1033–1050. http://doi.org/10.1002/joc.4420

Marengo, J. A., Nobre, C. A., Tomasella, J., Oyama, M. D., Sampaio de Oliveira, G., de Oliveira, R., … Brown, I. F. (2008). The Drought of Amazonia in 2005. Journal of Climate, 21(3), 495–516. http://doi.org/10.1175/2007JCLI1600.1

Moore, N., Arima, E., Walker, R., & Ramos da Silva, R. (2007). Uncertainty and the changing hydroclimatology of the Amazon. Geophys. Res. Lett, 34, 14707. http://doi.org/10.1029/2007GL030157

Nepstad, D. C., Stickler, C. M., Soares-Filho, B., & Merry, F. (2008). Interactions among Amazon land use, forests and climate: Prospects for a near-term forest tipping point. Philosophical Transactions of the Royal Society B: Biological Sciences, 363(1498), 1737–1746. http://doi.org/10.1098/rstb.2007.0036

Nobre, C. A., Sampaio, G., Borma, L. S., Castilla-Rubio, J. C., Silva, J. S., & Cardoso, M. (2016). Land-use and climate change risks in the Amazon and the need of a novel sustainable development paradigm. Proceedings of the National Academy of Sciences, 113(39), 10759–10768. http://doi.org/10.1073/pnas.1605516113

Oyama, M. D., & Nobre, C. A. (2003). A new climate-vegetation equilibrium state for Tropical South America. Geophysical Research Letters, 30(23), n/a-n/a. http://doi.org/10.1029/2003GL018600

Paccini, L., Espinoza, J. C., Ronchail, J., & Segura, H. (2018). Intra-seasonal rainfall variability in the Amazon basin related to large-scale circulation patterns: a focus on western Amazon–Andes transition region. International Journal of Climatology, 38(5), 2386–2399. http://doi.org/10.1002/joc.5341

Partal, T., & Kahya, E. (2006). Trend analysis in Turkish precipitation data. Hydrological Processes, 20(9), 2011–2026. http://doi.org/10.1002/hyp.5993

R Core Team. (2018). R: A language and environment for statistical computing. R Foundation for Statistical Computing. Vienna, Austria. Retrieved from http://www.r-project.org/

Rohrbeck, C. (2013). Detection of changes in variance using binary segmentation and optimal partitioning. Retrieved from https://www.semanticscholar.org/paper/Detection-of-changes-in-variance-using-binary-and-Rohrbeck/b132976b756634c02a8bdd77d4c530d02222561a

Ronchail, J., Cochonneau, G., Molinier, M., Guyot, J. L., De Miranda Chaves, A. G., Guimarães, V., & De Oliveira, E. (2002). Interannual rainfall variability in the Amazon basin and sea-surface temperatures in the equatorial Pacific and the tropical Atlantic Oceans. International Journal of Climatology, 22(13), 1663–1686. http://doi.org/10.1002/joc.815

Saad, S. I., da Rocha, H. R., Silva Dias, M. A. F., Rosolem, R., Saad, S. I., Rocha, H. R. da, … Rosolem, R. (2010). Can the deforestation breeze change the rainfall in amazonia? a case study for the BR-163 Highway Region. Earth Interactions, 14(18), 1–25. http://doi.org/10.1175/2010EI351.1

Saatchi, S. S., Houghton, r. A., Dos Santos Alvalá, r. C., Soares, j. V., & Yu, Y. (2007). Distribution of aboveground live biomass in the Amazon basin. Global Change Biology, 13(4), 816–837. http://doi.org/10.1111/j.1365-2486.2007.01323.x

Salati, E., Dall'Olio, A., Matsui, E., & Gat, J. R. (1979). Recycling of water in the Amazon Basin: An isotopic study. Water Resources Research, 15(5), 1250–1258. http://doi.org/10.1029/WR015i005p01250

Salviano, M. F., Daniel Groppo, J., & Pellegrino, G. Q. (2016). Trends Analysis of Precipitation and Temperature Data in Brazil. Revista Brasileira de Meteorologia, 31(1), 64–73. http://doi.org/10.1590/0102-778620150003

Santos, E. B., Lucio, P. S., & Silva, C. M. S. e. (2015). Precipitation regionalization of the Brazilian Amazon. Atmospheric Science Letters, 16(3), 185–192. http://doi.org/10.1002/asl2.535

Satyamurty, P., de Castro, A. A., Tota, J., da Silva Gularte, L. E., & Manzi, A. O. (2010). Rainfall trends in the Brazilian Amazon Basin in the past eight decades. Theoretical and Applied Climatology, 99(1–2), 139–148. http://doi.org/10.1007/s00704-009-0133-x

Sharma, D., & Babel, M. S. (2014). Trends in extreme rainfall and temperature indices in the western Thailand. International Journal of Climatology, 34(7), 2393–2407. http://doi.org/10.1002/joc.3846

Sheil, D., & Murdiyarso, D. (2009). How Forests Attract Rain: An Examination of a New Hypothesis. BioScience, 59(4), 341–347. http://doi.org/10.1525/bio.2009.59.4.12

Silva Junior, C. H. L., Almeida, C. T., Santos, J. R. N., Anderson, L. O., Aragão, L. E. O. C., &

Silva, F. B. (2018). Spatiotemporal rainfall trends in the Brazilian legal Amazon between the years 1998 and 2015. Water (Switzerland), 10(9), 1–16. http://doi.org/10.3390/w10091220

Sombroek, W. (2001). Spatial and temporal patterns of amazon rainfall. AMBIO: A Journal of the Human Environment, 30(7), 388–396. http://doi.org/10.1579/0044-7447-30.7.388

Spera, S. A., Galford, G. L., Coe, M. T., Macedo, M. N., & Mustard, J. F. (2016). Land-use change affects water recycling in Brazil's last agricultural frontier. Global Change Biology, 22(10), 3405–3413. http://doi.org/10.1111/gcb.13298

Vera, C., Silvestri, G., Liebmann, B., & González, P. (2006). Climate change scenarios for seasonal precipitation in South America from IPCC-AR4 models. Geophys. Res. Lett, 33, 13707. http://doi.org/10.1029/2006GL025759

Wilks, D. S. (2011). Statistical methods in the atmospheric sciences. Elsevier/Academic Press.

Wu, M., Schurgers, G., Ahlström, A., Rummukainen, M., Miller, P. A., Smith, B., & May, W. (2017). Impacts of land use on climate and ecosystem productivity over the Amazon and the South American continent. Environmental Research Letters, 12(5), 054016. http://doi.org/10.1088/1748-9326/aa6fd6

Xu, Z. X., Takeuchi, K., & Ishidaira, H. (2003). Monotonic trend and step changes in Japanese precipitation. Journal of Hydrology, 279(1–4), 144–150. http://doi.org/10.1016/S0022-1694(03)00178-1

Yin, L., Fu, R., Zhang, Y.-F., Arias, P. A., Fernando, D. N., Li, W., … Bowerman, A. R. (2014). What controls the interannual variation of the wet season onsets over the Amazon? Journal of Geophysical Research: Atmospheres, 119(5), 2314–2328. http://doi.org/10.1002/2013JD021349

Yoon, J. H., & Zeng, N. (2010). An Atlantic influence on Amazon rainfall. Climate Dynamics, 34(2), 249–264. http://doi.org/10.1007/s00382-009-0551-6

Zilli, M. T., Carvalho, L. M. V., Liebmann, B., & Silva Dias, M. A. (2017). A comprehensive analysis of trends in extreme precipitation over southeastern coast of Brazil. International Journal of Climatology, 37(5), 2269–2279. http://doi.org/10.1002/joc.4840

CHAPTER3. ANALYZING THE FIRST-ORDER RESPONSES OF ATMOSPHERE TO THE POTENTIAL REFORESTATION ACROSS THE AMAZON BASIN

Citation: Haghtalab. N., Moore, N., Nejadhashemi, A.P., (2021) Analyzing the First-Order Responses of Atmosphere to the Potential Reforestation Across the Amazon Basin, Journal of Geophysical Research: Atmosphere (under review)

Introduction

The land surface plays a vital role in the climate system. Partitioning of available energy into sensible and latent heat, and available water into runoff and evapotranspiration (ET) directly depends on the land surface biophysical characteristics (Pitman 2003). The land cover and land surface attributes affect the atmosphere primarily in two ways: first, through changing albedo and modifying the partitioning of reflected and absorbed incoming shortwave radiation; and second, through altering the partitioning of the absorbed energy into the sensible and latent heat fluxes depends on the vegetation aerodynamic properties, soil water balance, and canopy conductance. On the other hand, Land Cover Change (LCC) directly alters surface solar radiation, longwave radiation, and atmospheric turbulence. These alterations lead to changes in fluxes of momentum, heat, and water vapor through the mediation of albedo, ET, and roughness, as well as CO2 (Pielke et al. 2011, Alkama and Cescatti 2016). Deforestation generally provides higher albedo, less net radiation at the surface (Alton 2009), and higher surface temperatures locally but cooling globally (Devaraju et al. 2015). Replacing forest cover with croplands will alter land surface energy partitioning, its biophysical attributes, and vegetation dynamics (Zhu et al. 2019). In general, if a forest is replaced by bare soil, annual precipitation may decrease by up to 30% (Snyder et al. 2004), and over the tropics, it would reduce by 10% (about 110 mm/yr) (Bathiany et al. 2010).

Amazon intact forest generates more CAPE (convective available potential energy) and deep clouds due to greater humidity, while deforested areas generate more Sensible Heat (SH) to

Latent Heat (LH) and create lifting as a result of shallow convection (Wang et al. 2009). Across the Amazon Basin, deforestation has led to local reduction of rainfall and increased surface temperatures (Henderson-Sellers and Gornitz 1984; Dickinson and Kennedy 1992; Nobre et al. 1991, 2009). According to observations and simulations, conversion of forest to cropland in the Amazon Basin resulted in a decrease in precipitation (P) (da Silva et al. 2008b), a decrease in ET (Oliveira et al. 2014, Spera et al. 2016), an increase in temperature (Silvério et al. 2015), and indirectly intensified fire occurrence (Aragão et al. 2008). The onset of the rainy season (September 1st) has also delayed, on average, 11 days over the last thirty years across the highly deforested areas in the state of Rondonia, Brazil (Butt et al. 2011). In addition, the length of the dry season has been increased from 5 to 6 months (Costa and Pires 2010) and drought conditions are exacerbated as a result of deforestation (Bagley et al. 2014). Dirmeyer (2002) found that the impact of land surface variability on climate is more apparent at monthly time scales than at other timescales. Silva Dias et al. (2002) analyzed the interactions between clouds, rains, and the underlying land surface through biospheric processes in southwestern Rondônia, Brazil. They found that deforestation influences the atmosphere more during the dry season than during the wet season. They also reported a complex interaction between cloudiness, moisture transport, and fluxes during the wet season.

Several studies have focused on a wide variety of effects from deforestation on regional climate variability in the Amazon using General Circulation Models (GCMs: e.g., Nobre et al. 1991; Zeng et al. 1996; Werth and Avissar 2002; Schneider et al. 2006). Nobre et al. 2009 found that ocean-atmosphere interactions significantly influence the climate of Amazon and its changes as a result of deforestation using GCMs. Badger and Dirmeyer (2015) also used a GCM to capture the climate response to Amazon deforestation. They found that the sensitivity of climate

to LCC depends on the initial tree cover and type of irrigation. Some other studies have used satellite observations to assess crop responses to drought in the basin and found that due to reduced cloud cover, droughts induce a "greening-up" (Huete et al. 2006, Saleska et al. 2007) though other researchers have rejected this hypothesis (e.g., Brando et al. 2010; Xu et al. 2011). Therefore, models' outputs of the effects of deforestation on rainfall are not consistent and they have produced equivocal results. Model outputs are highly dependent on the scale of deforestation and the model resolution (D'almeida et al. 2007). Generally, available studies of land-atmosphere interactions have been done using multi-year time scales with single-column models, short-term experiments such as one week, or low-resolution GCMs.

On the other hand, understanding the effects of deforestation on the land surface energy and water budgets are complicated by 1) lack of statistically reliable approaches to identify non-linear systems feedbacks for land surface-atmosphere coupling and 2) lack of all-encompassing climate simulation methodologies. The conclusions of available studies are configuration dependent for example type of convection scheme or type of cloud parameterization. Global-scale models cannot deal with the effects of LCC effectively. Due to their computing resource and model design problems they cannot capture the topography, heterogeneity, and mesoscale convection at finer spatial scales (Avissar and Nobre 2002; da Silva and Avissar 2006). Whereas, at the regional scale, LCC can influence climate significantly (e.g., Moore et al. 2007; Pitman et al. 2009). Also, surface heterogeneity can increase local convection as a result of deforestation during the dry season, (Wang et al. 2000; Souza et al. 2000b; Baidya Roy and Avissar 2002) and influence transitions between wet and dry seasons (Fu et al. 2013; Wright et al. 2017).

In this research, we examined the sensitivity and magnitude of changes to the surface energy budget, including precipitation, due to potential new growth forests across the Amazon Basin. To

assess the sensitivity of fluxes of heat and moisture to the land cover change (here reforestation), we forced the Weather Research and Forecasting model (WRF)V3.9 with ESA (European Space Agency) land cover (current and reforested) and ERA_Interim boundary conditions for the 2009, 2013, and 2014 as they are ENSO neutral years. The results are presented at a seasonal temporal scale with an average of three years and the mean of the entire basin. To the best of our knowledge, there is no published work about the impact of potential reforestation on the atmosphere behavior across the entire Amazon Basin at these spatial and temporal scales during May-Nov and Dec-Apr. Available studies looked at small regions in the basin, used a short period (e.g. only May-Nov), or analyzed the impacts of different crops on the Amazon's atmosphere (e.g. Walker et al. 2009; Bagley et al. 2011; Medvigy et al. 2011; Lee et al. 2012; Khanna et al. 2017). Therefore, this research is unique as it investigates the land-atmosphere interactions across the entire Amazon Basin at a fine resolution to show the effects and locations of changes in the land surface biophysical characteristics on the fluxes of heat and moisture in the atmosphere.

Materials and Methods

Study area and simulation domain

Figure 10 shows the geographic location of the Amazon Basin, along with our simulation boundary. The Amazon Basin is expanded through Brazil, Peru, Colombia, Ecuador, and Bolivia. The basin's area is about 6 million km^2. The rainiest part of the basin is located on the Andes Cordillera (Espinoza et al. 2015; Paccini et al. 2018). The Amazon Basin provides more than 20% of the world's fresh water and is a hot spot for ecosystem diversity. The forest biomass holds 100 billion tons of carbon (Saatchi et al. 2007). Since the 1960s, forest cover has shrunken by 80% (Davidson et al. 2012).

The basin's climate varies from continuously rainy in the northwest to the long dry season in the east and south (Sombroek 2001, Davidson et al. 2012), where more conversion to agriculture occurred, which is referred to as the "Arc of Deforestation." Different synoptic-scale climate phenomena influence the climate of the basin. For example, El Nino Southern Oscillation (ENSO) influences the Amazon River flow on the eastern side of the basin during the El Nino years (Marengo 2004). However, during the La Nina years, flooding increases (Coe et al. 2002). Besides, the Atlantic Multidecadal Oscillation (AMO) affects the region differently. For instance, the drought of 2005 is attributed to AMO (Marengo et al. 2008). The Southern American Monsoon System brings rainfall to the southern portion of the basin with the maximum rainfall during DJF (December-January-February; austral summer) (Vera et al. 2006). During JJA (June-July-August; austral winter) the South America Convergence Zone (SACZ) contributes to the precipitation variability across the south of the Basin (Carvalho et al. 2004). During MAM (March-April-May), the rainfall regime is highly influenced by Intertropical Convergence Zone (ITCZ), which is highly variable (Fu et al. 2001).

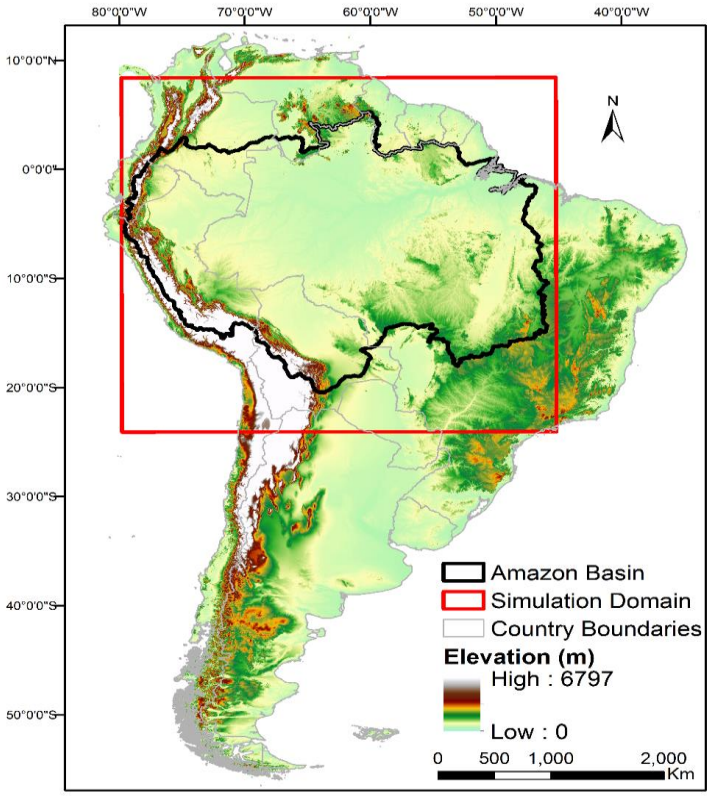

Figure 10. The Amazon basin; *The geographic location of the Amazon Basin in black, simulation domain in red, and topography of the Basin.*

Data

Since most remotely sensed derived land cover data are associated with uncertainty (Ge et al. 2007), accurate representation of land cover categories in climate models is very important. Land surface characteristics exert strong controls on the underlying atmospheric processes (Sertel et al. 2010). Up-to-date land cover classification affects simulated cumulative precipitation at the regional scale (Ge et al., 2007; Bagley et al. 2014). In this research, we used ESA 2009, which was reclassified based on US Geological Survey land cover classes to match the WRF settings and mosaicked to account for the differences in resolution. Since there is no significant change in land use from 2009 onward, we chose 2009 to be able to compare these

results to in-depth simulations for the floods of 2009 in a related study with the INFEWS hydrologists' team. For vertical boundary conditions, ERA_Interim with 80 km spatial resolution and 60 vertical levels and 6-hourly temporal resolution of 2009, 2013, and 2014 were used to force the model to simulate the effects of forest regrowth on the fluxes.

To validate the model precipitation output, we used daily rainfall datasets acquired from rain gauge stations of the Brazilian National Water Agency (ANA) and The Tropical Rainfall Measuring Mission (TRMM) with 0.25° spatial resolution. MODIS Land-Surface Temperature with 1 km spatial resolution is used to validate the simulated temperature.

WRF model setup

WRF.3.9 (The Weather Research and Forecasting model; Skamarock et al, 2008) is a three-dimensional, non-hydrostatic climate model widely used to do atmospheric research by scientific communities. Simulations were initialized at 00:00 UTC and the first 15 days were considered spin-up and were removed from the analysis. Early trials using longer spin-up proved to be computationally expensive and unlikely to significantly affect the sensitivity tests. The horizontal grid spacing was 16 km, with 38 levels of vertical levels up to 1000 m. The thickness of the lowest atmospheric layer is about 50 m on smooth topography. At this resolution, cumulus parameterization is necessary to resolve convection, clouds, and precipitation properly (Bagley et al. 2014). WRF offers several parametrizations for schemes such as physics, Land Surface Model (LSM), planetary boundary layer (PBL), cumulus. Model parameterization and performance are highly dependent on geographic location, the variables, season, and time of the year (e.g., Jankov et al. 2005, Cheng and Steenburgh 2005; Case et al. 2008; Ruiz et al. 2010b). Table 2 summarizes WRF parameterizations for this study, primarily based on previous studies. SSTs

(Sea Surface Temperature) come from ERA data to be time-consistent with the vertical boundary conditions.

Table 3. WRF parameterizations

Parameter	Scheme option
Longwave radiation scheme	Rapid Radiative Transfer Model
shortwave radiation	Dudhia scheme
surface layer	fifth-generation Pennsylvania State University–National Center for Atmospheric Research Mesoscale Model (MM5) scheme.
Cumulus scheme	Kain–Fritsch
Mp_physics	WSM6 Hong and Lim
LSM	NOAH
PBL	Yonsei University scheme

To quantify model performance, we calculated the root-mean-square error (RMSE) and systematic error (Percent Bias; PBias) on the areal basin mean of daily data. We also mapped the differences between the model outputs and observations at monthly and seasonal timescales for the basin to estimate model performance and examine the errors spatially. We resampled our observations based on the simulation outputs to eliminate spatial resolution discrepancies in our data and comparison.

Results and Discussion

Model validation

Figure 11 shows RMSE and PBias errors for both precipitation and temperature. We validated the simulated precipitation against ANA rain gauge measurements and TRMM reanalysis precipitation data and compared basin-wide averages.

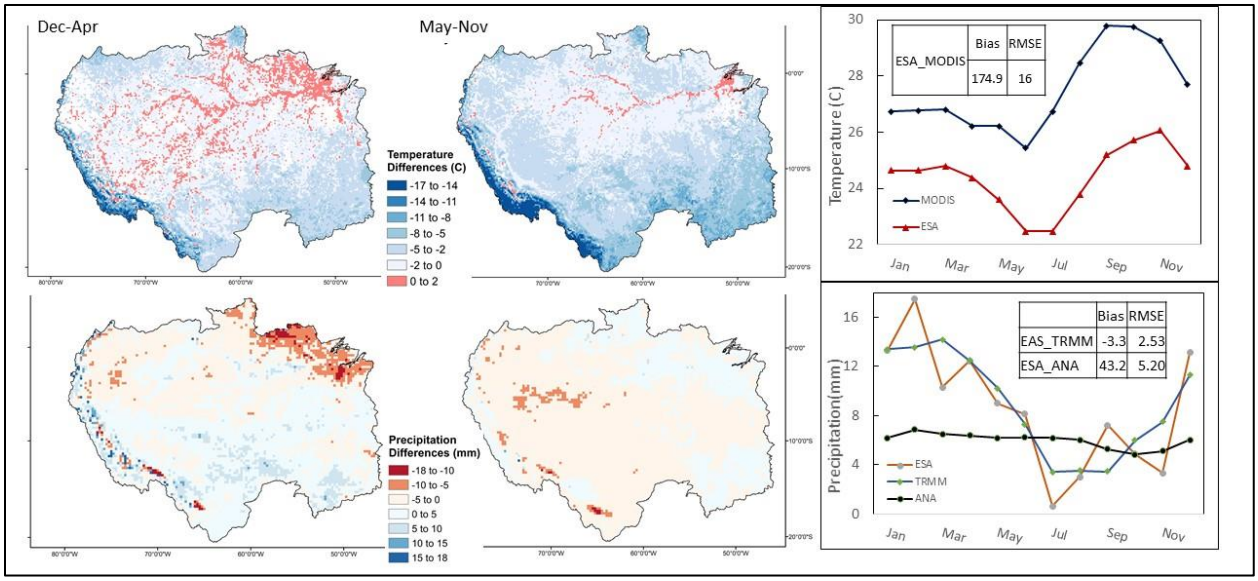

Figure 11. Model output validation*; Left: difference maps of model outputs and the observations at the seasonal scale. Right: Basin-wide average of mean monthly Temperature and Precipitation along with relative and systematic errors (Percent Bias)*

In general, the model simulated cooler temperatures than MODIS temperatures. The model underestimated the temperature up to 18° C at high altitudes (Figure 11), consistent with WRF's well-known cold bias at high altitudes (Réveillet et al. 2020). However, in lower altitudes in the center, East and South of the basing, the difference between simulated and observed values is about 0 to -2° C. The model performed better in simulating surface temperature (T) in May-Nov than Dec-Apr. Also, the model consistently simulated 5 mm less rainfall during May-Nov for most of the basin comparing to the observations. Because of the complex interaction between cloudiness, land surface, and precipitation in the Amazon Basin (Silva Dias et al. 2002), during Dec-Apr, the model overestimates P for the arc of deforestation by up to 5 mm/day compared to the observations. In terms of basin average, the temperature is being simulated with the same pattern as MODIS temperature but 1°C cooler. Simulated precipitation shows the same pattern as TRMM precipitation. The RMSE and Bias are reported in Figure 11.

To evaluate the spatial distribution of the model performance, a correlation between the model performance and elevation is shown in Figure 12. There is no strong correlation between P and elevation, but there is a strong negative correlation between T and elevation, as expected. As elevation increases, the model performed more poorly. For example, at higher altitudes in the Andes, the model simulated lower temperatures than observations (a well-known cold bias; c.f. Réveillet et al. 2020).

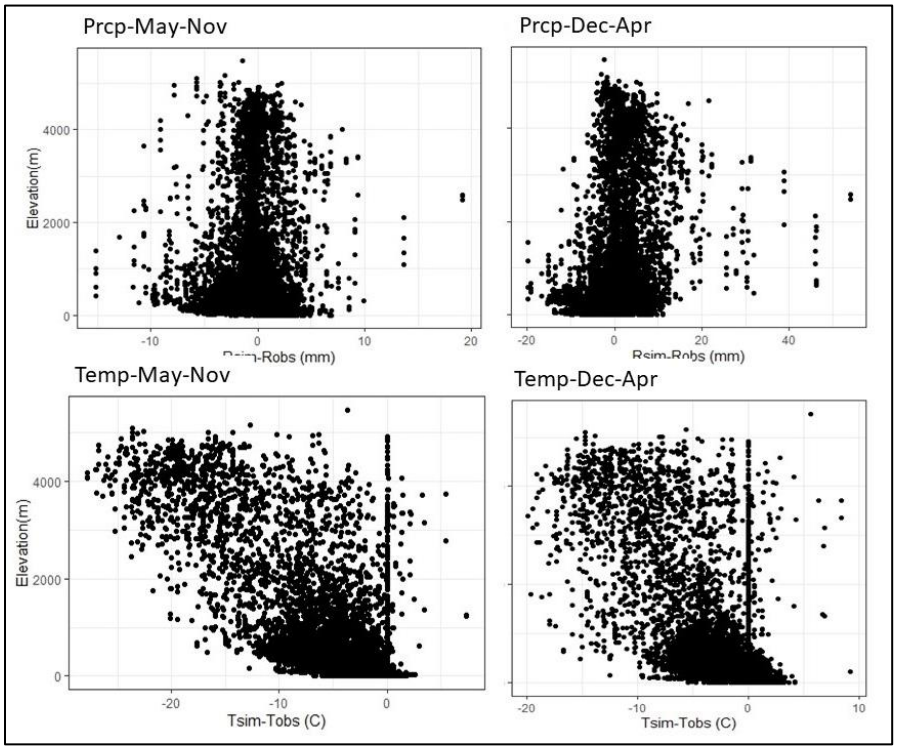

Figure 12. Correlation between topography and model performance*. The upper row shows precipitation and the bottom row shows temperature.*

Land cover change scenarios

The last 50 years have witnessed the conversion of forest to pasture and soy agriculture, driven by new road building. For deforested areas, this has brought reduced soil moisture, higher SH, seasonally bare soils, higher albedos, and lowered zero-plane displacement heights. Figure 13 shows maps of current and reforested land cover used in this study to analyze the sensitivity of the atmosphere to deforestation across the Amazon Basin. In this study, the only conversion

from forest to cropland has been considered. Every grid cell, which was primarily cropland, has been replaced by evergreen rainforest (although this is complex in the southeastern domain). As a result, the converted reforested area covers 5% of the basin, which is mostly located along the arc of deforestation and along the main stem of the Amazon river.

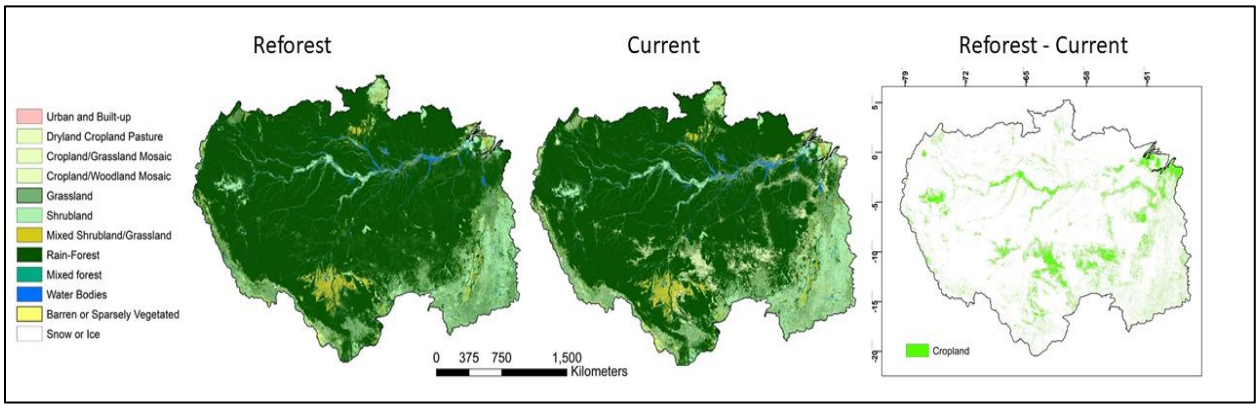

Figure 13. ESA land cover map used in the simulation*. In the Reforest map, all croplands are replaced by evergreen broadleaf forests. The reforested areas are shown on the difference map between the reforest and current land cover.*

The sensitivity of fluxes and Precipitation to land cover change across the basin

The results shown here are averaged across the three years of simulation. To assess the impacts of regrowth on fluxes and precipitation, we applied a Student t-test for each season time series at each grid point. In this test, the null statistical hypothesis states that the reforested and current population had the same mean (Hasler et al. 2009). Each grid point that could reject the null hypothesis at a 95% significance level is considered to have experienced a significant impact from the reforestation process. Although ENSO-neutral years, there exists interannual variability across the three years, and both positive and negative changes develop in response to reforestation.

Heat flux

Surface fluxes are related to the dynamics of the lower atmosphere and the efficiency of aerodynamic transfer between the lower atmosphere and the land surface (Zhang et al. 1996). LH

largely depends on surface moisture and transpiration rate, but they also depend on root depth, leaf area, and surface roughness (Davin and de Noblet-Ducoudré 2010, Ban-Weiss et al. 2011). On the arc of deforestation, the removal of moist forests reduces transpiration but also surface roughness and consequently reduces latent heat flux and water vapor in the atmosphere. This leads to decreased cloudiness and precipitation and increased SH flux not only on the deforested areas but on the intact forest in the northwest of the basin, which tends to intensify warming of the boundary layer (BL) and increase convection (Pitman 2003, Davin and de Noblet-Ducoudré 2010, de Noblet-Ducoudré et al. 2012). On the other hand, changes in the Leaf Area Index (LAI) due to deforestation influence the exchange of both SH and LH. Our results show that, all over the basin, the highest LAI occurs from July to November. The effects of LCC as reforestation on LH are shown in Figure 14 (only significant changes are shown). Throughout a year the spatial pattern of changes in LH is consistent with the reforestation pattern. However, an increase in the latent heat in May-Nov is more obvious and higher than in Dec-Apr especially on the arc of deforestation and NW of the basin. LH has increased by 30 Wm^{-2} during May-Nov and by 15 Wm^{-2} during Dec-Apr- - although there are some extreme increases in the north side of the region, most of the area shows an increase of about 15 Wm^{-2}. The highest amount of change in LH happened in November starting in July from 20 W m^{-2} to 50 W m^{-2} in September and to 20 W m^{-2} in November (map are provided as supplementary materials, Appendices B.1). Due to higher LAI, more surface moisture, higher transpiration rates, and higher roughness on reforested areas, LH has shown a persistent increase. Therefore, it indicates a high sensitivity of LH to surface vegetation cover biophysical characteristics.

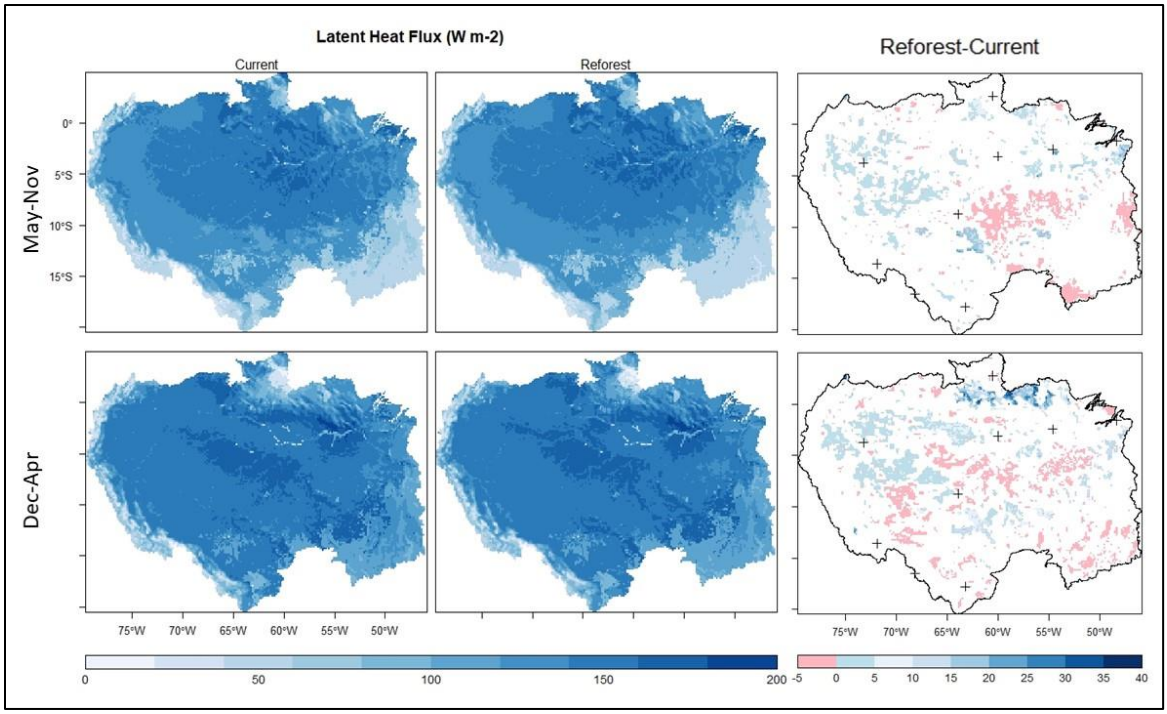

Figure 14. Mean daily seasonal Latent Heat Flux (LH) *with current and reforested land cover along with significant differences at α=95%. The plus signs on the difference maps indicate major cities.*

Removing rainforest leads to increased surface albedo, decreased interception, and a decrease in surface roughness. Therefore, replacing croplands with rainforest in the simulation decreased monthly albedo by about 14% and increased LAI up to 3 (m^3 m^{-2}) over the reforested area. The seasonal average of sensible heat flux and skin temperature (T_{SK}) are shown in Figures 15 and 16. We found visually no significant negative changes in domain averaged mean SH across the region with reforestation. Because the land surface has a complex relationship with the atmosphere, SH did not show significant sensitivity to changes in the land surface biophysical characteristics at a seasonal scale. However, at the monthly time scale, the cooling effect of reforestation is clear, especially at the end of the May-Nov time period. This finding is consistent with observations (e.g., Souza et al. 2000a; Wang et al. 2009; Li and Fu 2004), showing that SH is significantly lower over the forest than in pasture.

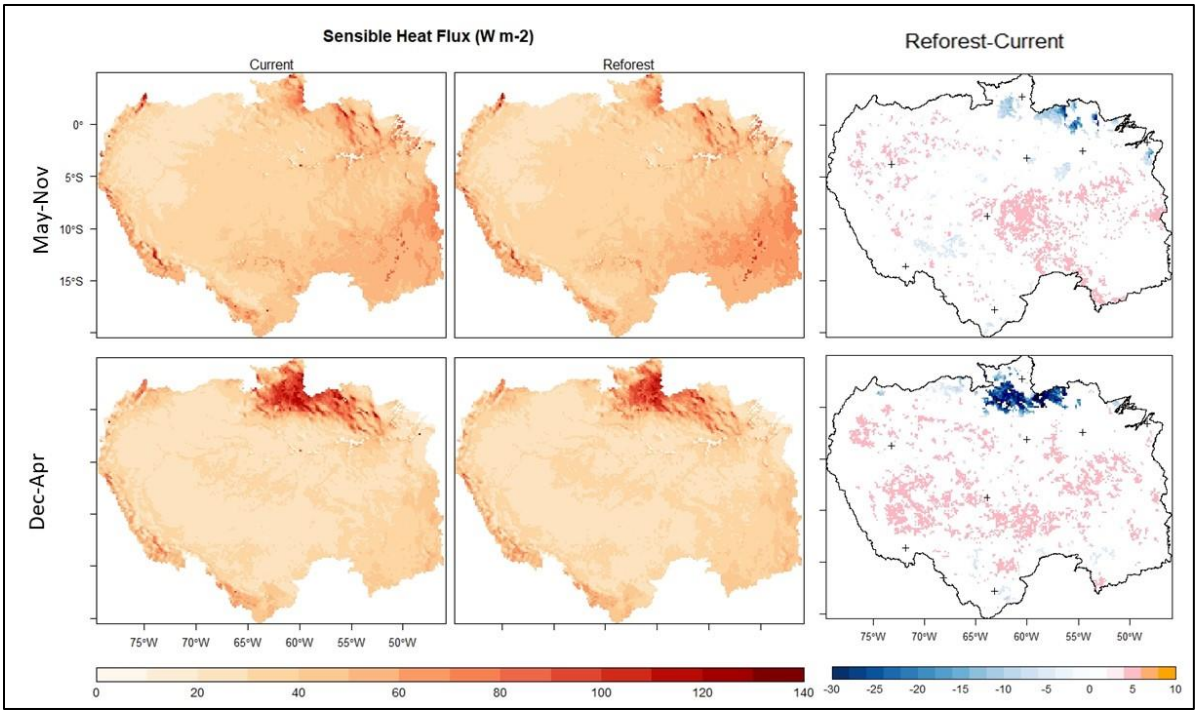

Figure 15. Mean daily seasonal sensible heat flux (SH) *with current and reforested land cover along with significant differences at α=95%. The plus signs on the difference maps indicate major cities.*

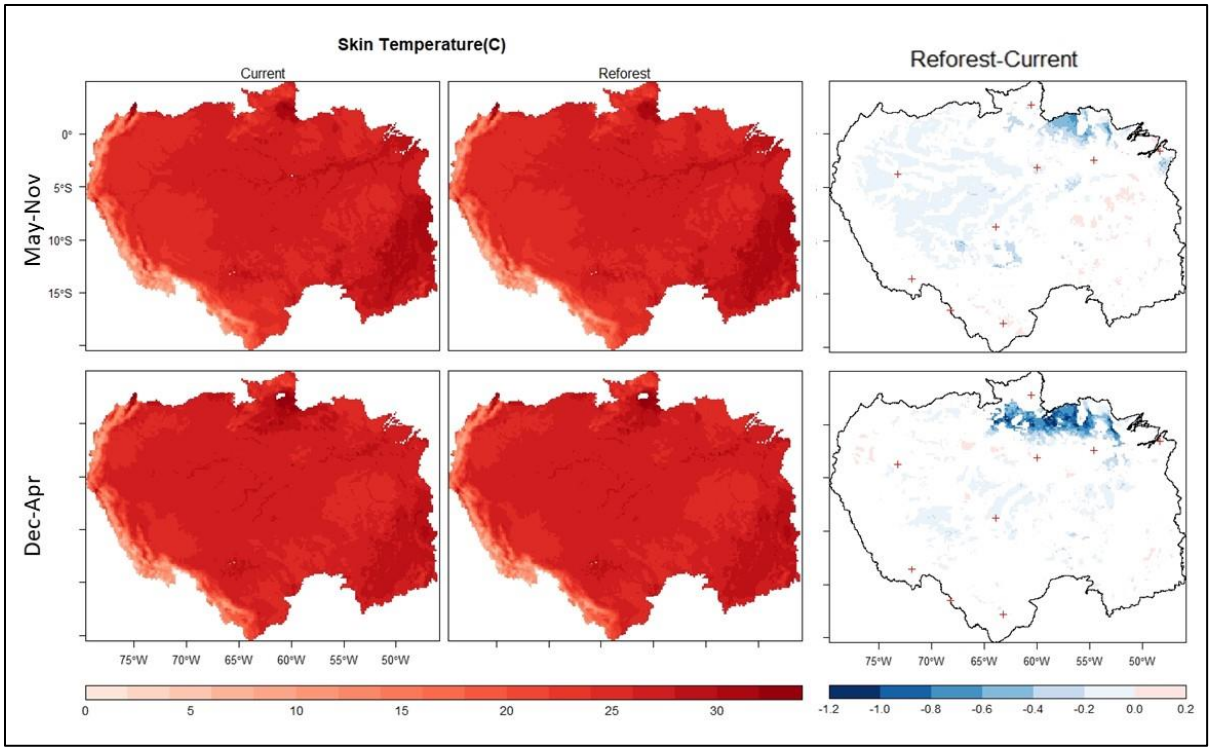

Figure 16. Mean daily seasonal skin temperature (TSK) *with current and reforested land cover along with significant differences at α=95%. Red plus signs on the difference maps indicate major cities.*

In May-Nov, by reforestation, T_{SK} decreased by 0.8^{oC} in the NE and by 0.5^{oC} on the west side of the basin (Figure 16). While during Dec-Apr T_{SK} decreased by 1.2oC by reforestation. The increased ET drives a significant increase in cloud cover that gets advected westward. The cooling effect of reforestation is clearer on a monthly scale, especially in August and September by about 2 $^{\circ C}$. This finding is consistent with Nobre et al (2009) which found 2 $^{\circ C}$ warmer air temperature as a result of deforestation, as well as Silvério et al (2015) which found 0.3 $^{\circ C}$ warmer surface temperature due to deforestation of the Xingu region along the arc of deforestation.

Moisture flux and precipitation

A significant amount of precipitation in the tropics is produced by moisture recycling. Especially during December to April, 50% to 75% of precipitation is through ET (Salati and Nobre 1991), and almost half of the precipitation originated from moisture released from the forest across the Amazon Basin (Kumagai and Porporato 2012; Phillips et al. 2009, Silva Dias et al. 2009, Malhi et al. 2008). Our results showed that reforestation significantly increased the domain-averaged available moisture to the atmosphere (Figure 17), mostly during May-Nov, by 27%. The maximum increase in moisture flux occurred in August and September, about 0.03 g m^{-2} s^{-1}, especially in northern Mato Grosso and southern Pará. All of these areas have had significant widespread deforestation. However, other heavily deforested areas in the simulations (along the rivers in the centroid of the basin) did not exhibit significant changes in moisture flux. These regions receive much more rainfall and have virtually no dry season. The value of 0.01 g m^{-2} s^{-1} in the difference panel of Figure 17 converts to approximately 25 mm/month, which is at the upper end of the RMSE measured by global ET products (Motta Paca et al. 2019).

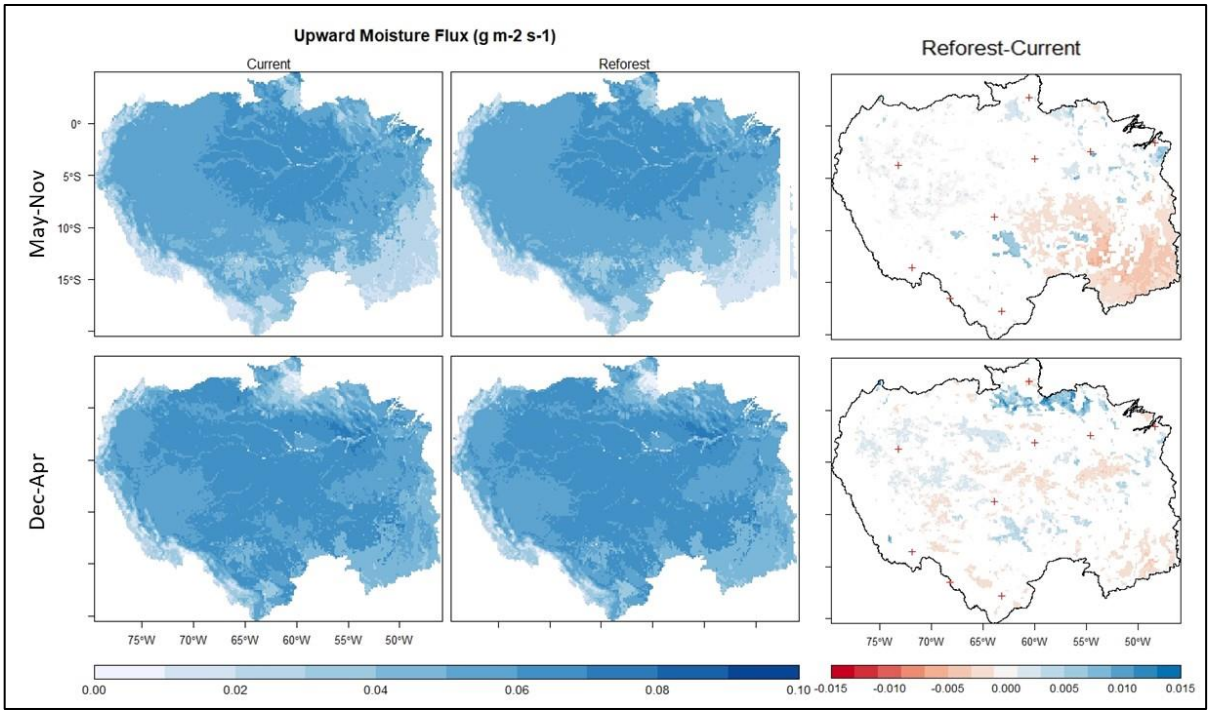

Figure 17. Mean daily seasonal Upward Moisture Flux (QFX) *with current and reforested land cover along with significant differences at α=95%. Red plus signs on the difference maps indicate major cities.*

During Dec-Apr, synoptic-scale atmospheric circulations bring moisture to the basin through thunderstorms and deep convection, as well as shallow convections triggered at the regional scale (Da Silva et al. 2008). During Dec-Apr, also at the synoptic scale, Rossby waves can propagate northward and produce precipitation at a regional scale (Da Silva 2008). Squall lines originating on the northeast coast of South America transport moisture and precipitation east toward the Andes. On the synoptic scale, although the positioning and strength of the ITCZ control different precipitation regimes in the region, El Nino can affect the Walker-type circulations and can thus affect the spatial distribution of the rainfall (Haghtalab et al. 2020; Richey et al. 1989). Therefore, the amount of rainfall is likely more dependent on synoptic-scale forcings such as the ITCZ and Walker-type cells and less on the localized reforestations, which we will explore. Reforestation provides moisture, but larger processes initiate rainfall. In this

study, mean seasonal precipitation showed increasing signals by 5 mm/day with forest regrowth. Changes occurred mostly on the west side of the region during May-Nov due to moisture transport and more cloud fraction over the west due to reforestation, which indicated the teleconnected impacts of reforestation on precipitation, as discussed in Souza et al (2000). The maximum increase in precipitation occurred during Dec-Apr at 5 mm/day, while during May-Nov the increase was about 3 mm/d with a spatially very consistent pattern (Figure 18); note similarities to Figure 5 of Badger and Dirmeyer (2015).

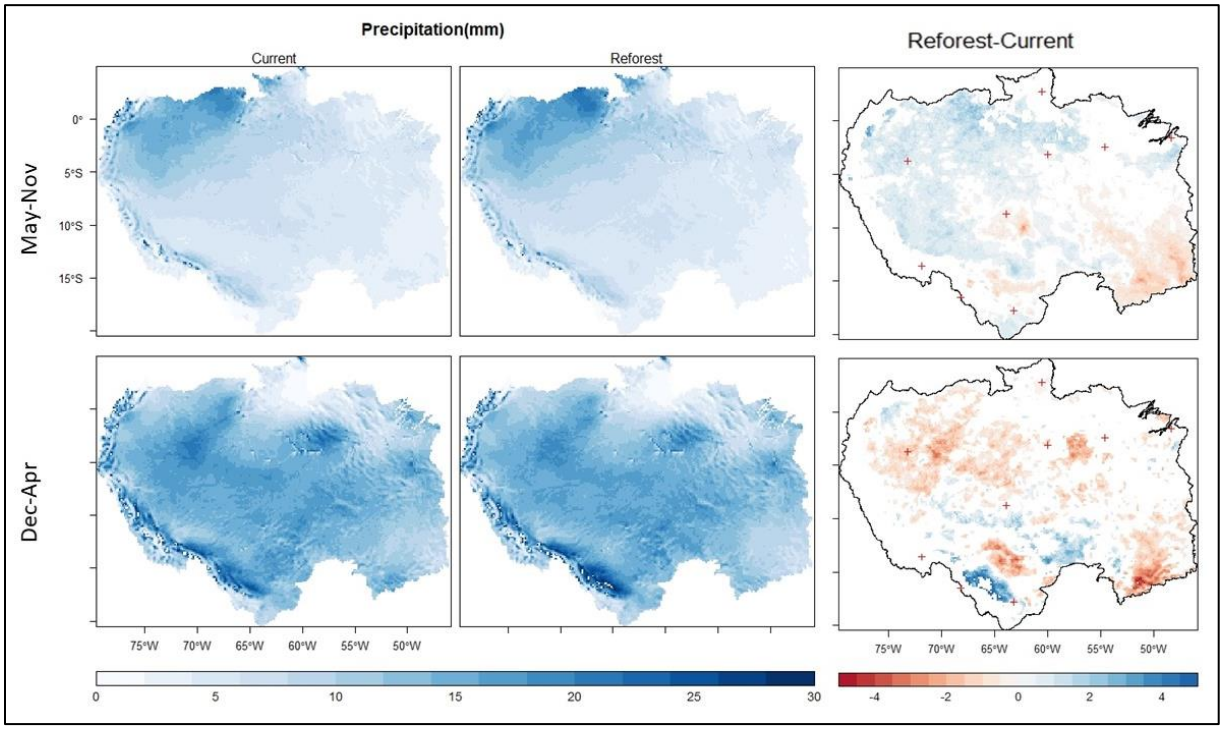

Figure 18. Mean daily seasonal precipitation (mm) *with current and reforested land cover along with significant differences at α=95%. Red plus signs on the difference maps indicate major cities.*

Thus, following potential reforestation in the Amazon Basin, changes in the biophysical characteristics of the land surface can affect the fluxes of heat and moisture behavior (Jonko et al. 2010). As such, deforestation across the Amazon Basin has made the atmosphere warmer with less moisture and LH, especially during May-Nov. Additionally, the number of extreme

precipitation events increased with deforestation. As expected, many of the patterns in Figures 14-18 generally follow the Arc of Deforestation, but others do not, and this cannot explain observed rainfall changes in other parts of the basin reported in other studies (Espinoza et al. 2019, Haghtalab et al. 2020). Some laterally translated features suggest that land cover creates perturbations that get advected elsewhere, and large patterns also exist that suggest continent/synoptic-scale processes are being modified as a result of deforestation. This suggests complex interactions between climate and LCC that we will explore in future work.

Conclusion

This paper examines the regional-scale impacts of potential reforestation on the energy and moisture budgets and precipitation across the Amazon Basin. Through analysis of changes in regional moisture and heat fluxes, we presented results from regional simulations showing that the land surface and atmosphere are interacting tightly across the basin. We found several principal outcomes. First, the effects of reforestation on the atmosphere were more evident during May-Nov. Second, spatial patterns of the changes in the atmosphere behavior due to reforestation were consistent with the pattern of LCC, with minimal tele-connected impacts. Third, although at the seasonal scale, the changes in SH were minimal, at the monthly scale, it simulated a decrease by 4 W m-2. Forth, mean T_{SK} at the seasonal scale decreased up to 1.2°C, which is consistent with several studies (e.g., Nobre et al. 1991; Snyder et al. 2004; Badger and Dirmeyer 2015). Fifth, reforestation also increased mean monthly LH as much as 50 W m-2 in September in certain areas, while available moisture to the atmosphere increased by 27%. Other studies found equivalent scale results but due to deforestation (e.g., Zhang et al. 1996; Hasler et al. 2009; Badger and Dirmeyer 2015). Sixth, seasonal precipitation increased by 5 mm/day in reforested areas throughout a year, illustrating the causal mechanisms between increased LH and

precipitation and emphasizing the mechanisms identified between wet season start and forest cover (Myneni et al. 2007).

Our results show that by altering the land surface biophysical characteristics— in this case, reforestation— temperature, evaporation fraction, moisture at the surface, and the ratio of LH flux to the SH flux are strongly modified. With a higher proportion of LH, PBL cools down, increases its humidity, and becomes shallower. This further affects the transfer of moisture and energy from the surface to the boundary layer, even influencing transfer to the free atmosphere. Although unavailable, parameters for young moist forests would improve these simulations further. Due to teleconnection mechanisms, changing the exchange of energy and moisture balance between the PBL and the free atmosphere influences tropical convection, impacting the intensity of high-level tropical outflow and providing a mechanism that could affect the extratropics (Snyder et al. 2004). Consequently, changes in the surface fluxes of energy and moisture due to LCC cause impacts beyond the areas of disturbances. Thus, it would be reasonable if deforestation force a disturbance in the general circulation, including the Hadley and Walker-type circulations.

Future work needs to focus on identifying the coupling strength of land cover changes to atmospheric processes to identify areas where rainfall is most sensitive to changes of the land surface and examining the extent to which changes in regional scale can alter the circumstances at the larger scale. Also, different time scales from hourly to daily to monthly evaluations should be considered to distinguish the sensitivity of time-sensitive processes such as cloud formation and convection, which determine the amount and timing of precipitation to reforestation.

APPENDIX

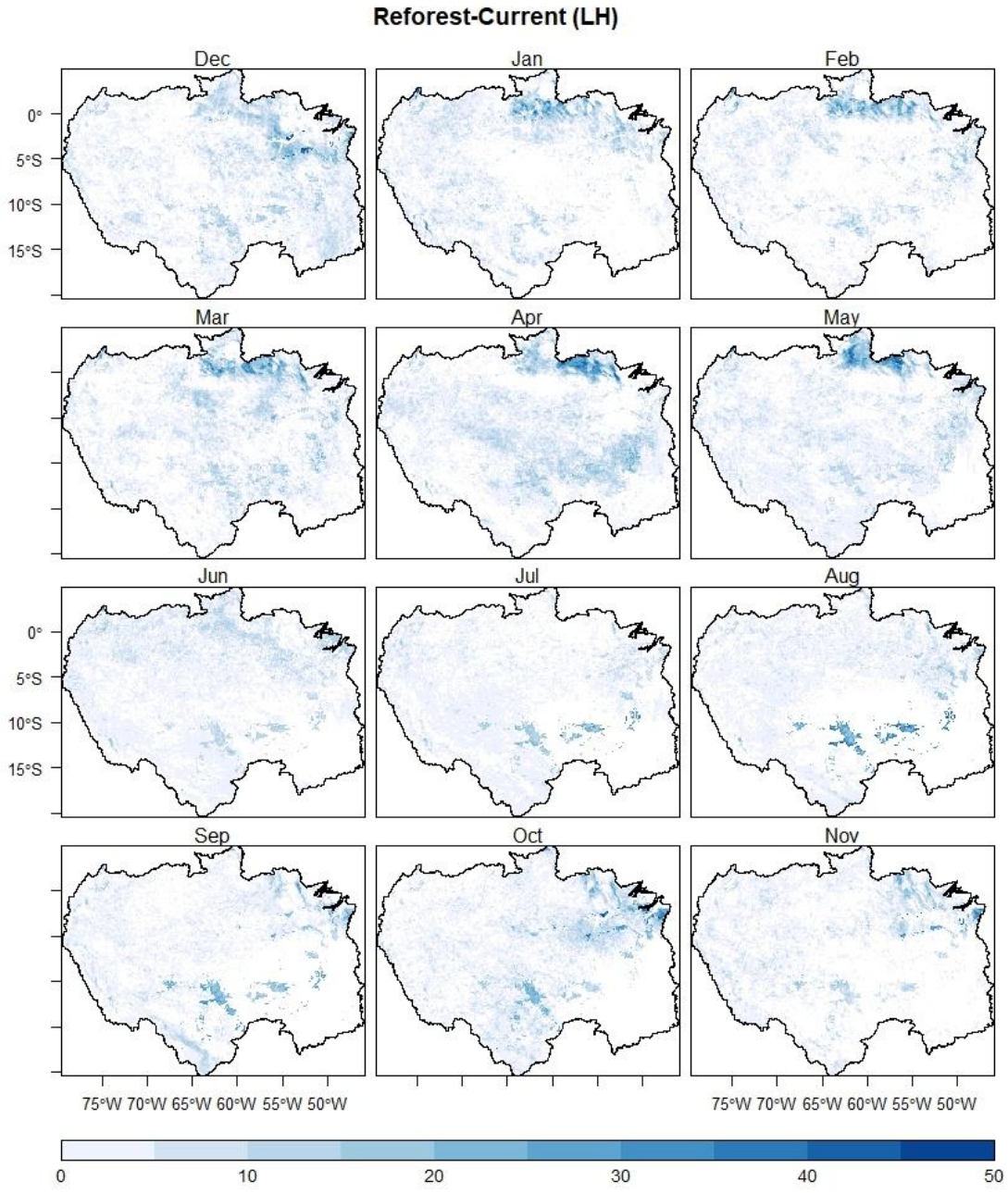

Figure 19. Differences of LH (wm^{-2}) *from control and reforested simulations at monthly timescale.*

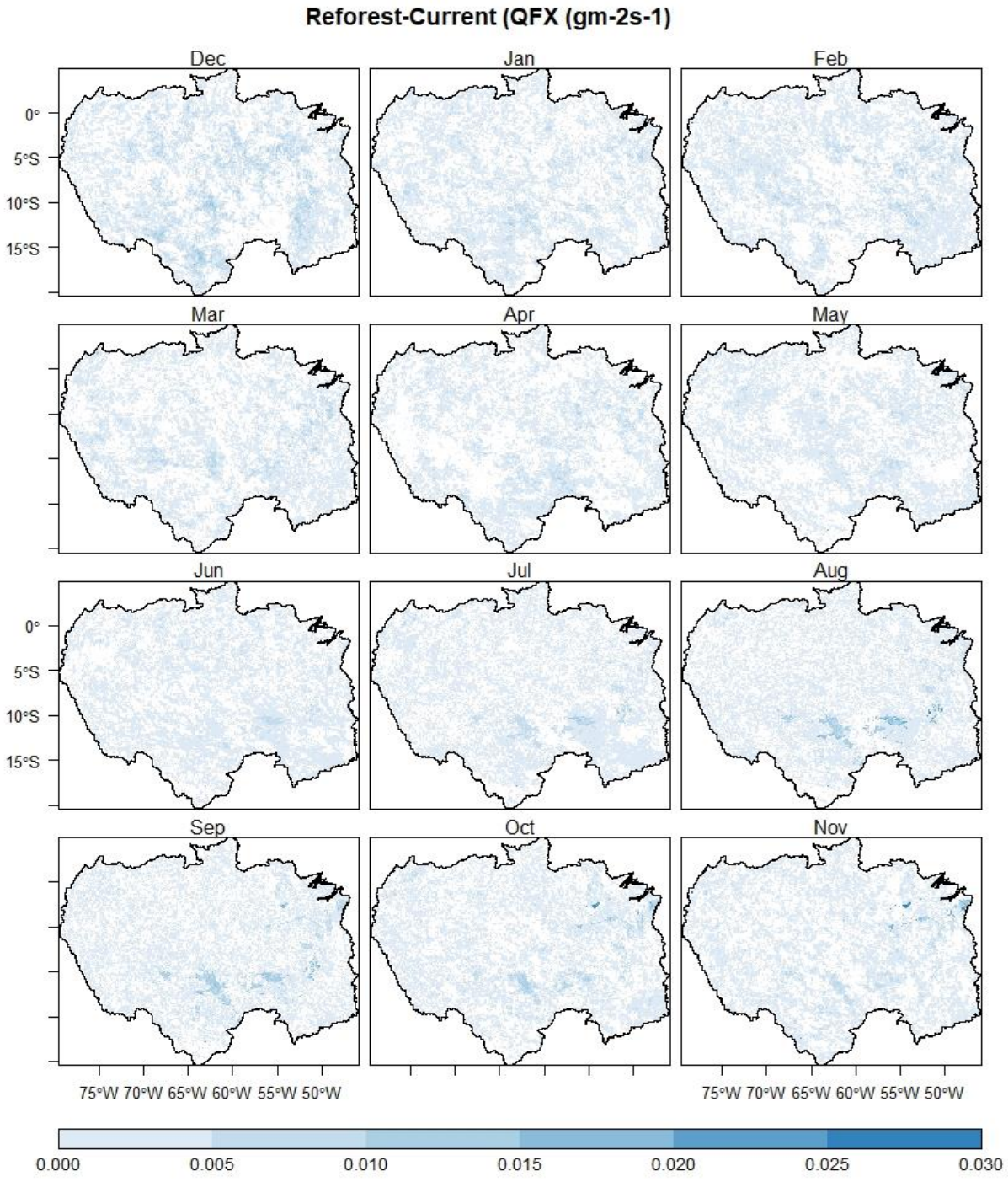

Figure 20. Differences of upward moisture flux (wm^{-2}) *from control and reforested simulations at monthly timescale.*

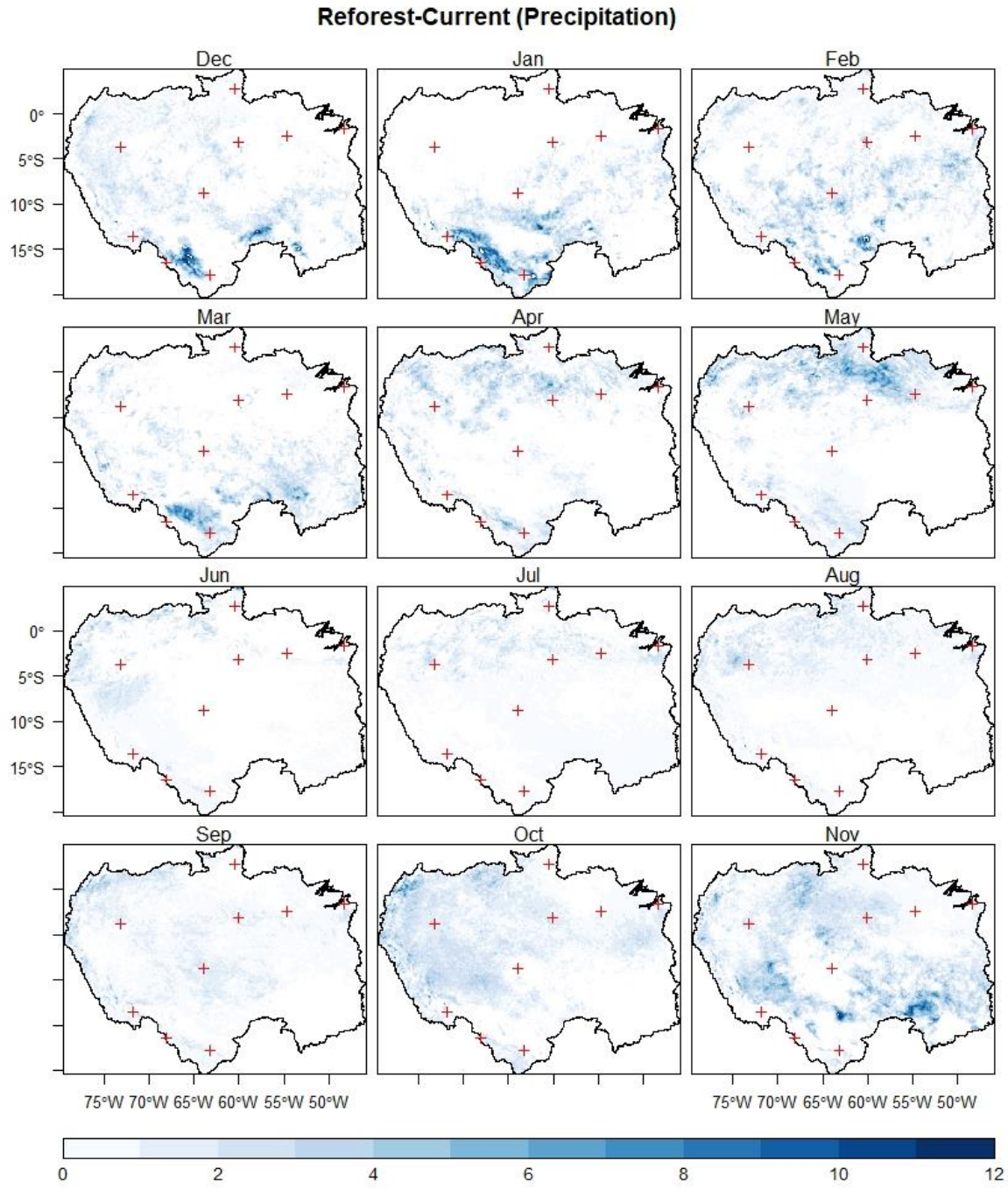

Figure 21. Differences of precipitation (mm) *from control and reforested simulations at monthly timescale.*

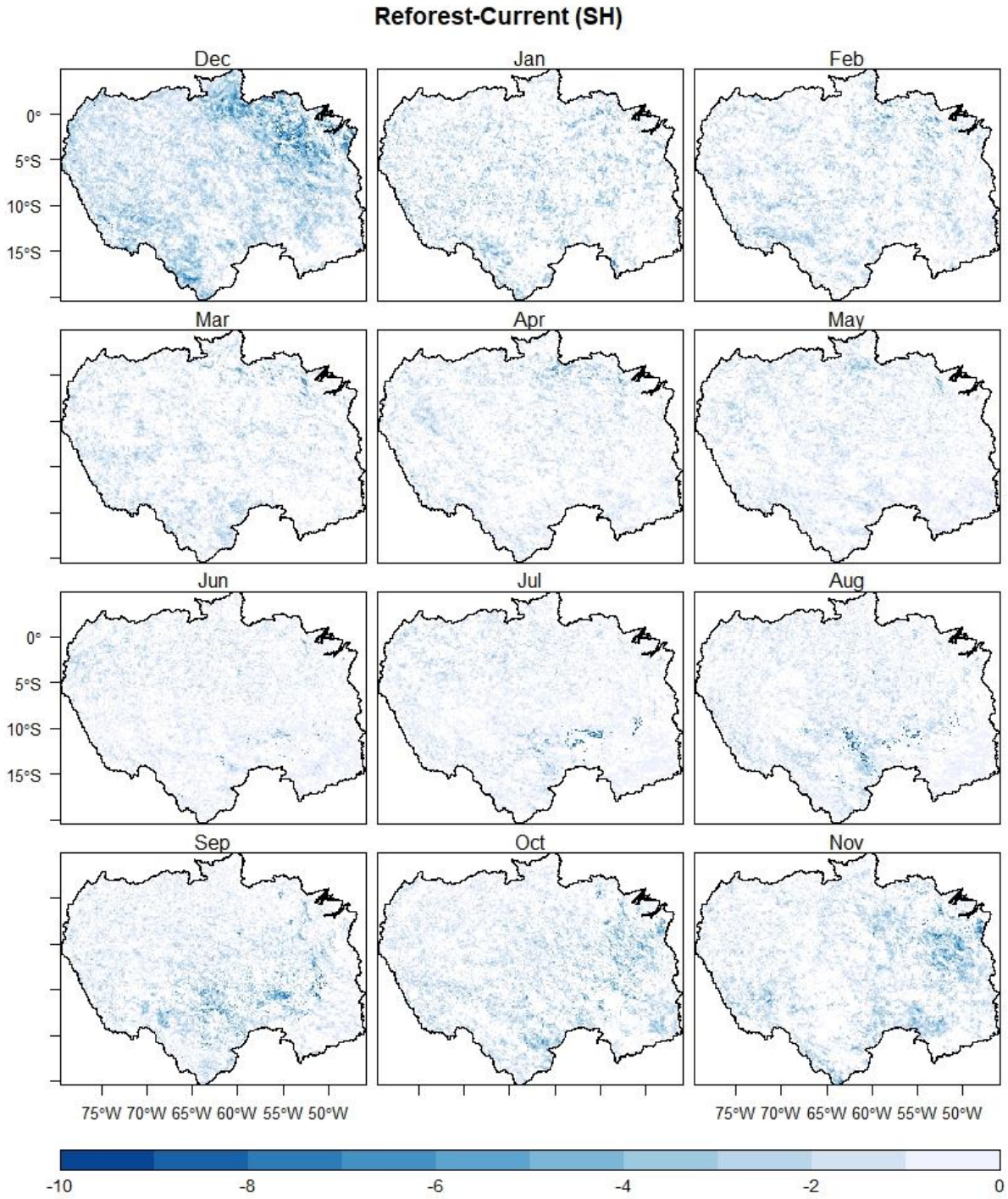

Figure 22. Differences of precipitation (mm) *from control and reforested simulations at monthly timescale.*

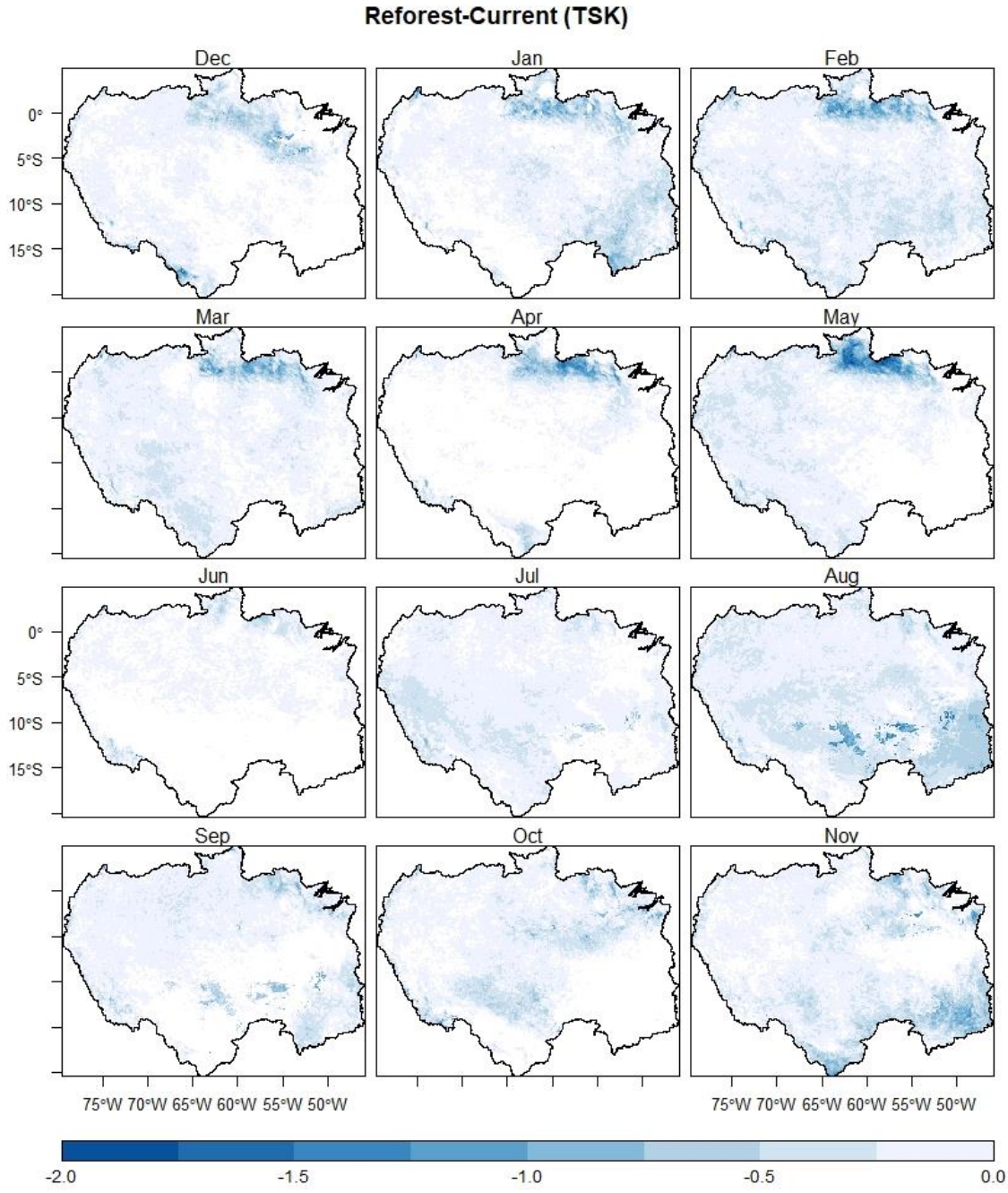

Figure 23. Differences of T_{sk} (ºC) *from control and reforested simulations at monthly timescale.*

REFERENCES

REFERENCES

Alkama, R., and A. Cescatti, 2016: Climate change: Biophysical climate impacts of recent changes in global forest cover. Science (80-.)., 351, 600–604, https://doi.org/10.1126/science.aac8083.

Alton, P., 2009: A simple retrieval of ground albedo and vegetation absorptance from MODIS satellite data for parameterisation of global Land-Surface Models. Agric. For. Meteorol., 149, 1769–1775, https://doi.org/10.1016/j.agrformet.2009.04.012.

Aragão, L. E. O. C., Y. Malhi, N. Barbier, A. Lima, Y. Shimabukuro, L. Anderson, and S. Saatchi, 2008: Interactions between rainfall, deforestation and fires during recent years in the Brazilian Amazonia. Philos. Trans. R. Soc. B Biol. Sci., 363, 1779–1785, https://doi.org/10.1098/rstb.2007.0026.

Avissar, R., and C. A. Nobre, 2002: Preface to special issue on the Large-Scale Biosphere-Atmosphere Experiment in Amazonia (LBA). J. Geophys. Res. D Atmos., 107, 1–2, https://doi.org/10.1029/2002JD002507.

Badger, A. M., and P. A. Dirmeyer, 2015: Climate response to Amazon forest replacement by heterogeneous crop cover. Hydrol. Earth Syst. Sci., 19, 4547–4557, https://doi.org/10.5194/hess-19-4547-2015.

Bagley, J. E., A. R. Desai, P. C. West, and J. A. Foley, 2011: A simple, minimal parameter model for predicting the influence of changing land cover on the land-atmosphere system. Earth Interact., 15, 1–32, https://doi.org/10.1175/2011EI394.1.

——, ——, K. J. Harding, P. K. Snyder, and J. A. Foley, 2014: Drought and deforestation: Has land cover change influenced recent precipitation extremes in the Amazon? J. Clim., 27, 345–361, https://doi.org/10.1175/JCLI-D-12-00369.1.

Baidya Roy, S., and R. Avissar, 2002: Impact of land use/land cover change on regional hydrometeorology in Amazonia. J. Geophys. Res. Atmos., 107, LBA 4-1-LBA 4-12, https://doi.org/10.1029/2000JD000266.

Ban-Weiss, G. A., G. Bala, L. Cao, J. Pongratz, and K. Caldeira, 2011: Climate forcing and response to idealized changes in surface latent and sensible heat. https://doi.org/10.1088/1748-9326/6/3/034032.

Bathiany, S., M. Claussen, V. Brovkin, T. Raddatz, and V. Gayler, 2010: Combined biogeophysical and biogeochemical effects of large-scale forest cover changes in the MPI earth system model. Biogeosciences, 7, 1383–1399, https://doi.org/10.5194/bg-7-1383-2010.

Brando, P. M., S. J. Goetz, A. Baccini, D. C. Nepstad, P. S. A. Beck, and M. C. Christman, 2010: Seasonal and interannual variability of climate and vegetation indices across the Amazon.

Proc. Natl. Acad. Sci., 107, 14685–14690, https://doi.org/10.1073/pnas.0908741107.

Butt, N., P. A. De Oliveira, and M. H. Costa, 2011: Evidence that deforestation affects the onset of the rainy season in Rondonia, Brazil. J. Geophys. Res. Atmos., 116, 2–9, https://doi.org/10.1029/2010JD015174.

Carvalho, L. M. V., C. Jones, B. Liebmann, L. M. V. Carvalho, C. Jones, and B. Liebmann, 2004: The South Atlantic Convergence Zone: Intensity, Form, Persistence, and Relationships with Intraseasonal to Interannual Activity and Extreme Rainfall. J. Clim., 17, 88–108, https://doi.org/10.1175/1520-0442(2004)017<0088:TSACZI>2.0.CO;2.

Case, J. L., W. L. Crosson, S. V Kumar, W. M. Lapenta, and C. D. Peters-Lidard, 2008: Impacts of High-Resolution Land Surface Initialization on Regional Sensible Weather Forecasts from the WRF Model. J. Hydrometeorol., 9, 1249–1266, https://doi.org/10.1175/2008JHM990.1.

Cheng, W. Y. Y., and W. J. Steenburgh, 2005: Evaluation of Surface Sensible Weather Forecasts by the WRF and the Eta Models over the Western United States. Weather Forecast., 20, 812–821, https://doi.org/10.1175/WAF885.1.

Coe, M. T., M. H. Costa, A. Botta, and C. Birkett, 2002: Long-term simulations of discharge and floods in the Amazon Basin. J. Geophys. Res., 107, 8044, https://doi.org/10.1029/2001JD000740.

Costa, M. H., and G. F. Pires, 2010: Effects of Amazon and Central Brazil deforestation scenarios on the duration of the dry season in the arc of deforestation. Int. J. Climatol., 30, 1970–1979, https://doi.org/10.1002/joc.2048.

D'almeida, C., C. J. Vörösmarty, G. C. Hurtt, J. A. Marengo, S. L. Dingman, and B. D. Keim, 2007: The effects of deforestation on the hydrological cycle in Amazonia: a review on scale and resolution. Int. J. Climatol. Int. J. Clim., 27, 633–647, https://doi.org/10.1002/joc.1475.

Davidson, E. A., and Coauthors, 2012: The Amazon basin in transition. Nature, 481, 321–328, https://doi.org/10.1038/nature10717.

Davin, E. L., and N. de Noblet-Ducoudre, 2010: Climatic impact of global-scale Deforestation: Radiative versus nonradiative processes. J. Clim., 23, 97–112, https://doi.org/10.1175/2009JCLI3102.1.

Devaraju, N., G. Bala, and R. Nemani, 2015: Modelling the influence of land-use changes on biophysical and biochemical interactions at regional and global scales. Plant, Cell Environ., 38, 1931–1946, https://doi.org/10.1111/pce.12488.

Dickinson, R. E., and P. Kennedy, 1992: Impacts on regional climate of Amazon deforestation. Geophys. Res. Lett., 19, 1947–1950, https://doi.org/10.1029/92GL01905.

Dirmeyer, P. A., 2002: An Evaluation of the Strength of Land–Atmosphere Coupling. J. Hydrometeorol., 2, 329–344, https://doi.org/10.1175/1525-

7541(2001)002<0329:aeotso>2.0.co;2.

Espinoza, J. C., S. Chavez, J. Ronchail, C. Junquas, K. Takahashi, and W. Lavado, 2015: Rainfall hotspots over the southern tropical Andes: Spatial distribution, rainfall intensity, and relations with large-scale atmospheric circulation. Water Resour. Res., 51, 3459–3475, https://doi.org/10.1002/2014WR016273.

Fu, R., R. E. Dickinson, M. Chen, H. Wang, R. Fu, R. E. Dickinson, M. Chen, and H. Wang, 2001: How Do Tropical Sea Surface Temperatures Influence the Seasonal Distribution of Precipitation in the Equatorial Amazon? J. Clim., 14, 4003–4026, https://doi.org/10.1175/1520-0442(2001)014.

——, and Coauthors, 2013: Increased dry-season length over southern Amazonia in recent decades and its implication for future climate projection. Proc. Natl. Acad. Sci. U. S. A., 110, 18110–18115, https://doi.org/10.1073/pnas.1302584110.

Ge, J., J. Qi, B. M. Lofgren, N. Moore, N. Torbick, and J. M. Olson, 2007: Impacts of land use/cover classification accuracy on regional climate simulations. J. Geophys. Res., 112, D05107, https://doi.org/10.1029/2006JD007404.

Haghtalab, N., N. Moore, B. P. Heerspink, and D. W. Hyndman, 2020: Evaluating spatial patterns in precipitation trends across the Amazon basin driven by land cover and global scale forcings. Theor. Appl. Climatol., 140, 411–427, https://doi.org/10.1007/s00704-019-03085-3.

Hasler, N., D. Werth, and R. Avissar, 2009: Effects of tropical deforestation on global hydroclimate: A multimodel ensemble analysis. J. Clim., 22, 1124–1141, https://doi.org/10.1175/2008JCLI2157.1.

Henderson-Sellers, A., and V. Gornitz, 1984: Possible climatic impacts of land cover transformations, with particular emphasis on tropical deforestation. Clim. Change, 6, 231–257, https://doi.org/10.1007/BF00142475.

Huete, A. R., and Coauthors, 2006: Amazon rainforests green-up with sunlight in dry season. Geophys. Res. Lett., 33, L06405, https://doi.org/10.1029/2005GL025583.

Jankov, I., W. A. Gallus, M. Segal, B. Shaw, and S. E. Koch, 2005: The Impact of Different WRF Model Physical Parameterizations and Their Interactions on Warm Season MCS Rainfall. Weather Forecast., 20, 1048–1060, https://doi.org/10.1175/WAF888.1.

Jonko, A. K., A. Hense, and J. J. Feddema, 2010: Effects of land cover change on the tropical circulation in a GCM. Clim. Dyn., 35, 635–649, https://doi.org/10.1007/s00382-009-0684-7.

Khanna, J., D. Medvigy, S. Fueglistaler, and R. Walko, 2017: Data for Nature Climate Change article “Regional dry-season climate changes due to three decades of Amazonian deforestation.”

Kumagai, T., and A. Porporato, 2012: Drought-induced mortality of a Bornean tropical rain forest amplified by climate change. J. Geophys. Res. Biogeosciences, 117, https://doi.org/10.1029/2011JG001835.

Lee, S.-J., E. H. Berbery, S.-J. Lee, and E. H. Berbery, 2012: Land Cover Change Effects on the Climate of the La Plata Basin. J. Hydrometeorol., 13, 84–102, https://doi.org/10.1175/JHM-D-11-021.1.

Li, W., and R. Fu, 2004: Transition of the Large-Scale Atmospheric and Land Surface Conditions from the Dry to the Wet Season over Amazonia as Diagnosed by the ECMWF Re-Analysis. J. Clim., 17, 2637–2651, https://doi.org/10.1175/1520-0442(2004)017<2637:TOTLAA>2.0.CO;2.

Mahmood, R., and Coauthors, 2014: Land cover changes and their biogeophysical effects on climate. Int. J. Climatol., 34, 929–953, https://doi.org/10.1002/joc.3736.

Malhi, Y., and Coauthors, 2006: The regional variation of aboveground live biomass in old-growth Amazonian forests. Glob. Chang. Biol., 12, 1107–1138, https://doi.org/10.1111/j.1365-2486.2006.01120.x.

Marengo, J. A., 2004: Interdecadal variability and trends of rainfall across the Amazon basin. Theor. Appl. Climatol., 78, 79–96, https://doi.org/10.1007/s00704-004-0045-8.

Marengo, J. A., and Coauthors, 2008: The Drought of Amazonia in 2005. J. Clim., 21, 495–516, https://doi.org/10.1175/2007JCLI1600.1.

Medvigy, D., R. L. Walko, R. Avissar, D. Medvigy, R. L. Walko, and R. Avissar, 2011: Effects of Deforestation on Spatiotemporal Distributions of Precipitation in South America. J. Clim., 24, 2147–2163, https://doi.org/10.1175/2010JCLI3882.1.

Moore, N., E. Arima, R. Walker, and R. Ramos da Silva, 2007: Uncertainty and the changing hydroclimatology of the Amazon. Geophys. Res. Lett., 34, L14707, https://doi.org/10.1029/2007GL030157.

Myneni, R. B., and Coauthors, 2007: Large seasonal swings in leaf area of Amazon rainforests. Proc. Natl. Acad. Sci. U. S. A., 104, 4820–4823, https://doi.org/10.1073/pnas.0611338104.

Nobre, C. A., P. J. Sellers, and J. Shukla, 1991: Amazonian Deforestation and Regional Climate Change. J. Clim., 4, 957–988, https://doi.org/10.1175/1520-0442(1991)004<0957:ADARCC>2.0.CO;2.

Nobre, P., M. Malagutti, D. F. Urbano, R. A. F. De Almeida, and E. Giarolla, 2009: Amazon deforestation and climate change in a coupled model simulation. J. Clim., 22, 5686–5697, https://doi.org/10.1175/2009JCLI2757.1.

Oliveira, P. T. S., M. A. Nearing, M. S. Moran, D. C. Goodrich, E. Wendland, and H. V. Gupta, 2014: Trends in water balance components across the Brazilian Cerrado. Water Resour. Res., 50, 7100–7114, https://doi.org/10.1002/2013WR015202.

Paccini, L., J. C. Espinoza, J. Ronchail, and H. Segura, 2018: Intra-seasonal rainfall variability in the Amazon basin related to large-scale circulation patterns: a focus on western Amazon–Andes transition region. Int. J. Climatol., 38, 2386–2399, https://doi.org/10.1002/joc.5341.

Phillips, O. L., and Coauthors, 2009: Drought sensitivity of the amazon rainforest. Science (80-.)., 323, 1344–1347, https://doi.org/10.1126/science.1164033.

Pielke, R. A., and Coauthors, 2011: Land use/land cover changes and climate: modeling analysis and observational evidence. Wiley Interdiscip. Rev. Clim. Chang., 2, 828–850, https://doi.org/10.1002/wcc.144.

Pitman, A. J., 2003: The evolution of, and revolution in, land surface schemes designed for climate models. Int. J. Climatol., 23, 479–510, https://doi.org/10.1002/joc.893.

——, and Coauthors, 2009: Uncertainties in climate responses to past land cover change: First results from the LUCID intercomparison study. Geophys. Res. Lett., 36, 1–6, https://doi.org/10.1029/2009GL039076.

Réveillet, M., S. MacDonell, S. Gascoin, C. Kinnard, S. Lhermitte, and N. Schaffer, 2020: Impact of forcing on sublimation simulations for a high mountain catchment in the semiarid Andes. Cryosph., 14, 147–163, https://doi.org/10.5194/tc-14-147-2020.

Richey, J. E., C. Nobre, and C. Deser, 1989: Amazon River discharge and climate variability: 1903 to 1985. Science (80-.)., 246, 101–103, https://doi.org/10.1126/science.246.4926.101.

Ruiz, J. J., C. Saulo, and J. Nogués-Paegle, 2010: WRF Model Sensitivity to Choice of Parameterization over South America: Validation against Surface Variables. Mon. Weather Rev., 138, 3342–3355, https://doi.org/10.1175/2010MWR3358.1.

Saatchi, S. S., R. A. HOUGHTON, R. C. DOS SANTOS ALVALÁ, J. V. SOARES, and Y. YU, 2007: Distribution of aboveground live biomass in the Amazon basin. Glob. Chang. Biol., 13, 816–837, https://doi.org/10.1111/j.1365-2486.2007.01323.x.

Saleska, S. R., K. Didan, A. R. Huete, and H. R. da Rocha, 2007: Amazon Forests Green-Up During 2005 Drought. Science (80-.)., 318, 612–612, https://doi.org/10.1126/science.1146663.

Schneider, E. K., M. Fan, B. P. Kirtman, and P. A. Dirmeyer, 2006: Potential Effects of Amazon Deforestation on Tropical Climate. 1–29.

Sertel, E., A. Robock, and C. Ormeci, 2010: Impacts of land cover data quality on regional climate simulations. Int. J. Climatol., 30, 1942–1953, https://doi.org/10.1002/joc.2036.

Shukla, J., and Coauthors, Influence of Land-Surface Evapotranspiration on the Earth's Climate. Science,.

Silva Dias, M. A., R. Avissar, and P. Silva Dias, 2009: Modeling the Regional and Remote Climatic Impact of Deforestation. Amazonia and Global Change, 251–260.

Silva Dias, M. A. F. F., and Coauthors, 2002: Cloud and rain processes in a biosphere-atmosphere interaction context in the Amazon Region. J. Geophys. Res. D Atmos., 107, 8072, https://doi.org/10.1029/2001JD000335.

da Silva, R. R., and R. Avissar, 2006: The hydrometeorology of a deforested region of the amazon basin. J. Hydrometeorol., 7, 1028–1042, https://doi.org/10.1175/JHM537.1.

——, D. Werth, and R. Avissar, 2008a: Regional impacts of future land-cover changes on the Amazon basin wet-season climate. J. Clim., 21, 1153–1170, https://doi.org/10.1175/2007JCLI1304.1.

——, ——, ——, R. R. da Silva, D. Werth, and R. Avissar, 2008b: Regional impacts of future land-cover changes on the Amazon basin wet-season climate. J. Clim., 21, 1153–1170, https://doi.org/10.1175/2007JCLI1304.1.

Silvério, D. V., P. M. Brando, M. N. Macedo, P. S. A. Beck, M. Bustamante, and M. T. Coe, 2015: Agricultural expansion dominates climate changes in southeastern Amazonia: The overlooked non-GHG forcing. Environ. Res. Lett., 10, 104015, https://doi.org/10.1088/1748-9326/10/10/104015.

Snyder, P. K., C. Delire, and J. A. Foley, 2004: Evaluating the influence of different vegetation biomes on the global climate. Clim. Dyn., 23, 279–302, https://doi.org/10.1007/s00382-004-0430-0.

Sombroek, W., 2001: Spatial and Temporal Patterns of Amazon Rainfall. AMBIO A J. Hum. Environ., 30, 388–396, https://doi.org/10.1579/0044-7447-30.7.388.

Souza, E. P., N. O. Renno, and M. A. F. S. Dias, 2000a: Convective circulations induced by surface heterogeneities. J. Atmos. Sci., 57, 2915–2922, https://doi.org/10.1175/1520-0469(2000)057<2915:CCIBSH>2.0.CO;2.

Souza, E. P., N. O. Rennó, M. A. F. S. Dias, E. P. Souza, N. O. Rennó, and M. A. F. S. Dias, 2000b: Convective Circulations Induced by Surface Heterogeneities. https://doi.org/10.1175/1520-0469(2000)057<2915:CCIBSH>2.0.CO;2.

Spera, S. A., G. L. Galford, M. T. Coe, M. N. Macedo, and J. F. Mustard, 2016: Land-use change affects water recycling in Brazil's last agricultural frontier. Glob. Chang. Biol., 22, 3405–3413, https://doi.org/10.1111/gcb.13298.

Vera, C., G. Silvestri, B. Liebmann, and P. González, 2006: Climate change scenarios for seasonal precipitation in South America from IPCC-AR4 models. Geophys. Res. Lett, 33, 13707, https://doi.org/10.1029/2006GL025759.

Walker, R., N. J. Moore, E. Arima, S. Perz, C. Simmons, M. Caldas, D. Vergara, and C. Bohrer, 2009: Protecting the Amazon with protected areas. Proc. Natl. Acad. Sci. U. S. A., 106, 10582–10586, https://doi.org/10.1073/pnas.0806059106.

Wang, J., R. L. Bras, E. A. B. Eltahir, J. Wang, R. L. Bras, and E. A. B. Eltahir, 2000: The

Impact of Observed Deforestation on the Mesoscale Distribution of Rainfall and Clouds in Amazonia. http://dx.doi.org/10.1175/1525-7541(2000)001<0267:TIOODO>2.0.CO;2, https://doi.org/10.1175/1525-7541(2000)001<0267:TIOODO>2.0.CO;2.

——, and Coauthors, 2009: Impact of deforestation in the Amazon basin on cloud climatology. Proc. Natl. Acad. Sci. U. S. A., 106, 3670–3674, https://doi.org/10.1073/pnas.0810156106.

Werth, D., and R. Avissar, 2002: The local and global effects of Amazon deforestation. J. Geophys. Res., 107, 8087, https://doi.org/10.1029/2001JD000717.

Wright, J. S., R. Fu, J. R. Worden, S. Chakraborty, N. E. Clinton, C. Risi, Y. Sun, and L. Yin, 2017: Rainforest-initiated wet season onset over the southern Amazon. Proc. Natl. Acad. Sci. U. S. A., 114, 8481–8486, https://doi.org/10.1073/pnas.1621516114.

Xu, L., A. Samanta, M. H. Costa, S. Ganguly, R. R. Nemani, and R. B. Myneni, 2011: Widespread decline in greenness of Amazonian vegetation due to the 2010 drought. Geophys. Res. Lett., 38, n/a-n/a, https://doi.org/10.1029/2011GL046824.

Zeng, N., R. E. Dickinson, and X. Zeng, 1996: Climatic impact of Amazon deforestation - A mechanistic model study. J. Clim., 9, 859–883.

Zhang, H., K. McGuffie, and A. Henderson-Sellers, 1996: American Meteorological Society Impacts of Tropical Deforestation . Part II : The Role of Large-Scale Dynamics Author (s): H . Zhang , K . McGuffie and A . Henderson-Sellers Published by : American Meteorological Society Stable URL : https://www.jstor.o. J. Clim., 9, 2498–2521.

Zhu, Y., R. H. Zong, and T. Y. Zhang, 2019: Deforestation effects on land surface energy coupling: A data-driven perspective. E3S Web Conf., 96, 8–11, https://doi.org/10.1051/e3sconf/20199602001.

CHAPTER 4. MULTIVARIATE PREDICTORS OF SOIL MOISTURE - PRECIPITATION COUPLING AT THE REGIONAL SCALE

in collaboration with
Nathan Moore

Introduction

Land surface-atmosphere (L-A) interaction is defined as the extent to which perturbations in the land surface state can affect the planetary boundary layer (PBL) through its effects on turbulent surface fluxes (Betts 2009). Soil moisture is a critical component of L-A interactions. It is the most important land surface parameter that influences the variability of the atmosphere at the seasonal to sub-seasonal temporal scale (Zhang et al. 2008). Soil moisture influences the surface energy and water balance components by influencing evapotranspiration (ET) and latent heat flux (LH) (Zhang et al. 2011). Therefore, precipitation anomalies can be attributed to soil moisture anomalies through alteration of land surface fluxes (Schlosser and Milly 2002). For instance, higher evaporation can be produced with a wetter soil that can result in more precipitation due to higher local recycling and its effects on larger scale circulations leading to strong soil moisture feedbacks (Koster et al. 2000; Dirmeyer and Brubaker 2007; Zhang et al 2008), and through enhancing the vegetation breeze (e.g., Medvigy et al. 2011).

The interaction between soil moisture and precipitation is straightforward, but the feedback path from soil moisture to precipitation is complicated and hard to measure (Seneviratne et al. 2010) as it has both direct and indirect effects (Guillod et al. 2015). Indirect effects include altering the planetary boundary condition, modification of circulation patterns, and influences of the soil moisture from outside of the region, while direct effects include the ones related to moisture recycle over the region (Goessling and Reick 2011). Also, soil moisture can control the evolution of heavy rainfall and extreme precipitation events. For instance, Sorensson and

Menendez (2011) reported that in western North America, land surface characteristics control the persistence of extreme rainy days indicating that feedbacks between the occurrence of heavy rainfall and soil moisture can be either positive or negative depending on the region.

Early studies of soil moisture-atmosphere interactions started in the 1980s (e.g., (Shukla and Mintz 1982; Yeh et al. 1984) showing significant climate sensitivities to ET and soil moisture anomalies. However after 2000, major advances occurred such as multi-model studies (e.g., Guo et al. 2006; Koster et al. 2006; Seneviratne et al. 2006; Koster et al. 2009; Pitman et al. 2009; Koster et al. 2010); observational and in situ measurements (e.g., Findell and Eltahir 1997; Baldocchi and Xu 2007); new remotely sensed measurements (e.g., Tapley et al. 2004; Owe et al. 2008; Jeu et al. 2008); and new diagnostic approaches (e.g., Chen and Dirmeyer 2016; Devanand et al. 2020).

Global circulation models (GCMs) have coarse grid spacings, and this particularly affects how precipitation forcing is simulated which may cause problems in the representation of the parameters across scales (Dirmeyer et al. 2018). GCM results retain large uncertainties in the analysis of L-A interactions, especially when downscaled to regional and local scales (Pitman et al. 2009; Wei et al. 2010). For example, the GLACE (Global Land-Atmosphere Coupling Experiment) demonstrated the spatial distribution of coupling strength of soil moisture-atmosphere coupling through dozens of GCM models and multidimensional average distributions of L-A coupling strength (Koster et al. 2004, Guo et al. 2006). However, GLACE experiments have systematic errors as compared with observed interactions between land and atmosphere at the local to regional scales (e.g., Dirmeyer et al. 2006). Also, Wei et al. (2010) suggested that those GCMs in GLACE may overestimate L-A coupling strength on a globally averaged basis due to exhibit too much variance at intra-seasonal scales at lower latitudes.

Besides, the lack of large-scale observational assessments of L-A coupling is still a major challenge in assessing models' performance (Gue et al. 2006; Santanello et al. 2011).

The regional climate regime is an important determinant factor in soil moisture-atmosphere feedbacks. For instance, GLACE found that transitional zones between dry and wet climates exhibit a strong L-A coupling during boreal summer (Koster et al. 2004; Koster et al. 2006; Guo et al. 2006). However, with the coarse resolution and simple parametrization of the GCMs, they could only provide limited information on L-A coupling strength at scales smaller than global (Dirmeyer et al. 2006). Zhang et al. (2008) used observations to examine L-A coupling strength in the northern hemisphere during boreal summer. They found strong coupling over transitional zones from arid to semiarid or from semi-humid forest to grassland. In a similar study, Dirmeyer et al. (2018) validated model representation of surface fluxes and L-A at the global scale against flux tower observations. They found that coupling strength is highly dependent on model parameterization and uncertainty in observations.

L-A coupling and feedbacks across the tropics have been showing very high uncertainty (A. K. Betts and Silva Dias 2010). Given the land surface state being the main driver of climate variability in the tropics (Zeng and Neelin 1999), precise measurement of this coupling remains elusive. Lack of observational data and consistent model parametrization have hampered the precise measuring of L-A coupling strength.

Many metrics have been used to assess L-A coupling. However, the two most commonly used metrics are the GLACE variance-based metric (Koster et al. 2002) and the correlation-based metric (Dirmeyer et al. 2018). These metrics measure the effects of soil moisture on the evolution and variability of precipitation considering state variables, boundary conditions, and fluxes. Other available metrics consider feedbacks among factors other than soil moisture-

precipitation such as soil moisture-temperature (Miralles et al. 2014), a coupling drought index based on interactions between temperature and humidity (Roundy et al. 2014), or conditional correlation focused on soil moisture memory and 21 days total precipitation (Mei and Wang 2012). Despite sophisticated LSMs in climate models, some critical relationships and parameters are not well understood at fine resolutions. Therefore, it is essential to quantify the L-A coupling strength at a fine spatial resolution (Dirmeyer et al. 2018). For example, the water holding capacity of soil which is a key parameter of L-A coupling (e.g., Milly and Dunne 1994) is highly variable among climate models (Seneviratne et al. 2006a) or is missing in the diagnoses metrics (Jach et al. 2020).

Quantitative analysis of L-A coupling strength at a fine spatial resolution for the Amazon basin is rare. While Wang et al. (2020) analyzed the sensitivity of the WRF model to parameter perturbation in modeling hot spots of coupling at the daily time scale and 50 km spatial resolution for the amazon basin, we examine the sensitivity of spatial pattern of hot spots at regional spatial scale to commonly used metrics at monthly time scales over 10 years. Ultimately, we develop a multivariable metric of L-A coupling measurement for the Amazon basin. To do this, we will quantify soil moisture-precipitation (SM-P) coupling strength by applying two popular L-A coupling measurement metrics (GLACE-type and correlation-based) at the regional scale, to provide a theoretical analysis of underlying processes. Then, by finding the key variables and their interactions in L-A coupling, we will suggest a new metric to find the hot spots of L-A coupling at a monthly time scale. To do this, 10 years of climate simulations (2005-2015) have been performed using WRF V3.9 (The Weather Research and Forecasting model; Skamarock et al. 2008) for the Amazon Basin. The first section focuses on measuring the coupling strength of L-A interactions using diagnostic metrics. Next, we analyze the physical

relationships and processes controlling L-A interactions on hot spots of coupling. We also look for insights in developing a new metric considering more physical relationships, interactions, and lag times between variables. The outcome of this paper will provide a detailed analysis of the effects of scale and complexity in L-A coupling measurement.

Materials and Methods

Simulation set-up

The simulation domain covers the entire Amazon Basin in South America. WRFV3.9 is forced by the ERA_Interim boundary condition at 0.5 ^{o} x 0.5^{o} spatial resolution and 6h temporal resolution. Two sets of experiments are designed to address the research questions. The control experiment (CLT) is set to run from 2005 to 2015 using Noah LSM. In this experiment, soil moisture interacts with the atmosphere actively. In the No-Soil-Moisture experiment (NSM) the soil moisture is not interacting with the atmosphere (following the GLACE experiment). Simulations are initialized at 00:00 UTC and each year started independently. Each first 15 days period is omitted as spin-up. Early trials using longer spin-up proved to be computationally expensive and unlikely to significantly affect the results. The horizontal grid spacing is 16 km, with 38 levels of vertical levels up to 1000 m. The thickness of the lowest atmospheric layer is about 50 m on smooth topography. At this resolution, cumulus parameterization is necessary to resolve convection, clouds, and precipitation properly (Bagley et al. 2011). The model uses WSM6 (Hong and Leetmaa 1999) as its MP-physics scheme, Yonsei University scheme as a PBL, MM5 scheme for Surface layer, and Kain–Fritsch scheme for cumulus parameterization. Figure 10 shows the simulation domain.

Land-atmosphere coupling metrics

In this study, we aim to evaluate the spatial patterns of two available L-A coupling measuring metrics. These metrics have been developed and applied at a global scale using reanalysis data and GCMs simulations. Here we will apply them at the regional scale across the Amazon Basin to qualitatively examine the extent to which these metrics show similar behavior across scales.

A: Variance based metric

The GLACE experiments were designed to examine and quantify the strength of L-A coupling using dozens of GCMs. The goal was to evaluate the degree to which atmosphere and precipitation generations are influenced by soil moisture anomalies (Koster et al, 2002). Following their methodology, two sets of experiments were designed. Control (CNL) experiment consists of 10 years (2005-2015) of simulations with interactive soil moisture. In No-Soil-Moisture (NSM) experiment we removed the soil moisture interaction by using the simplest LSM. The data are aggregated in monthly values for all 10 years.

To quantify the degree of "similarity" between two time series of precipitation, first, we calculate monthly totals of precipitation (P), at each grid cell, which provides 10 monthly totals. Then we calculate the annual average of precipitation for each grid cell (P). Then for each time period n,

$$\hat{P}_n = 1/10 \sum_{i=1}^{12} P\,ni \quad , \qquad (1)$$

Where P is monthly totals of precipitation, $\hat{P}$ denotes the average of monthly totals over 10 years of simulations. Then the variance of P across all years (δ^2p) and variance of $\hat{P}$ across all time periods ($\delta^2\hat{P}$) is calculated. Finally, we measure the time series similarity at each grid cell by calculating Ωp.

$$\Omega p = \frac{10\delta 2\hat{P} - \delta 2p}{9\delta 2p} \qquad (2)$$

If each year produces the same time series of P, then δ^2p equals $\delta^2\hat{P}$ and Ωp will be 1. Ωp varies from 0 to 1, with values approaches 1 indicating a greater degree of precipitation similarity.

By repeating the calculation using the NSM experiment, we are able to calculate the coupling strength for each grid cell.

$$I_G = \Omega p\ (NSM) - \Omega p\ (CNL) \qquad (3)$$

Where Ωp (CNL) represents the similarity in precipitation time series induced by all factors, while Ωp (NSM) represents the similarity induced by everything but land surface states, and I_G denotes the GLACE-based index. This gives us the first-order indication of influences of soil moisture on the evolution of the atmosphere and fraction of variance explained by the prescription of subsurface soil moisture variables.

B: Correlation-based metric

Studies have shown that near-surface humidity, temperature, and growth of boundary layer influence the effects of SM anomalies on the lower atmosphere (Betts et al. 2004; Conil et al. 2007; Zhang et al. 2011b). Dirmeyer (2011) introduced a new correlation-based index to quantify the strength of L-A coupling. They hypothesized that analyzing correlations between the terrestrial leg of the coupling -i.e., land surface state variables and surface fluxes- and between the atmospheric leg of the coupling – i.e., surface fluxes and atmospheric state – may represent the feedback. For example, a positive correlation between soil moisture and LH (terrestrial leg) shows that soil moisture controls flux variability indicating a moisture limited state as opposed to an energy-limited state. Since the interactions between land and atmospheric variables are highly complex to be measured by using simplistic linear correlations, statistical coupling indices have

been introduced to measure the strength of effects of causally related variables within the land-atmosphere system (Devanand et al 2020). These indices will quantify the "sensitivity" or "strength" of L-A coupling. Here we quantify the strength of L-A coupling using two-legged coupling metrics following previous studies (e.g. Dirmeyer, 2011; Dirmeyer et al., 2018, Devanand et al. 2020) using variables of CNL simulation only. To quantitatively measure the strength of the atmospheric and terrestrial segments of the L-A feedback, these metric uses correlations between atmospheric states, surface fluxes, and land surface states. Surface fluxes are the driving variables, and the atmospheric state is the response variable in the atmospheric segment. Whereas, in the terrestrial segment of the coupling, the driving variable will be the land surface state and the surface fluxes are the response variables. The variance will be incorporated into the driving variables to make sure it has adequate variability in time to propagate the change in the response variables.

$$I = \sigma(a)\frac{db}{da} = r(a,b)\sigma(b) \qquad (4)$$

Where *I* denotes the coupling index, a is the driving variable and b is the response variable, σ is the standard deviation of the variable in time, r is the correlation in time, and $\frac{db}{da}$ is the slope of the linear regression fit line describing "b" dependent on "a" (Dirmeyer et al. 2018). We calculated these indices using daily values grouped in a month for 10 years of simulations. Indices are shown at a 95% significant level. We used multiple terrestrial coupling indices that employ daily soil moisture in the top 10 cm soil layer as the driving variable and LH, SH, Upward Moisture Flux (QFX), and specific humidity (SpH) as the response variables. To calculate the strength of the atmospheric segment, we used SH and LH as the forcing variables and precipitation (prcp) as the response variables.

C: Multivariable predictor of hot spots of strong coupling

To find key variables and their interactions in L-A coupling, we conducted multivariable stepwise regression of 7 variables involved in L-A interactions within the boundary layer, considering their interactions and lag times to identify novel relationships that might warrant further relationship. Here is the model in R:

$$Prcp \sim SH + LH + QFX + SpH + T2 + SM + prcp\text{-}21 + LH{:}SM + SM{:}prcp\_21 + LH{:}prcp\_21 + SH{:}T2 + SH{:}LH \quad (5)$$

Where prcp_21 represents accumulated rainfall in the past 21 days, SM:prcp_21 term indicates the interaction between the past 21 days accumulated rainfall and mean monthly soil moisture per day for that month to represent the lag time effect on precipitation variability. 21-day soil moisture memory is defined based on Wei et al. (2008) analysis which indicates that for the topsoil layer, the optimal soil moisture memory is 21 days. Only significant values ($P<0.05$ and R^2 >90%) are considered. Then, we applied models for each month to calculate the hot spots in the basin using aggregated monthly values of CNL simulation.

Results

A:Variance based metric

Figure 19 shows a spatial distribution of the coupling index (I_G) following GLACE. A higher value of the coupling index shows stronger feedback in the system indicating that soil moisture controls the evolution of the atmosphere in the areas of strong coupling. The response of the surface fluxes to the imposed surface states is one explanation of widespread low I_G. Low values indicate that precipitation is controlled more by atmosphere dynamics than land conditions. The coupling is inconsistently evident in the arc of deforestation and the transitional zone between Cerrado and forest. While the GLACE experiment located the strong hot spots of coupling on the

areas far from the arc of deforestation, we found a consistent pattern of hot spots of strong coupling across the arc of deforestation, and near urban areas such as Porto Velho and Santa Cruz de La Sierra. In the areas with weaker coupling, which are mostly located on the intact forest, since energy is the determinant factor, soil moisture anomalies do not influence the atmosphere.

Comparing with GLACE results (Koster et al 2002), we found that coupling strength is highly variable depending on parameterizations and spatial and temporal resolution. If the time period of the aggregated analysis is longer for instance from daily to monthly, seasonal, and annual scale, the index shows higher values, because the internal variabilities of the atmospheric variables bounce each other out as we scale up our analysis. Also, as the spatial resolution of the simulation changes (from global to regional) the spatial pattern and quantitative value of the index change as well. The hot spots of strong coupling are located on Savanna and Cerrado biomes in the southeast and northeast and the arc of deforestation, particularly south of Belem.

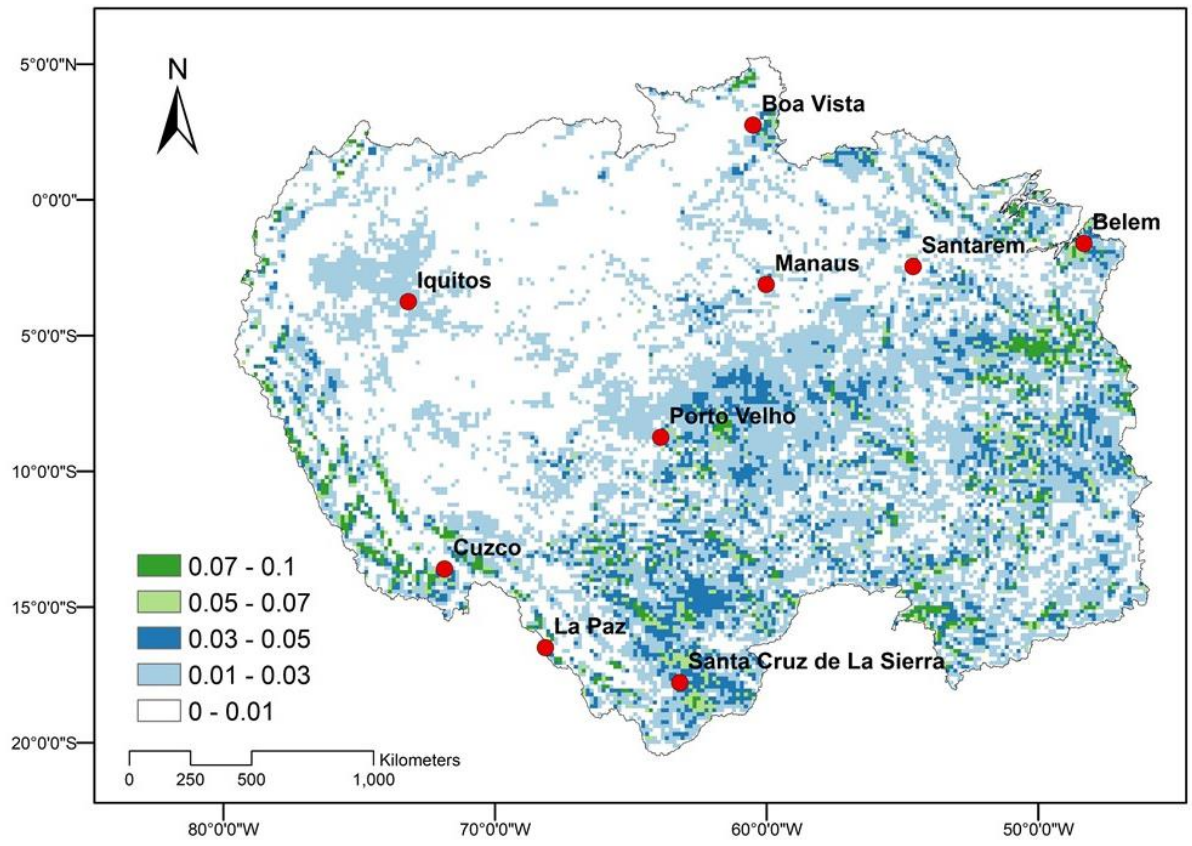

Figure 24. GLACE-type L-A coupling measurement at a regional scale.

B: Correlation-based metric

The results of the correlation-based index (*I*) are presented in Figures 25- 27 for both terrestrial and atmospheric segments. These results are significant at a 95% confidence level. Starting with the terrestrial segment, SM showing a high correlation with fluxes especially during May-Nov when the moisture is the limiting factor of the system. SM and SH are strongly coupled across the arc of deforestation at the end of May-Nov and early in Jul-Dec. Inverse correlations between SM and SH highlight the influence of soil moisture variability in the northernmost part of the domain, with the only notable southern coupling during Aug-Oct.

SM and LH show a positive correlation at the end of the May-Nov time period and early in Dec-Apr. *I* is very high along the arc of deforestation, urbanized areas, and Cerrado during the boreal summer and early fall highlighting hot spots of strong L-A coupling. The monthly maps

show that hot spots of positive SM_LH correlation are predominantly located across the semi-arid-humid southeastern ecotone during the dry season, where there is the highest soil moisture-driven variance in LH. This also occurs near the savanna at the northern edge of the domain. Negative SM-LH correlation during Dec-Apr suggests that soil moisture is weakly driven by fluxes and it does not typically exert feedbacks on the atmosphere since soil moisture is very high especially in March and April.

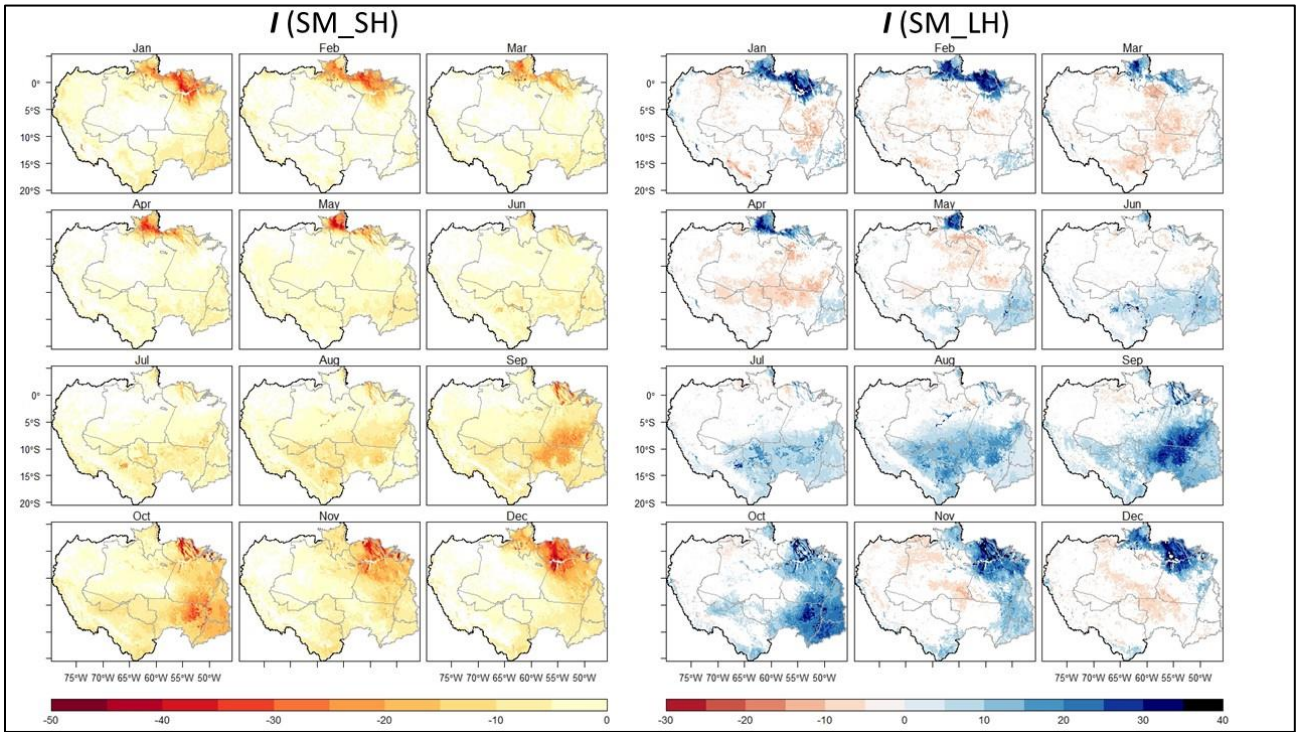

Figure 25. Correlation-based Coupling Index (I) for SM_LH on the left and SM_SH on the right *panel at monthly time scale.*

Figure 26 shows *I* between SM-SpH highlighting the direct impact of SM on SpH within the boundary layer. As SM increases SpH increases accordingly, indicating a strong interaction especially during the dry season and early in Dec-Apr. SM-SpH coupling is stronger in May, Sep, and Dec, and weaker in other months. SM also influences the variability of upward moisture flux at the surface (QFX). At the end of the dry season (Jun-Jul-Aug-Sep-Oct) SM-QFX are highly correlated positively across the arc of deforestation while at the end of Dec-Apr (Mar-

Apr-May) the inverse correlation more to the north indicates the effects of other parameters than soil moisture in the variability of QFX.

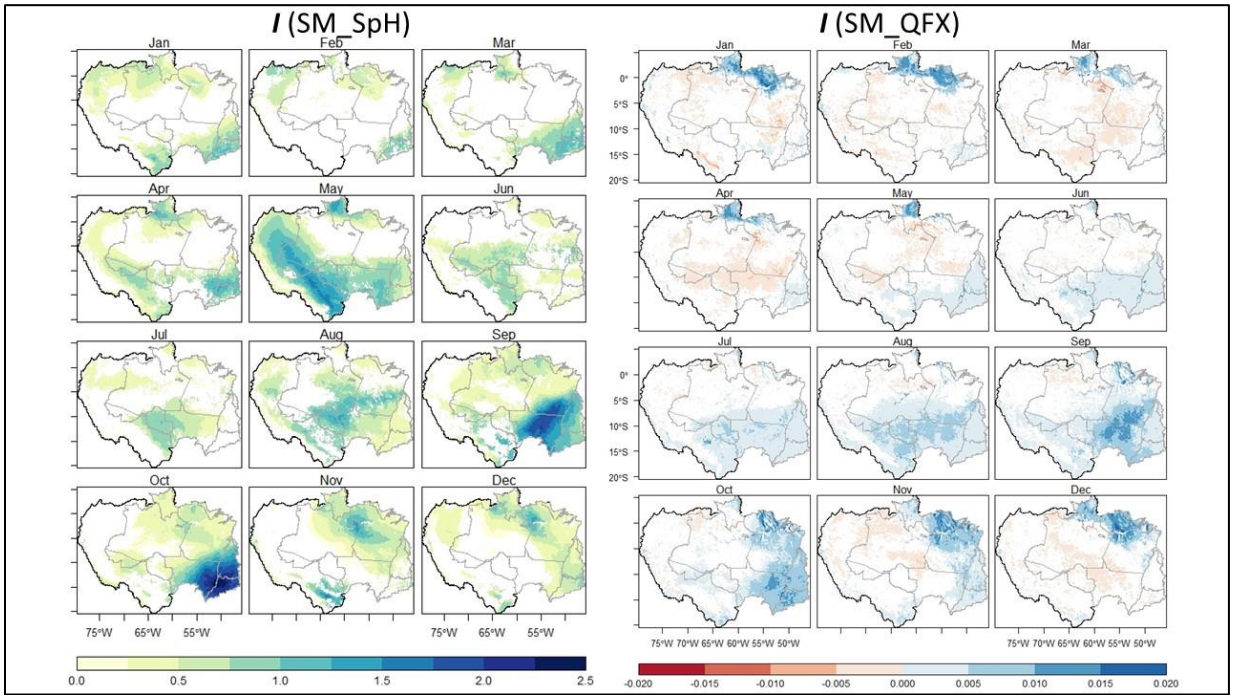

Figure 26. Correlation-based Coupling Index (I) for SM_QFX on the left and SM_SpH on the right *panel at the monthly time scale.*

Unlike the terrestrial segment, relationships and interactions are physically more complicated in the atmospheric segment. Figure 27 shows *I* for LH_prcp on the left and SH-prcp on the right. LH and precipitation are weakly correlated across the region for most months, but they are inversely correlated in March and April and positively correlated in Aug-Sep-Oct. This indicates that LH-prcp interacting is complicated and non-linear. On the other hand, SH shows a persistent negative correlation with precipitation but spatially varying. The interaction is high in April and May along the arc of deforestation, and in October and December over the Cerrado biome on the Southeast of the basin.

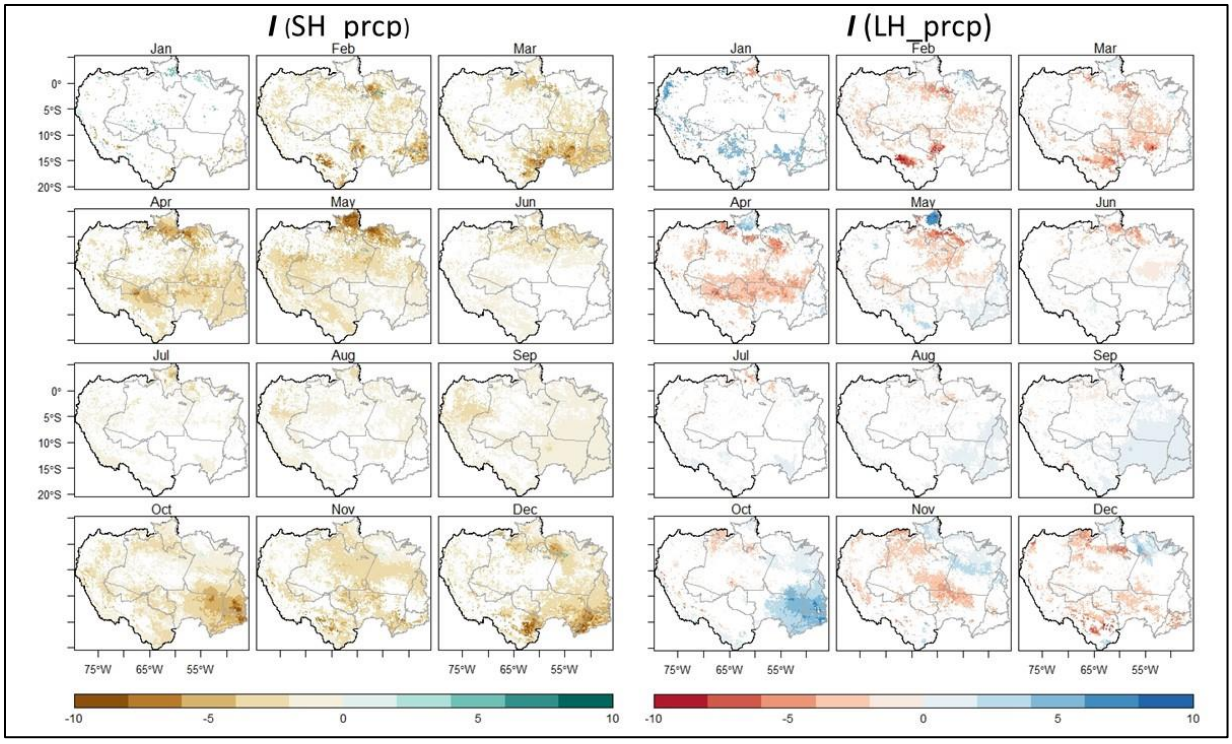

Figure 27. Correlation-based Coupling Index (I) for LH_prcp on the left and SH_prcp on the right *panel at monthly time scale.*

Discussion

Measuring L-A coupling strength is an approach to quantitatively assess the interactions between the land surface state and the atmosphere state which is variable across regions (Koster et al. 2004) and depends on model parametrization (Koster et al. 2002). This raises the question of which factors play a more important role in L-A coupling. We found that factors and their influence in L-A coupling vary depending on the spatial location and time of a year. The following section focuses on the physical processes involved in L-A interactions.

Terrestrial Segment

Generally, in tropical rain forests, light and solar energy are limiting factors for photosynthesis and ET, while water and soil moisture in savannah and semi-arid regions are the limiting factors regulating surface fluxes and L-A interactions (Gentine et al 2019). Thus, most of the feedbacks

between precipitation and surface fluxes are strong in climatically transitional ecotones such as the northeastern Savanna and southeastern Cerrado of Amazonia.

In the terrestrial segment of L-A coupling, interactions are straightforward. As it is shown in figures 24 and 25, SM interacts with fluxes across the region directly. A positive significant correlation between soil moisture and fluxes indicates that variations in soil moisture drive variations in the fluxes. This occurs where there is some degree of soil moisture deficit that controls the variability of fluxes. A negative correlation between soil moisture and QFX in Mar, Apr, May, and Dec on the urbanized areas and south of the basin shows that available energy to the system is the controlling factor and soil moisture is plentiful.

Soil moisture LH feedback is predominantly positive during Jun-Oct in the center and southeast of the basin over Cerrado and urbanized areas. Regions of negative feedback are due to cloud covers. Low soil moisture can lead to increased boundary layer cloudiness when the atmosphere is unstable (Ek and Holtslag 2004). This higher cloud cover may increase the chance of precipitation resulting in negative feedback between SM-LH on the arc of deforestation and the center of the basin (Figure 20). Also, increased soil moisture can lead to decreased precipitation if the atmosphere is humid and thermal forcing is insufficient to initiate deep convection (Buermann et al. 2001) as we see for May in Figure 26. Moreover, as soil moisture decreases, the amount of available soil moisture for plants becomes limited which may lead to reducing ET depending on plant species (Seneviratne et al. 2010). Decreased ET can lead to higher SH in the boundary layer (Figure 25) in the eastern semiarid regions at various times of the year. This coupling leads to a warmer atmosphere as a result.

Tropical forest in Amazonia absorbs more solar energy than most ecosystems around the world. Taking advantage of soil moisture in the basin, this energy is unevenly partitioned to more

LH than SH (Hasler et al 2009; Spera et al. 2016). Although the Amazon basin receives a substantial amount of energy throughout the year, the wetter portion of the basin during the rainy months receives less incident energy due to cloudiness, thus less LH is expected.

On the other hand, in the drier portion of the basin during the dry season, plants become the dominant users of soil moisture and control ET in the boundary layer. With more xeric plants, less ET and LH will be available, thus SH increases (Nepstad et al. 2008). Therefore, during the dry season, synergies between climate and vegetation cover control much of the observed variability of energy and water balances in the Amazon (Coe et al. 2016).

An important effect of SM on near-surface climate is its role in controlling near-surface temperature. Whenever total energy partitioned to LH is limited by soil moisture, more energy will be available in form of SH which leads to higher temperatures in the system. This increase may lead to the occurrence of extreme heat events and heat waves (Zhang et. 2009). Generally, decreased ET leads to higher SH and a warmer atmosphere which these simulations show along the arc of deforestation towards the end of the dry season. Potential positive feedback between ET and SH indicates that increased T_{sk} increase evaporative demand, thus leads to a potential increase in ET, resulting in a further decrease in soil moisture.

Atmosphere Segment

The major components of L-A interactions are surface turbulent fluxes and associated momentum, energy, water, and trace gases exchange between the land surface and atmosphere (Restrepo-Coupe et al. 2013).

In the wetter part of the Amazon basin, net radiation peaks in the dry season (Jun-Oct) due to decreases in cloud cover and precipitation generated from shallow convection. Therefore, as incident solar radiation increases, both ET and Gross Primary Production (GPP) increase.

Transpiration will be maximum as well during the May-Nov “dry season” in the western basin (where there is effectively no dry season). In the east, water stress will be a controlling factor across the savannah and Cerrado. In contrast with the perennially wet and green western Amazon, the seasonal cycle of fluxes and precipitation are more pronounced on the center and east side of the basin with the marked dry season. Light changes between dry and wet seasons due to cloud cover is one of the primary reasons for changes in the seasonality of surface fluxes in addition to leaf flush out (Morton et al. 2014, 2016; Anber et al. 2015, Saleska et al. 2016).

A fundamental consideration in the study of moisture flux and moisture cycle in the Amazon Basin is to assess sources of moisture to the system. Early studies (e.g., Eltahir and Bras, 1994; Trenberth, 1999) focused on moisture recycling, but recent studies show that the recycling ratio for the basin ranges from 25% to 35% (Zemp et al., 2014). Also, upstream sources of moisture influence the downstream rainfall over tropics (Hoyos et al., 2018). For example, downstream rainfall amounts double for those air masses passing over extensive vegetation compared with those passing over sparsely vegetated areas (Spracklen et al. 2012). Moisture recycling plays a critical role across ecotones.

Shallow convection formation frequently depends on SH, LH, and their partitioning (Tawfik et al. 2015). Across the Amazon basin, shallow convection occurs more over patchwork landscapes while they are absent over cooler and more humid river basins (Rieck et al 2015). Shallow convection is highly dependent on CAPE which in turn depends on fluxes within the boundary layer. In comparison, deep convection (usually forced by mesoscale and large-scale circulations) has been viewed as less dependent on surface fluxes states (Roy and Avissar 2002). This mechanism may be more relevant in feedback in transitional dry-to-wet regions. Dec-Apr precipitation is dominated by deep convection; however, during May-Nov, precipitation happens

due to “pop-corn-type” shallow convection which is directly related to the land surface state and is more locally triggered (Ghate and Kollias 2016). Although shallow convection produces less rainfall than deep convection, it will affect deep convection through its influence on heat fluxes and moisture transportation to the lower troposphere. In addition, feedback between shallow convection and surface radiation is important to be considered, since they are preferentially triggered over a drier surface, have a small life cycle, and therefore they are more directly linked to the land surface states and underlying surface conditions (Gentine et al. 2019). This is the case in eastern and southern parts of the basin which have distinct dry and wet seasons. For example, in the southeast on Cerrado during the wet season, especially Feb, Mar, and Apr, CAPE is limited, and shallow convection brings precipitation to the region. Therefore, the surface state does not significantly influence the atmosphere in these months.

Deficiencies of available metrics

Correlations can neither explain causality nor estimate indirect relationships in coupling. Covariance analysis (lag correlation), on the other hand, can be affected by autocorrelation between parameters and in precipitation only without any contribution of soil moisture which can influence the lag correlation between SM and precipitation (e.g., Wei et al. 2008). In addition, some diagnosed lag correlations can be artifacts of data handling (e.g., Salvucci et al. 2002). Moreover, as tele-connected processes, the land surface can influence precipitation remotely due to the advection of convective cells away from the surfaces that initiated them (Zhang and Frederiksen 2003). Soil characteristics such as temperature, texture, and heat storage capacity may also have memories on monthly to seasonal time scales (Amenu et al 2005).

Despite such noise in the signal, a way to measure L-A coupling is to identify empirical relationships by displaying the variables as a function of one another. However, this method cannot

show the causality, it is very useful to identify coupling mechanisms at L-A interactions and explore the key parameters in the coupled system. For this reason, here we provide a multivariable regression analysis of parameters involved in L-A interactions within the boundary layer, considering their interactions and lag times.

Theoretically, soil texture plays an important role in soil thermal and hydraulic processes such as soil temperature and volumetric soil moisture content thus have a significant effect on the evolution of PBL and precipitation (He et al. 2016). Soil texture can influence the amount and distribution of water in the soil, control plants' functions which indirectly can impact ET. Therefore, it is critical to consider this parameter in L-A coupling measurement. Figure 29 shows the spatial distribution of soil texture across the Amazon Basin. But, due to poor correlation between soil texture and fluxes variability and precipitation ($R2 < 0.005$), here we omitted it from our analysis. Since the existing soil texture in our simulation has a very coarse spatial resolution of 5 arc min which equals 8.3 km at the equator, we recommend future studies test our new index using finer spatial scale soil texture data.

Table 4 in supplementary materials shows the key parameters in L-A coupling and their influence at the monthly timescale on precipitation. Our analysis is significant and strong with $R2 > 0.90$ and P-value < 0.001. Our results show that multiple variables, as well as their interaction terms, should be considered in L-A interaction studies. We included 7 variables and their interactions in our regression model. We found that the interactions between variables often play more important roles than isolated single variables (as it is used in other studies e.g., Diremeyer et al 2011). Generally, LH:SH interaction shows a key parameter in L-A coupling in almost all months, and LH:SM consistently shows significant impacts on L-A coupling strength across all months. Also, QFX and SpH are among the key variables in L-A coupling analysis which are

robust and consistent across most months. Additionally, the relationship between soil moisture memory and precipitation is significant and has a strong effect on L-A coupling as is shown in Appendix Besides, in Jan-Feb-Mar, LH:SM, QFX, LH:prcp21, and SpH are recognized as the critical parameters in L-A coupling. In April QFX does not play an important role in the coupling. In May in addition to previous parameters, SM:prcp21 and T2 are among those influential parameters. In Jun, Aug, Sep, and Nov all factors are critical while in July and Oct LH:SM does not show any impact on the coupling strength. And in Dec LH:SH is not as significant as SM:prcrp_21 and LH:SM.

Figure 28 shows the spatial distribution of hot spots of strong coupling for each month using the multivariable regression equation for each month. This figure indicates that, variables impact the L-A coupling differently depending on the time of the year and spatial location of the phenomena.

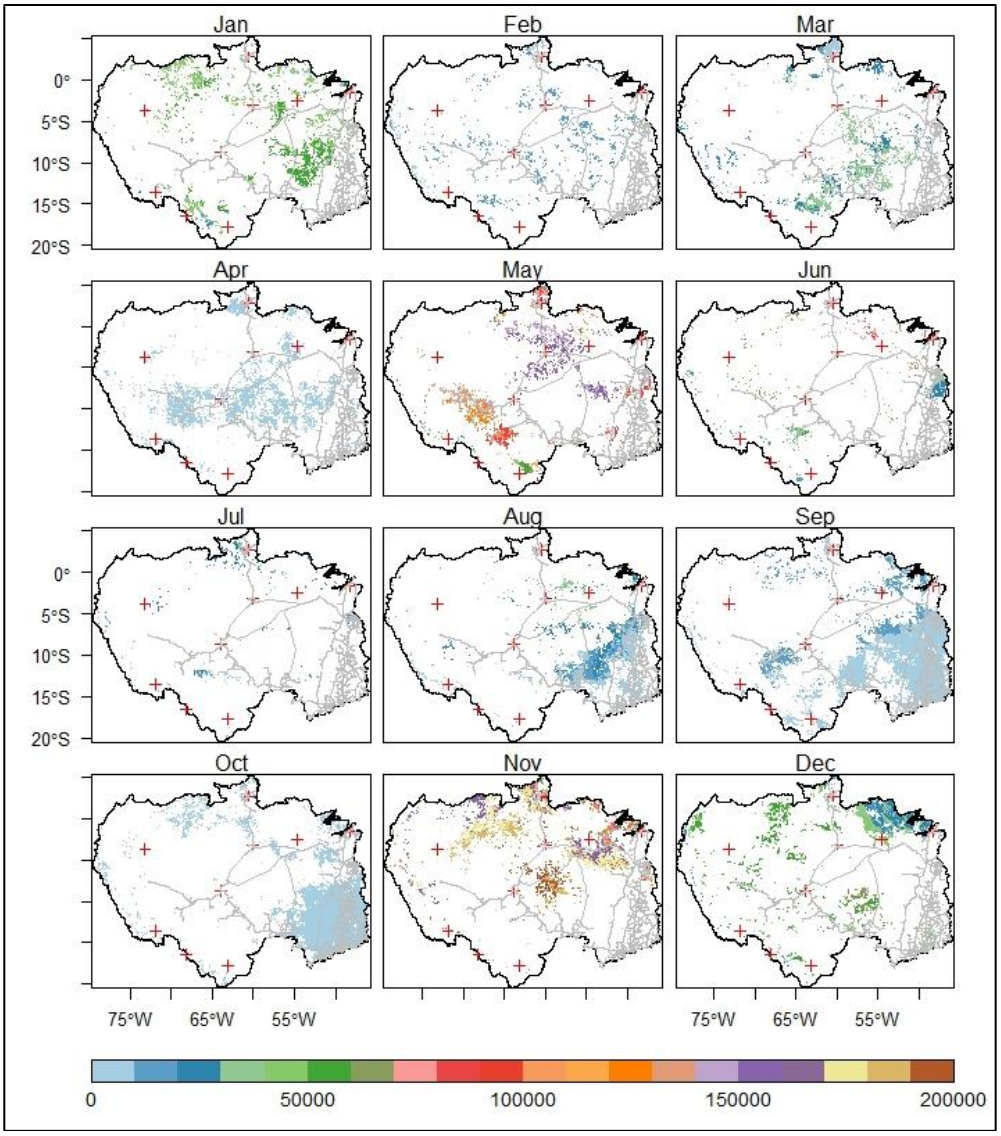

Figure 28. multivariable regression index at monthly time scale*. Gray lines represent major highways in Brazil and red plus signs indicate the location of major cities. The higher values show that more variables are involved for those regions.*

Areas in blue in Aug, Sep, and Oct show the hot spots are located on the Cerrado ecotone of the southeastern Amazon and along major highways. The blue color indicates that the coupling is not too complicated, and it can be measured by excluding non-important parameters from the analysis. But, in May, hot spots are located around Manaus which is urbanized (shown in appendix) indicating that in this area atmosphere is highly sensitive to land surface changes. Also, in Nov, hot spots are located near highways and major cities, where human disturbances

are maximum. Although figure 23 qualitatively shows the hotspots of L-A coupling, it provides valuable insight for future investigation on L-A coupling.

Conclusion

The L-A coupling strength measurement is an approach to quantify the relationship between the land surface and the atmosphere state. In this study, we measured L-A coupling strength at the regional scale across the Amazon basin, found the physical processes involved in this interaction, and examined the key parameters in L-A coupling to improve the existing metrics of L-A coupling strength.

Comparing our results to those of GLACE and Dirmeyer et al (2011), we found that coupling strength is subject to regional variability. It depends on model parameterization and temporal and spatial scale of analysis. Although our results of hot spots of strong L-A coupling across the Amazon basin show -to some extent- overlap with the previous analysis at the global scale, some key regions especially transitional zones between dry and wet, savanna, and Cerrado were missing at the global scale analyses. We found that strong L-A coupling lies mainly in the transitional zone between wet and dry regions (Savanna and Cerrado) during the boreal summer. We provided a comprehensive demonstration of a high correlation between land surface states and atmosphere by applying the correlation-based metric (I) on the terrestrial leg and atmospheric leg of coupling at a monthly time scale. We found that although interactions between land surface parameters such as soil moisture with fluxes (LH and SH) are straightforward, the interactions between fluxes and the atmosphere state, especially precipitation are highly complex, and is not possible to capture all the complexity by applying simple linear correlations. Therefore, the question remains about the important factors in L-A coupling. A lack of common definition along with the fact that different studies and metrics address different

quantities and processes (Knist et al. 2017) complicates the comparability of studies on L-A coupling strength. Additionally, disparate atmospheric models and resolutions, high land surface complexity, and lack of observations make assessments difficult as well (Santanello et al. 2011). Furthermore, many studies have been performed on a global scale and rather coarse resolutions.

Tropical energy, water, and the carbon cycle are not isolated, rather they interact actively. It is essential to consider this interaction in measuring L-A coupling strength. Besides, it is worth noting that SM and fluxes' relationships may vary with temporal scale. The high sensitivity of monthly SH to soil moisture anomalies does not necessarily mean they will be sensitive at a daily or annual scale. Therefore, the complexity of L-A interaction cannot be measured only by using a simple linear correlation and cannot be inferred directly from this analysis of coupling strength. For this reason, we applied stepwise regression analyses using seven variables, their interactiona as well as soil moisture memory to find the key parameters in L-A coupling in the boundary layer. We found that interactions between parameters and physical processes play a more important role in L-A interactions indicating the complexity of relationships. Developing a multivariate metric of measuring L-A coupling strength is a useful tool in seasonal and sub-seasonal climate forecasting. Soil moisture is possibly the main source of forecast skill for summer precipitation predictability (Findell et al. 2006), thus monitoring soil moisture in identified hot spots of strong L-A coupling will improve monthly to seasonal precipitation forecast.

We recommend that future studies focus on cloud-land surface feedback in L-A coupling since it regulates light, temperature, and water vapor deficit over the tropical forest, and such feedbacks have received less attention in studies. Also, the omitted relationship between physical processes, especially atmospheric composition and chemical reactions and aerosols, adds

uncertainty in coupling analysis. Additionally, soil texture and drainage are two important factors influencing soil physical characteristics, which are not considered here, need to get attention in future L-A coupling studies. Besides, it is necessary to consider the influences of remote forcing and non-local drivers. This is important over the tropics because of the strong coupling between convection and large-scale forcings.

APPENDIX

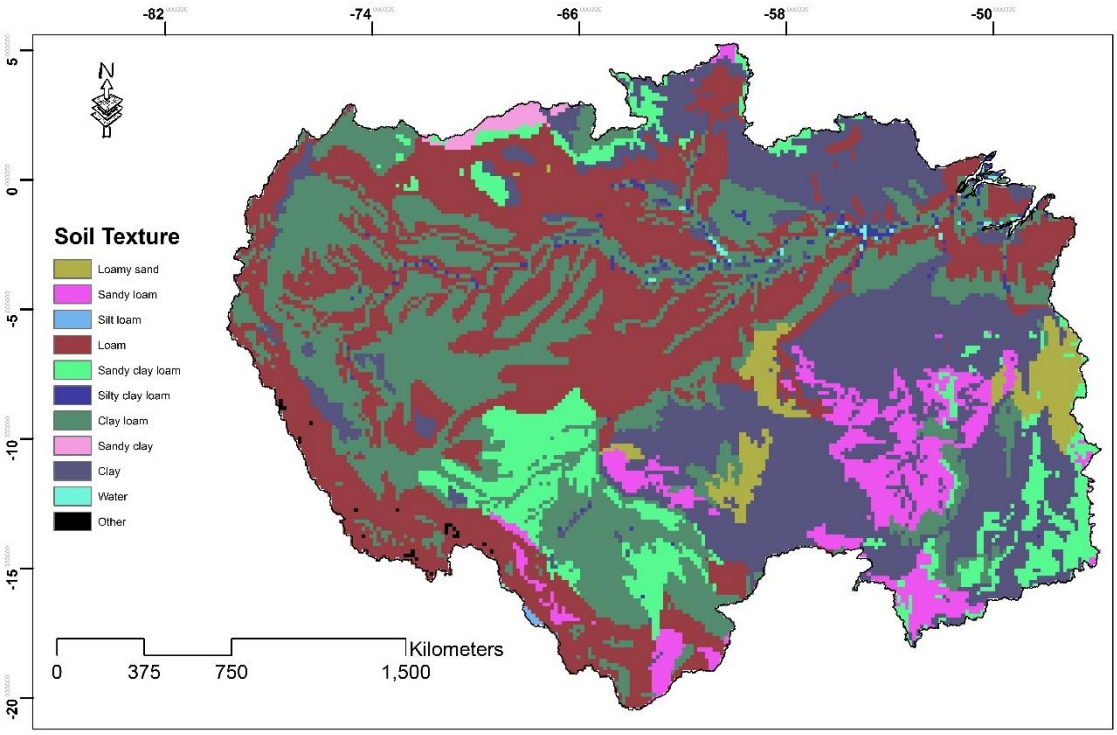

Figure 29. Soil texture categories *based on Food and Agriculture Organization soil database at 5 arc min spatial resolution.*

Table 4. Key parameters in land-atmosphere coupling *(P_value< 2.2e-16)*

Month	*Key variables*	*Coefficient*	R^2
Jan	*LH:SM*	*0.13*	*0.92*
	QFX	*80430*	
	SH:LH	*-0.0001*	
	SH:T2	*0.00116*	
	SM:prcp_21	*-0.01937*	
	LH:prcp_21	*-0.00004*	
	SpH	*-335*	
Feb	*SH:LH*	*-0.00002*	*0.97*
	LH:prcp_21	*-0.00001*	
	LH:SM	*0.01680*	
	QFX	*298564.2*	
	SpH	*106.08380*	
	T2	*-0.05062*	
Mar	*SH:T2*	*-0.00021*	*0.94*
	SH:LH	*-0.00014*	
	LH:SM	*0.02682*	
	LH:prcp_21	*-0.00005*	
	QFX	*493800*	
	SpH	*169.1*	
Apr	*SM:prcp_21*	*-0.00247*	*0.97*
	SH:T2	*-0.00061*	
	SH:LH	*-0.00025*	
	LH:SM	*0.06453*	
	LH:prcp_21	*-0.0001*	
	SpH	*195.5*	
May	*SH:LH*	*0.00006*	*0.98*
	SM:prcp_21	*0.00394*	
	LH:prcp_21	*0.00001*	
	LH:SM	*0.03486*	
	T2	*-0.1011*	
	QFX	*-2799000*	
	SpH	*412.7*	

Table 4 (cont'd)

Jun	*SH:LH*	*0.00003*	*0.99*
	SM:prcp_21	*-0.00699*	
	LH:prcp_21	*-0.00004*	
	LH:SM	*0.00966*	
	SH:T2	*-0.00025*	
	QFX	*-1369000*	
	SpH	*72.35*	
Jul	*SH:LH*	*-0.00013*	*0.99*
	SM:prcp_21	*-0.00285*	
	LH:prcp_21	*0.00003*	
	SH:T2	*-0.00023*	
	QFX	*-507500*	
	SpH	*46.73*	
Aug	*SH:LH*	*0.00001*	*0.99*
	SM:prcp_21	*0.02039*	
	LH:prcp_21	*0.00005*	
	LH:SM	*-0.00263*	
	SH:T2	*-0.00006*	
	QFX	*525000*	
	SpH	*28.18*	
Sep	*SH:LH*	*-0.00012*	*0.99*
	SM:prcp_21	*0.02387*	
	LH:prcp_21	*0.00001*	
	LH:SM	*-0.00246*	
	SH:T2	*-0.00009*	
	QFX	*202800*	
	SpH	*84.34*	
Oct	*SH:LH*	*-0.00012*	*0.98*
	SM:prcp_21	*0.01338*	
	LH:prcp_21	*-0.00001*	
	SH:T2	*0.00094*	

Table 4 (cont'd)

	SpH	*178.6*	
Nov	*SH:LH*	*0.00011*	*0.97*
	SM:prcp_21	*0.00915*	
	LH:prcp_21	*0.00001*	
	LH:SM	*0.02575*	
	SH:T2	*0.00177*	
	QFX	*2768000*	
	SpH	*333.9*	
Dec	*SM:prcp_21*	*-0.00656*	*0.96*
	LH:prcp_21	*-0.00002*	
	LH:SM	*0.00660*	
	SH:T2	*0.00092*	
	QFX	*859300*	
	SpH	*-96.04*	

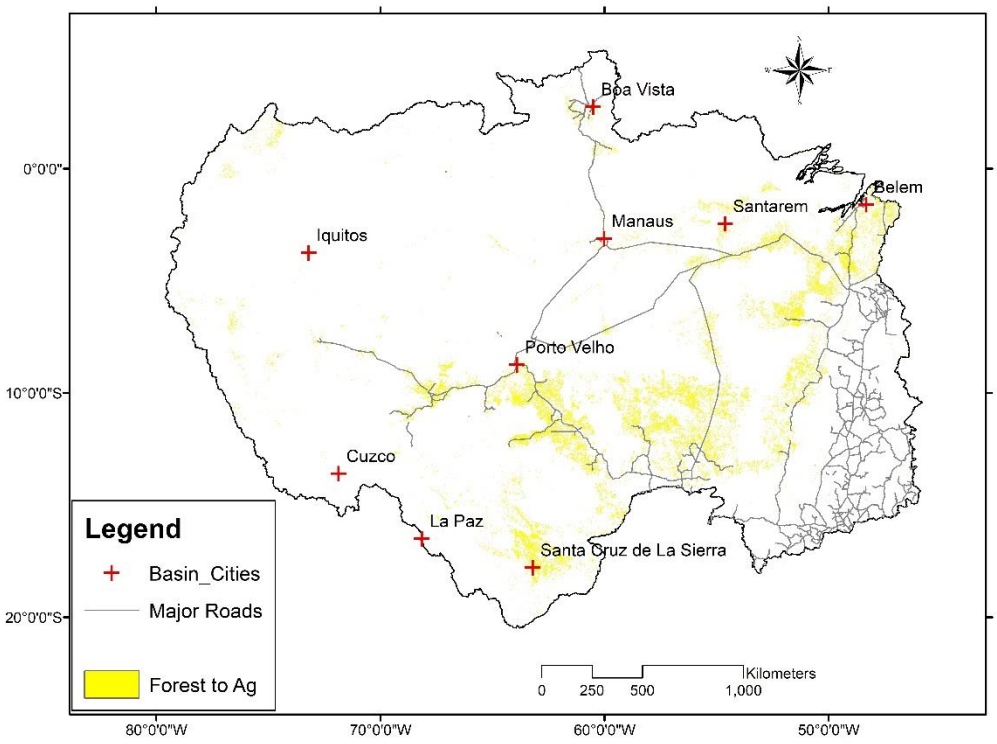

Figure 30. Land cover change from forest to agriculture across the Amazon Basin. *Major high ways and major cities are shown on the map. This map indicates that most of deforestations have occurred along the high ways and around urbanized areas*

REFERENCES

REFERENCES

Amenu, Geremew G., Praveen Kumar, and Xin Zhong Liang. 2005. "Interannual Variability of Deep-Layer Hydrologic Memory and Mechanisms of Its Influence on Surface Energy Fluxes." Journal of Climate 18 (23): 5024–45. https://doi.org/10.1175/JCLI3590.1.

Bagley, Justin E, Ankur R Desai, Paul C West, Jonathan A Foley, Justin E Bagley, Ankur R Desai, Paul C West, and Jonathan A Foley. 2011. "A Simple, Minimal Parameter Model for Predicting the Influence of Changing Land Cover on the Land–Atmosphere System $^{+}$." Earth Interactions 15 (29): 1–32. https://doi.org/10.1175/2011EI394.1.

Baidya Roy, Somnath, and Roni Avissar. 2002. "Impact of Land Use/Land Cover Change on Regional Hydrometeorology in Amazonia." Journal of Geophysical Research Atmospheres 107 (20): LBA 4-1-LBA 4-12. https://doi.org/10.1029/2000JD000266.

Baldocchi, Dennis D., and Liukang Xu. 2007. "What Limits Evaporation from Mediterranean Oak Woodlands - The Supply of Moisture in the Soil, Physiological Control by Plants or the Demand by the Atmosphere?" Advances in Water Resources 30 (10): 2113–22. https://doi.org/10.1016/j.advwatres.2006.06.013.

Betts, Alan K. 2009. "Land-Surface-Atmosphere Coupling in Observations and Models." Journal of Advances in Modeling Earth Systems 1 (3): n/a--n/a. https://doi.org/10.3894/james.2009.1.4.

Betts, Alan K., and Maria Assunção F. Silva Dias. 2010. "Progress in Understanding Land-Surface-Atmosphere Coupling from LBA Research." Journal of Advances in Modeling Earth Systems 2 (2): 6. https://doi.org/10.3894/JAMES.2010.2.6.

Betts, R. A., P. M. Cox, M. Collins, P. P. Harris, C. Huntingford, and C. D. Jones. 2004. "The Role of Ecosystem-Atmosphere Interactions in Simulated Amazonian Precipitation Decrease and Forest Dieback under Global Climate Warming." Theoretical and Applied Climatology 78 (1–3): 157–75. https://doi.org/10.1007/s00704-004-0050-y.

Buermann, W., J. Dong, X. Zeng, R. B. Myneni, and R. E. Dickinson. 2001. "Evaluation of the Utility of Satellite-Based Vegetation Leaf Area Index Data for Climate Simulations." Journal of Climate 14 (17): 3536–50. https://doi.org/10.1175/1520-0442(2001)014<3536:EOTUOS>2.0.CO;2.

Chen, Liang, and Paul A. Dirmeyer. 2016. "Adapting Observationally Based Metrics of Biogeophysical Feedbacks from Land Cover/Land Use Change to Climate Modeling." Environmental Research Letters. https://doi.org/10.1088/1748-9326/11/3/034002.

Coe, M. T., D. V. Silverio, M. Bustamante, M. Macedo, J. Shimbo, P. M. Brando, M. T. Coe, et al. 2016. "Feedbacks between Land Cover and Climate Changes in the Brazilian Amazon and Cerrado Biomes - NASA/ADS." AGUFM, GC23I-08.

https://ui.adsabs.harvard.edu/abs/2016AGUFMGC23I..08C/abstract.

Conil, Sebastien, H. Douville, and S. Tyteca. 2007. “The Relative Influence of Soil Moisture and SST in Climate Predictability Explored within Ensembles of AMIP Type Experiments.” Climate Dynamics 28 (2–3): 125–45. https://doi.org/10.1007/s00382-006-0172-2.

Devanand, Anjana, Maoyi Huang, David M. Lawrence, Colin M. Zarzycki, Zhe Feng, Peter J. Lawrence, Yun Qian, and Zhao Yang. 2020. “Land Use and Land Cover Change Strongly Modulates Land-Atmosphere Coupling and Warm-Season Precipitation Over the Central United States in CESM2-VR.” Journal of Advances in Modeling Earth Systems 12 (9): 1–23. https://doi.org/10.1029/2019MS001925.

Dirmeyer, Paul A. 2011. “The Terrestrial Segment of Soil Moisture-Climate Coupling.” Geophysical Research Letters 38 (16): 1–5. https://doi.org/10.1029/2011GL048268.

Dirmeyer, Paul A., and Kaye L. Brubaker. 2007. “Characterization of the Global Hydrologic Cycle from a Back-Trajectory Analysis of Atmospheric Water Vapor.” Journal of Hydrometeorology 8 (1): 20–37. https://doi.org/10.1175/JHM557.1.

Dirmeyer, Paul A., Liang Chen, Jiexia Wu, Chul Su Shin, Bohua Huang, Benjamin A. Cash, Michael G. Bosilovich, et al. 2018. “Verification of Land-Atmosphere Coupling in Forecast Models, Reanalyses, and Land Surface Models Using Flux Site Observations.” Journal of Hydrometeorology 19 (2): 375–92. https://doi.org/10.1175/JHM-D-17-0152.1.

Dirmeyer, Paul A., Randal D. Koster, and Zhichang Guo. 2006. “Do Global Models Properly Represent the Feedback between Land and Atmosphere?” Journal of Hydrometeorology 7 (6): 1177–98. https://doi.org/10.1175/JHM532.1.

Ek, M. B., and A. A.M. Holtslag. 2004. “Influence of Soil Moisture on Boundary Layer Cloud Development.” Journal of Hydrometeorology 5 (1): 86–99. https://doi.org/10.1175/1525-7541(2004)005<0086:IOSMOB>2.0.CO;2.

Findell, Kirsten L, and Elfatih A B Eltahir. 1997. “An Analysis of the Soil Moisture-Rainfall Feedback, Based on Direct Observations from Illinois.” Water Resources Research 33 (4): 725–35. https://doi.org/10.1029/96WR03756.

Findell, Kirsten L, Thomas R Knutson, P C D Milly, Kirsten L Findell, Thomas R Knutson, and P C D Milly. 2006. “Weak Simulated Extratropical Responses to Complete Tropical Deforestation.” Journal of Climate 19 (12): 2835–50. https://doi.org/10.1175/JCLI3737.1.

Gentine, Pierre, Adam Massmann, Benjamin R. Lintner, Sayed Hamed Alemohammad, Rong Fu, Julia K. Green, Daniel Kennedy, and Jordi Vilà-Guerau De Arellano. 2019. “Land-Atmosphere Interactions in the Tropics - A Review.” Hydrology and Earth System Sciences 23 (10): 4171–97. https://doi.org/10.5194/hess-23-4171-2019.

Ghate, Virendra P., and Pavlos Kollias. 2016. “On the Controls of Daytime Precipitation in the Amazonian Dry Season.” Journal of Hydrometeorology 17 (12): 3079–97. https://doi.org/10.1175/JHM-D-16-0101.1.

Goessling, H. F., and C. H. Reick. 2011. “What Do Moisture Recycling Estimates Tell Us? Exploring the Extreme Case of Non-Evaporating Continents.” Hydrology and Earth System Sciences 15 (10): 3217–35. https://doi.org/10.5194/hess-15-3217-2011.

Guillod, Benoit P, Boris Orlowsky, Diego G Miralles, Adriaan J Teuling, and Sonia I Seneviratne. 2015. “Reconciling Spatial and Temporal Soil Moisture Effects on Afternoon Rainfall.” Nature Communications 6 (1): 6443. https://doi.org/10.1038/ncomms7443.

Guo, Zhichang, Paul A. Dirmeyer, Randal D. Koster, Y. C. Sud, Gordon Bonan, Keith W. Oleson, Edmond Chan, et al. 2006a. “GLACE: The Global Land–Atmosphere Coupling Experiment. Part II: Analysis.” Journal of Hydrometeorology 7 (4): 611–25. https://doi.org/10.1175/JHM511.1.

Hasler, Natalia, David Werth, and Roni Avissar. 2009. “Effects of Tropical Deforestation on Global Hydroclimate: A Multimodel Ensemble Analysis.” Journal of Climate 22 (5): 1124–41. https://doi.org/10.1175/2008JCLI2157.1.

He, J. J., Y. Yu, L. J. Yu, C. M. Yin, N. Liu, S. P. Zhao, and X. Chen. 2016. “Effect of Soil Texture and Hydraulic Parameters on WRF Simulations in Summer in East China.” Atmospheric Science Letters 17 (10): 538–47. https://doi.org/10.1002/asl.690.

Hong, Song-You, and Ants Leetmaa. 1999. “An Evaluation of the NCEP RSM for Regional Climate Modeling.” Journal of Climate 12 (2): 592–609. https://doi.org/10.1175/1520-0442(1999)012<0592:AEOTNR>2.0.CO;2.

Jach, Lisa, Kirsten Warrach-Sagi, Joachim Ingwersen, Eigil Kaas, and Volker Wulfmeyer. 2020. “Land Cover Impacts on Land-Atmosphere Coupling Strength in Climate Simulations With WRF Over Europe.” Journal of Geophysical Research: Atmospheres 125 (18). https://doi.org/10.1029/2019JD031989.

Jeu, Richard A.M., W. Wagner, T. R.H. Holmes, A. J. Dolman, N. C. Giesen, and J. Friesen. 2008. “Global Soil Moisture Patterns Observed by Space Borne Microwave Radiometers and Scatterometers.” Surveys in Geophysics 29 (4–5): 399–420. https://doi.org/10.1007/s10712-008-9044-0.

Koster, R. D., S. P. P. Mahanama, T. J. Yamada, Gianpaolo Balsamo, A. A. Berg, M. Boisserie, P. A. Dirmeyer, et al. 2010. “Contribution of Land Surface Initialization to Subseasonal Forecast Skill: First Results from a Multi-Model Experiment.” Geophysical Research Letters 37 (2): n/a-n/a. https://doi.org/10.1029/2009GL041677.

Koster, R D, Z Guo, P a. Dirmeyer, G B Bonan, E Chan, P M Cox, C T Gordon, et al. 2006. “GLACE: The Global Land – Atmosphere Coupling Experiment. Part I: Overview.” Journal of Hydrometeorology 7: 611–25. https://doi.org/http://dx.doi.org/10.1175/JHM511.1.

Koster, Randal D., Paul A. Dirmeyer, Andrea N. Hahmann, Ruben Ijpelaar, Lori Tyahla, Peter Cox, and Max J. Suarez. 2002. “Comparing the Degree of Land-Atmosphere Interaction in Four Atmospheric General Circulation Models.” Journal of Hydrometeorology 3 (3): 363–75. https://doi.org/10.1175/1525-7541(2002)003<0363:CTDOLA>2.0.CO;2.

Koster, Randal D., Zhichang Guo, Rongqian Yang, Paul A. Dirmeyer, Kenneth Mitchell, and Michael J. Puma. 2009. “On the Nature of Soil Moisture in Land Surface Models.” Journal of Climate 22 (16): 4322–35. https://doi.org/10.1175/2009JCLI2832.1.

Koster, Randal D, Max J Suarez, Agnès Ducharne, Marc Stieglitz, and Praveen Kumar. 2000. “A Catchment-Based Approach to Modeling Land Surface Processes in a General Circulation Model: 1. Model Structure.” Journal of Geophysical Research: Atmospheres 105 (D20): 24809–22. https://doi.org/10.1029/2000JD900327.

Medvigy, David, Robert L Walko, Roni Avissar, David Medvigy, Robert L Walko, and Roni Avissar. 2011. “Effects of Deforestation on Spatiotemporal Distributions of Precipitation in South America.” Journal of Climate 24 (8): 2147–63. https://doi.org/10.1175/2010JCLI3882.1.

Mei, Rui, and Guiling Wang. 2012. “Summer Land-Atmosphere Coupling Strength in the United States: Comparison among Observations, Reanalysis Data, and Numerical Models.” Journal of Hydrometeorology 13 (3): 1010–22. https://doi.org/10.1175/JHM-D-11-075.1.

Milly, P. C.D., and K. A. Dunne. 1994. “Sensitivity of the Global Water Cycle to the Water-Holding Capacity of Land.” Journal of Climate 7 (4): 506–26. https://doi.org/10.1175/1520-0442(1994)007<0506:SOTGWC>2.0.CO;2.

Miralles, Diego G, Adriaan J Teuling, Chiel C Van Heerwaarden, and Jordi Vilà Guerau De Arellano. 2014. “Mega-Heatwave Temperatures Due to Combined Soil Desiccation and Atmospheric Heat Accumulation.” Nature Geoscience 7 (5): 345–49. https://doi.org/10.1038/ngeo2141.

Nepstad, Daniel C, Claudia M Stickler, Britaldo Soares-Filho, and Frank Merry. 2008. “Interactions among Amazon Land Use, Forests and Climate: Prospects for a near-Term Forest Tipping Point.” Philosophical Transactions of the Royal Society B: Biological Sciences 363 (1498): 1737–46. https://doi.org/10.1098/rstb.2007.0036.

Owe, Manfred, Richard de Jeu, and Thomas Holmes. 2008. “Multisensor Historical Climatology of Satellite-Derived Global Land Surface Moisture.” Journal of Geophysical Research 113 (F1): F01002. https://doi.org/10.1029/2007JF000769.

Pitman, A J, N De Noblet-Ducoudré, F T Cruz, E L Davin, G B Bonan, V Brovkin, M Claussen, et al. 2009. “Uncertainties in Climate Responses to Past Land Cover Change: First Results from the LUCID Intercomparison Study.” Geophysical Research Letters 36 (14): 1–6. https://doi.org/10.1029/2009GL039076.

Rieck, Malte, Cathy Hohenegger, and Pierre Gentine. 2015. “The Effect of Moist Convection on Thermally Induced Mesoscale Circulations.” Quarterly Journal of the Royal Meteorological Society 141 (691): 2418–28. https://doi.org/10.1002/qj.2532.

Roundy, Joshua K., Craig R. Ferguson, and Eric F. Wood. 2014. “Impact of Land-Atmospheric Coupling in CFSv2 on Drought Prediction.” Climate Dynamics 43 (1–2): 421–34. https://doi.org/10.1007/s00382-013-1982-7.

S¨Orensson, Anna A., and Claudio G. Men´Endez. 2011. “Summer Soil—Precipitation Coupling in South America.” Tellus A: Dynamic Meteorology and Oceanography 63 (1): 56–68. https://doi.org/10.1111/j.1600-0870.2010.00468.x.

Salvucci, Guido D., Jennifer A. Saleem, and Robert Kaufmann. 2002. “Investigating Soil Moisture Feedbacks on Precipitation with Tests of Granger Causality.” Advances in Water Resources 25 (8–12): 1305–12. https://doi.org/10.1016/S0309-1708(02)00057-X.

Santanello, Joseph A., Christa D. Peters-Lidard, Sujay V. Kumar, Joseph A. Santanello Jr., Christa D. Peters-Lidard, and Sujay V. Kumar. 2011a. “Diagnosing the Sensitivity of Local Land–Atmosphere Coupling via the Soil Moisture–Boundary Layer Interaction.” Journal of Hydrometeorology 12 (5): 766–86. https://doi.org/10.1175/JHM-D-10-05014.1.

Schlosser, C Adam, and P C D Milly. 2002. “A Model-Based Investigation of Soil Moisture Predictability and Associated Climate Predictability.” Journal of Hydrometeorology 3 (4): 483–501. https://doi.org/10.1175/1525-7541(2002)003<0483:AMBIOS>2.0.CO;2.

Seneviratne, Sonia I., Daniel Lüthi, Michael Litschi, and Christoph Schär. 2006a. “Land–Atmosphere Coupling and Climate Change in Europe.” Nature 443 (7108): 205–9. https://doi.org/10.1038/nature05095.

Seneviratne, Sonia I, Thierry Corti, Edouard L Davin, Martin Hirschi, Eric B Jaeger, Irene Lehner, Boris Orlowsky, and Adriaan J Teuling. 2010. “Investigating Soil Moisture-Climate Interactions in a Changing Climate: A Review.” Earth-Science Reviews 99 (3–4): 125–61. https://doi.org/10.1016/j.earscirev.2010.02.004.

Shukla, J, and Y Mintz. 1982. “Influence of Land-Surface Evapotranspiration on the Earth’s Climate.” Science (New York, N.Y.) 215 (4539): 1498–1501. https://doi.org/10.1126/science.215.4539.1498.

Shukla, J, Y Mintz, Randal D. Koster, Paul A. Dimeyer, J Shukla, Y Mintz, Zhichang Guo, et al. “Influence of Land-Surface Evapotranspiration on the Earth’s Climate.” Science (New York, N.Y.), March. http://www.ncbi.nlm.nih.gov/pubmed/17788673.

Skamarock, W. C., Klemp, J. B., Dudhia, J., Gill, D. O., Barker, D., Duda, M. G., …Powers, J G. 2008. “A Description of the Advanced Research WRF Version 3 | OpenSky.” University Corporation for Atmospheric Research. https://doi.org/doi:10.5065/D68S4MVH.

Spera, Stephanie A, Gillian L Galford, Michael T Coe, Marcia N Macedo, and John F Mustard. 2016. “Land-Use Change Affects Water Recycling in Brazil’s Last Agricultural Frontier.” Global Change Biology 22 (10): 3405–13. https://doi.org/10.1111/gcb.13298.

Tapley, Byron D., Srinivas Bettadpur, John C. Ries, Paul F. Thompson, and Michael M. Watkins. 2004. “GRACE Measurements of Mass Variability in the Earth System.” Science 305 (5683): 503–5. https://doi.org/10.1126/science.1099192.

Tawfik, Ahmed B., Paul A. Dirmeyer, and Joseph A. Santanello. 2015. “The Heated Condensation Framework. Part II: Climatological Behavior of Convective Initiation and

Land-Atmosphere Coupling over the Conterminous United States." Journal of Hydrometeorology 16 (5): 1946–61. https://doi.org/10.1175/JHM-D-14-0118.1.

Wang, Chen, Yun Qian, Qingyun Duan, Maoyi Huang, Larry K. Berg, Hyeyum H. Shin, Zhe Feng, et al. 2020. "Assessing the Sensitivity of Land-Atmosphere Coupling Strength to Boundary and Surface Layer Parameters in the WRF Model over Amazon." Atmospheric Research 234 (November 2019): 104738. https://doi.org/10.1016/j.atmosres.2019.104738.

Wei, Jiangfeng, Robert E. Dickinson, and Haishan Chen. 2008a. "A Negative Soil Moisture-Precipitation Relationship and Its Causes." Journal of Hydrometeorology 9 (6): 1364–76. https://doi.org/10.1175/2008JHM955.1.

Wei, Jiangfeng, Paul A. Dirmeyer, and Jingyong Zhang. 2010. "Land-Caused Uncertainties in Climate Change Simulations: A Study with the COLA AGCM." Quarterly Journal of the Royal Meteorological Society 136 (648): 819–24. https://doi.org/10.1002/qj.598.

Yeh, T-C., R T Wetherald, S Manabe, T-C. Yeh, R T Wetherald, and S Manabe. 1984. "The Effect of Soil Moisture on the Short-Term Climate and Hydrology Change—A Numerical Experiment." Monthly Weather Review 112 (3): 474–90. https://doi.org/10.1175/1520-0493(1984)112<0474:TEOSMO>2.0.CO;2.

Zeng, Ning, and J. David Neelin. 1999. "A Land-Atmosphere Interaction Theory for the Tropical Deforestation Problem." Journal of Climate 12 (2–3): 857–72. https://doi.org/10.1175/1520-0442(1999)012<0857:alaitf>2.0.co;2.

Zhang, Huqiang, and C. S. Frederiksen. 2003. "Local and Nonlocal Impacts of Soil Moisture Initialization on AGCM Seasonal Forecasts: A Model Sensitivity Study." Journal of Climate 16 (13): 2117–37. https://doi.org/10.1175/1520-0442(2003)16<2117:LANIOS>2.0.CO;2.

Zhang, Jingyong, Wei-Chyung Wang, and L Ruby Leung. 2008. "Contribution of Land-Atmosphere Coupling to Summer Climate Variability over the Contiguous United States." Journal of Geophysical Research 113 (D22): D22109. https://doi.org/10.1029/2008JD010136.

fZhang, Jingyong, Wei Chyung Wang, and Jiangfeng Wei. 2008. "Assessing Land-Atmosphere Coupling Using Soil Moisture from the Global Land Data Assimilation System and Observational Precipitation." Journal o Geophysical Research Atmospheres 113 (17): 1–14. https://doi.org/10.1029/2008JD009807.

Zhang, Jingyong, Lingyun Wu, and Wenjie Dong. 2011. "Land-Atmosphere Coupling and Summer Climate Variability over East Asia." Journal of Geophysical Research Atmospheres 116 (5): 1–14. https://doi.org/10.1029/2010JD014714.

CHAPTER 5. CONCLUSIONS

Summary and Opportunities for Future Research

For decades, researchers have documented the changes in atmosphere behavior and precipitation variability (e.g., Ronchail et al. 2002; Santos et al. 2015; Marengo and Espinoza 2016; Silva Junior et al. 2018) across the Amazon basin. However, the results are inconsistent and sometimes contradictory due to a lack of reliable observations and diverse model parametrizations. In addition, in global scale studies, determinant factors of atmosphere behavior at the local and regional scale are poorly characterized, such as convective triggering potential, moisture fluxes, or land cover changes; this makes it essential to assess land-atmosphere interaction at finer spatial resolution. Therefore, using high spatio-temporal resolution datasets and simulations is required to enhance understanding in precipitation change analysis and land-atmosphere interaction studies.

In this dissertation, chapter 2 presents the statistical analysis of spatio-temporal trends in precipitation amount, intensity, and timing from 1982 to 2018 using high-resolution gridded precipitation data (i.e. CHIRPS at 0.05^{o} spatial resolution). New indices are developed to address precipitation timing, intensity, and amount. The Mann-Kendall test is performed on daily indices to capture trends in the data, and a change point detection technique has been applied to find very wet or very dry years across the basin. We found that most of the Amazon basin has experienced precipitation shifts, many of which are significant. Generally, while the western regions have trended wetter, the eastern and southern regions have trended dryer. Wetting trends occur following the spatial pattern of extreme rainfall events, with very little similarity to changes in the number of dry days. This change shows that the distribution of rainfall has changed to more intense rainfall in some areas and reduced intensity in others. Although gridded datasets are

useful to analyze changes and trends, there is still significant uncertainty associated with them. There is a strong need to have high temporal resolution observations to be able to validate gridded datasets. Also, the spatial pattern of trends is very likely modulated by a combination of factors including ENSO, SSTs, the ITCZ/SACZ transition, strengthening Hadley and Walker circulations, and deforestation. Since lack of observations is a big challenge, I recommend that future research focus on applying this study's approach on observations, as they become available, to examine the trends in precipitation amount, intensity, and timing. In this way, a solid comparison of the different gridded datasets including reanalysis data would be available to minimize the uncertainty in climate studies. Also, further high-resolution regional modeling is necessary to quantitatively identify the causality of the global forcings such as ENSO and ITCZ versus regional forcings such as deforestation and topography.

Following the results of chapter 2, the goal of chapter 3 is to examine the extent to which changes in land cover biophysical characteristics (i.e. reforestation) across the basin can potentially influence the atmosphere behavior across the basin. For this purpose, we simulated changes in heat and moisture fluxes due to tropical reforestation for three ENSO-neutral years (2009, 2013, and 2014) using WRF V3.9. We found that 1) the effects of reforestation on the atmosphere were mostly evident during May to November, 2) spatial patterns of the changes in the atmosphere behavior were consistent with the pattern of land cover change, and 3) the cooling effect of reforestation was evident at the seasonal scale. With a higher proportion of LH due to reforestation, the PBL cools, increases in humidity, and becomes shallower. This further affects the transfer of moisture and energy from the surface to the boundary layer, even influencing transfer to the free atmosphere. Although unavailable, parameters for secondary or young moist forests would improve these simulations further. Due to teleconnection

mechanisms, changing the exchange of energy and moisture balance between the PBL and the free atmosphere influences tropical convection, impacts the intensity of high-level tropical outflow, and provides a mechanism that could affect the extra-tropics (Snyder et al. 2004). Consequently, changes in the surface fluxes of energy and moisture due to LCC cause impacts beyond the areas of disturbances. Thus, it would be reasonable if the land cover change in form of reforestation forces disturbances in the general circulation, including the Hadley and Walker-type circulations through tele-connected mechanisms. The results of this research provide valuable insight into the effects of human disturbances on the atmosphere and precipitation. However, a detailed analysis of influences of different land covers such as farming, savannah, grassland, seasonal agriculture, bare land, and double cropping should be considered in future research. This would be possible to address by repeating this approach using the NOAH-MP land surface model coupled with WRF. Therefore, a comprehensive analysis of the effects of monthly and seasonal changes in land surface biophysical characteristics such as albedo and LAI on the atmosphere's behavior including precipitation amount, occurrences of extreme heat events, floods, and droughts would be feasible. In addition, I recommend future studies focus on evaluating the influences of internal forcing versus external forcing on precipitation variability as well as finding a tipping point and ecosystem tolerance to the changes in precipitation amount and intensity. Also, analyzing tele-connected mechanisms to examine the extent to which changes in regional scale can alter the circumstances at the larger scale is recommended. Finally, evaluation should be done at different time scales from hourly to daily to monthly to distinguish the sensitivity of time-sensitive processes such as cloud formation and convection, which determine the amount and timing of precipitation, to reforestation.

Following the discoveries of chapter 3, chapter 4 is designed to quantitatively evaluate the land-atmosphere (L-A) coupling strength across the Amazon basin. The goal is to identify the coupling strength of land cover changes to atmospheric processes to identify areas where rainfall is most sensitive to changes in the land surface. In this research, by applying the two most popular L-A coupling strength metrics, detailed analysis of the physical processes involved in L-A interaction are explained and hot spots of strong L-A coupling are determined. Finally, by finding the key parameters in L-A coupling, a new multivariate index of coupling measurement is suggested. As a result, we found that hot spots of strong coupling are located in transitional zones between wet and dry ecotones, Savannah, Cerrado, and urbanized areas. Besides, we found that the spatio-temporal scale of analysis is a critical factor in measuring L-A coupling strength. Also, we figured that this analysis depends on model parameterization and is subject to regional variability. Although our results of hot spots of strong L-A coupling across the Amazon basin show -to some extent- overlap with the previous analysis at the global scale, some key regions especially transitional zones between dry and wet, savanna, and Cerrado were missing from the global scale analyses. Moreover, due to the insufficiency of the linear regression used in previous studies, we applied multiple regression on the most important parameters in L-A coupling to highlight the key parameters. We found that interactions between parameters and physical processes play a more important role in L-A interactions indicating the complexity of relationships. Qualitative mapping of hot spot intensity shows distinct clusters of coupling that vary in space and time. Developing a multivariable metric for measuring L-A coupling strength is a useful tool in seasonal and sub-seasonal climate forecasting. Although soil moisture is the main surface variable that affects near-surface moisture availability, soil texture could be another important parameter that modulates the hydrologic dynamics of the land surface. We recommend

future studies focus on analyzing the effects of soil texture on the evolution of precipitation across the tropics. Incorporating accurate soil texture with a high spatial resolution is challenging. Therefore, simulation results can be affected by the quality of soil texture data. Future work should consider using high accuracy up-to-date soil texture data in the simulations and do a comprehensive analysis of the changes in atmosphere behavior. In addition, we recommend that future studies focus on cloud-land surface feedbacks in L-A coupling since it regulates light, temperature, and water vapor deficit over the tropical forest, and such feedbacks have received less attention in studies. Also, the omitted relationships between physical processes (especially atmospheric composition, chemical reactions, and aerosols) add uncertainty in coupling analysis. Further, it is necessary to consider the influences of remote forcing and non-local drivers. This is important over the tropics because of the strong coupling between convection and large-scale forcings.

Broader Impacts

This dissertation focuses on evaluating climate variability and coupling strength of land-atmosphere interactions across the amazon basin. The overall discoveries of this dissertation provide useful information and direction for researchers, atmospheric scientists, policymakers, and governments. It can also potentially increase the human population's safety and prosperity by providing insight for disaster management, land preservation, and adaptation.

Chapter 2 already has been mentioned by the "Discover" magazine as solid evidence showing that the Amazon basin is getting drier over time and it might die in the near future. Also, this chapter is a good reference to show the government and policymakers that the climate of the basin is changing and it will continue to change if proper actions are not taken. Besides, understanding the trends in precipitation amount, intensity, and timing will offer valuable information for the prediction of future trends which can be used in future planning, policymaking, disaster management, and adaptation.

Chapter 3 shows the extent to which land cover change (i.e. reforestation) has affected the atmosphere behavior and precipitation patterns across the Amazon Basin. The results highlight the importance of land preservation and rehabilitation. This chapter provides solid knowledge about how human disturbances can influence the natural system and processes in specific areas. This chapter argues the fundamental knowledge required for adaptation, social science studies, and forest protection.

The outstanding results of chapter 4 can benefit various sectors such as atmospheric science research in which it provides a new point of view of looking at land-atmosphere interactions by integrating all important parameters involved in this relationship instead of only measuring single factor linear regression used in the old fashion methodologies. Although the results

provide a qualitative measure of the coupling, it is a good way to look at the complex relationship between land and atmosphere and shows the need for a complex metric. Also, this chapter highlights the areas where the coupling is the strongest and provides unique information to the government about the regions that have to be preserved. Therefore, this chapter brings a new perspective to the land-atmosphere interaction studies by highlighting the importance of scale and parameters in such studies. It suggests new directions for future research and recommends a comprehensive analysis of the relationships in the complicated land-atmosphere system.

Besides all mentioned broader impacts, this research helped me to grow and develop my understanding of human-environment interactions. This research showed me that systematic thinking and process-based analysis of natural phenomena are critical to understanding the relationships and interactions between various parts of a system. I found that given the high complexity of the natural processes, human-environment interactions are not linear thus need to be addressed properly and linear single variable correlation is not enough to capture all the complexity of the system. Additionally, this research demonstrated the importance of the scale of analysis in addressing the complexity and interactions in a coupled land-atmosphere system. Further, through this research, I discovered that how human disturbances at the local scale can propagate to and influence regional and global scale phenomena on areas beyond the disturbed regions. For example, deforestation in the Amazon basin can influence the ITCZ timing and pattern which then could affect the amount, intensity, and timing of precipitation in the tropics.

REFERENCES

REFERENCES

Marengo, J. A., and J. C. Espinoza. 2016. “Extreme Seasonal Droughts and Floods in Amazonia: Causes, Trends and Impacts.” International Journal of Climatology 36 (3): 1033–50. https://doi.org/10.1002/joc.4420.

Ronchail, Josyane, Gérard Cochonneau, Michel Molinier, Jean Loup Guyot, Adriana Goretti De Miranda Chaves, Valdemar Guimarães, and Eurides De Oliveira. 2002. “Interannual Rainfall Variability in the Amazon Basin and Sea-Surface Temperatures in the Equatorial Pacific and the Tropical Atlantic Oceans.” International Journal of Climatology 22 (13): 1663–86. https://doi.org/10.1002/joc.815.

Santos, Eliane Barbosa, Paulo Sérgio Lucio, and Cláudio Moisés Santos e Silva. 2015. “Precipitation Regionalization of the Brazilian Amazon.” Atmospheric Science Letters 16 (3): 185–92. https://doi.org/10.1002/asl2.535.

Silva Junior, Celso H.L., Catherine T. Almeida, Jessflan R.N. Santos, Liana O. Anderson, Luiz E.O.C. Aragão, and Fabrício B. Silva. 2018. “Spatiotemporal Rainfall Trends in the Brazilian Legal Amazon between the Years 1998 and 2015.” Water (Switzerland) 10 (9): 1–16. https://doi.org/10.3390/w10091220.

Snyder, P. K., C. Delire, and J. A. Foley. 2004. “Evaluating the Influence of Different Vegetation Biomes on the Global Climate.” Climate Dynamics 23 (3–4): 279–302. https://doi.org/10.1007/s00382-004-0430-0.